320
AA

PRELIMINARY REPORT

RISK ASSESSMENT FOR ICE DAMAGE TO SUBSEA PIPELINES

Submitted to

Minerals Management Service
U.S. Department of the Interior

Submitted by

C-CORE
St. John's, NF Canada

December 22, 1999

Table of Contents

1.0 Rationale for Risk Assessment Strategies 1-1
- 1.1 Background 1-1
- 1.2 Project Objectives 1-2
- 1.3 Project Scope 1-3

2.0 Ice Gouge/Soil/Pipeline Interaction Analysis 2-1
- 2.1 Overview of the Interaction Process 2-1
- 2.2 Driving Force Models 2-4
  - 2.2.1 Chari Model 2-4
  - 2.2.2 FENCO Model 2-4
  - 2.2.3 COGLA Model 2-5
  - 2.2.4 AARI Model 2-5
  - 2.2.5 C-CORE Model 2-5
  - 2.2.6 Assessment of Driving Force Models 2-6
- 2.3 Seabed Reaction Force and Soil Failure Models 2-6
  - 2.3.1 Chari Model 2-6
  - 2.3.2 FENCO Model 2-7
  - 2.3.3 COGLA Model 2-7
  - 2.3.4 Surkov Model 2-7
  - 2.3.5 AARI Model 2-7
  - 2.3.6 Kioka and Saeki Model 2-8
  - 2.3.7 C-CORE Model 2-8
  - 2.3.8 Assessment of Soil Failure Models 2-9
- 2.4 Subgouge Deformation Models 2-10
  - 2.4.1 Experimental and Field Investigations 2-10
  - 2.4.2 COGLA Model 2-11
  - 2.4.3 C-CORE Model 2-12
  - 2.4.4 Finite Element Analysis 2-13
  - 2.4.5 Assessment of Subgouge Deformation Models 2-17
- 2.5 Buried Pipeline Response Models 2-17
  - 2.5.1 ASCE Model 2-18
  - 2.5.2 AARI Model 2-19
  - 2.5.3 C-CORE Model 2-19
  - 2.5.4 Continuum Finite Element Models 2-20
  - 2.5.5 Assessment of Buried Pipeline Response Models 2-25

3.0 Environmental and Physical Data 3-1
3.1 General Framework for Assessing Pipeline Risk 3-1
3.1.1 Gouge Dimensions 3-1
3.1.2 Gouge Frequency 3-1
3.1.3 Age of Ice Gouges 3-2
3.2 Beaufort Sea 3-3
3.2.1 Geographic Region 3-3
3.2.2 Available Data 3-4
3.2.3 Method of Analysis 3-6
3.3 Lake Erie 3-6
3.3.1 Geographic Location 3-6
3.3.2 Available Data 3-7
3.3.3 Method of Analysis 3-8
3.4 Sakhalin Island 3-8
3.4.1 Geographic Location 3-8
3.4.2 Available Data 3-9
3.4.3 Method of analysis 3-9
3.5 Grand Banks 3-10
3.5.1 Geographic Location 3-10
3.5.2 Available Data 3-10
3.5.3 Method of Analysis 3-12
3.5.3.1 Iceberg Scour Model

4.0 Ice Gouge Risk Framework 4-1
4.1 Overview 4-1
4.1.1 Basis 4-1
4.1.2 Objectives and Constraints 4-1
4.1.3 Approach 4-1
4.2 Target Safety Levels 4-2
4.2.1 Overall Target Safety Levels 4-2
4.2.2 Apportioning Ice Gouge Risk 4-3
4.3 Design Gouge Parameters 4-4
4.3.1 Gouge Depth 4-4
4.3.2 Gouge Width 4-5
4.3.3 Joint Distribution of Gouge Depth and Width 4-5
4.3.4 Limit States Approach 4-5

5.0 Assessment of Model Uncertainty 5-1
5.1 Deterministic Model Analysis 5-2
5.1.1 Baseline Model Parameters 5-3
5.1.2 Variant Model Scenarios 5-3
5.2 Pipeline Response Analysis 5-4
5.2.1 Pipeline Strain Response 5-4
5.3 Pipeline Design Issues 5-6

5.4 Pipeline Response Model Uncertainty 5-7
5.4.1 Inherent Model Characteristics 5-8
5.4.2 Ice Gouge/Soil/Pipeline Interaction Model 5-8
5.4.3 Addressing Uncertainty Issues 5-10

References

Appendix A AARI Ice/Seabed Interaction Model

Appendix B Subgouge Deformation Models

Appendix C Buried Pipeline Response Models

Appendix D Scour Forces and Subscour Deformations - Experimental Observations

Appendix E Pipeline Strain Response Analysis

1.0 Rationale for Risk Assessment Strategies

1.1 Background

Marine pipelines are an effective and economic means for the transportation of oil and gas products from development fields in ice covered waters. Natural hazards such as ice gouging represents a significant threat to the safe operation and structural integrity of marine pipelines. The mitigation of potential environmental damage and economic impact due to pipeline failure is of primary concern. Public concern and perceived risk, economic development, target levels of safety and consequence are integral components of the design process. Consequently, the development of accurate and robust engineering models, as well as the characterisation and modelling of uncertainty are considered to be critical areas in the pipeline risk assessment process.

Buried marine pipelines can be subjected to ground motion due to natural processes such as landslide, liquefaction or earthquake events. For the arctic environment, ice gouging represents a significant threat to the structural integrity of marine pipelines. This is recognized by API RP 2N (1995) and API RP 1111 (1999).

Initial efforts for determining the minimum pipeline trench depth focused on the maximum gouge depth. The existence of large deformation zones extending with depth beneath the gouge was not considered. Been et al. (1990) recognized the potential for subgouge disturbance which was associated with a soil shearing mechanism. The importance of subgouge deformations was realised through the Pressure Ridge Ice Scour Experiment (PRISE) investigations (Clark et al., 1998). In PRISE, an engineering model was developed to assess the influence of ice gouge events on buried marine pipelines (Woodworth-Lynas et al., 1996). Comparison of field studies on relict gouge events with centrifuge modelling experiments has supported the importance of

and extent of subgouge deformation (Woodworth-Lynas, 1998; Woodworth-Lynas et al., 1998). This has a significant impact on pipeline design.

The development of statistical and mechanical models defining ice feature/soil interaction to predict design ice gouge parameters and engineering models defining the coupled soil/pipeline response are relatively well established. Model sensitivity and parameter uncertainty of existing analytical tools has not been properly assessed in terms of the influence and consequence on pipeline risk assessment strategies. The importance in pipeline design has been recognised by CSA Z662 (1999) and DNV (1996) through of incorporation of risk assessment guidelines.

Consequently, this project has been initiated to address the risk of marine pipelines subject to ice gouge events and the uncertainties associated with engineering assessment tools.

1.2 Project Objectives

The program objectives can be summarised as

- to review current practice for assessing risk of ice damage to marine pipelines
- to establish a rational, modelling framework for risk assessment
- to identity and characterize sources of risk uncertainty
- to evaluate inherent uncertainty in the environmental data and numerical models on risk estimates
- to prioritize areas of data collection and model development in order to reduce risk uncertainty

1.3 Project Scope

The initial phase focused on the fundamental mechanics governing the interaction of an ice feature with the seabed. Factors that influence the ice/soil interaction process and pipeline behaviour subject to ice gouge events were investigated. The engineering models include driving forces, seabed reaction or gouge forces, subgouge soil deformations and pipeline response.

A review of available physical data; for example, gouge statistics, geotechnical, ice regime, and required met-ocean data, was conducted for a range of geographic locations. The selected areas included the Grand Banks, Lake Erie, Sakhalin and Beaufort Sea. Appropriate characterisation of the data sets was performed to satisfy the objectives.

Quantitative risk models for determining annual probabilities associated with direct ice/pipeline contact or pipeline damage due to large soil displacements have been evaluated. The analytical or numerical models play a significant role in the uncertainty of ice gouge risk estimates for marine pipelines. The confidence associated with risk estimates depends on an accurate assessment, source characterisation and quantification of both parameter and model uncertainty. Sensitivity analyses will be conducted to evaluate the influence of uncertainty for reliability based design methods of marine pipelines in an ice gouge environment.

Finally, the results of the study will prioritize critical areas for future research requirements or data collection programs in order to reduce the inherent uncertainty and increase the reliability of risk estimates.

2.0 Ice Gouge/Soil/Pipeline Interaction Analysis

The fundamental parameters characterising the complex ice gouge/soil/pipeline interaction process and the analytical methods defining the event are reviewed.

2.1 Overview of the Interaction Process

A schematic illustration of an underwater view of a pressure ridge gouge event observed in the Russian arctic is presented in Figure 2.1-1. Although the geometry depicted is chaotic in nature, conceptually the ice feature is generally treated as a blunt indentor, which may be more characteristic of multi-year pressure ridges keels, icebergs or stamukhas (i.e. grounded ridges).

The dominant mechanisms governing the penetration of an ice feature into the seabed and the resultant creation of a gouge (i.e. depression or furrow) are illustrated in Figure 2.1-2. The plan view is shown in Figure 2.1-2(a) where a three-dimensional rupture surface forms as the ice feature advances and the deformed soil clears to the gouge edge. In the direction of motion, the profile Section A-A′, a dead wedge or zone of relatively stable soil mass develops adjacent to the keel. During the ice gouge event, soil is pushed forward, within the rupture surface, and develops a frontal mound (i.e. spoil heap or berm). For steady-state gouge processes, a dynamic equilibrium is developed where the "plowed" soil in the failure zone is balanced with creation of the frontal mound and side berms due to the coupled clearing mechanisms.

To characterise the soil deformation response, three zones have been postulated (Palmer et al., 1989) and are illustrated in Figure 2.1-1(b). The upper layer (Zone 1) represents the failure surface associated with intense plastic deformation. The intermediary layer (Zone 2) is subjected to large deformation and the transition from Zone 1 to Zone 2 is generally defined by yield soil response functions with the strain amplitude decaying with increasing soil depth. Zone 3 is wholly elastic response and defines the extent of the subgouge displacement field profile.

Ice gouge/soil/pipeline interaction scenarios can be broadly defined in two categories:

- Direct contact
- Load transfer

The first case would represent surficial or buried pipelines within Zone 1 where pipeline structural integrity would probably be compromised. The primary focus of this report, is the latter case, which is defined by the subgouge displacement field and relative motion between the pipeline and surrounding soil. In addition, the elastic response of Zone 3 is not considered, as the pipeline design would most likely be overly conservative.

Methods to analyse ice gouge/soil/pipeline interaction can be classified as:

- Statistical
- Deterministic
- Hybrid

For these engineering assessment tools, the objective is to define appropriate boundary conditions (e.g. gouge dimensions, ice gouge/seabed forces) which are required to estimate the pipeline response to ice gouge events. The overall philosophy is illustrated in Figure 2.1-3.

The data sources for statistical methods are environmental factors (e.g. driving forces, ice feature geometry) and physical gouge characteristics (e.g. gouge depth, width). To predict pipeline response, the environmental distributions have to be incorporated in some closed form algorithm. Conversely, gouge statistics can either independently assess design pipeline burial depth estimates or complement mechanical models defining ice gouge/seabed interaction forces.

For statistically significant parent distributions, the advantages for utilising physical ice gouge data sets are that the model is unbiased and representative of the interaction scenarios. Furthermore, knowledge of the complex ice gouge process is implicit. In addition to uncertainty, which will be addressed later, the main penalties are project lead-time and cost required for development of the database.

Deterministic analysis can be used as an independent assessment tool or augmented with statistical and/or empirical data. Pipeline response can be investigated through sensitivity analysis or discrete computations viewed as a subset within a risk-based framework (e.g. Monte Carlo simulation).

The advantages are the ability to conduct parametric evaluation of governing variables, to assess ice gouge/seabed interaction forces, to estimate upper limits on gouge depths, to investigate interaction scenarios not recorded in the statistical database. Limitations include technical knowledge and computational resources.

The issues addressed should not be viewed as inherently discrete components. In fact, coupled hybrid strategies developed on a rational basis, which complement and enhance the pipeline risk assessment model, are advantageous. The deterministic components outlined in this section and illustrated in Figure 2.1-3 will be discussed.

An evaluation of the deterministic engineering tools for ice gouge/soil/pipeline interaction analysis will be presented. The concepts and models reviewed will include driving forces, soil failure, subgouge deformation and pipeline response. Factors with respect to statistical analysis and physical characteristics of ice gouge events are considered in later sections.

2.2 Driving Force Models

Typically, driving force models couple statistical data of environmental processes (e.g. wind, current) and ice feature geometry with mechanical models that define ice gouge seabed interaction. The model bases can be generally considered as (i) work energy methods, (ii) force equilibrium methods or (iii) hybrid.

The energy method is a dynamic analysis that considers the ice feature kinetic energy (i.e. $KE = \frac{1}{2} m v^2$), whereas the force method assumes a steady state process governed by static equilibrium (i.e. $\Sigma F = 0$). Driving force models are typically used in conjunction with seabed force models to model the ice gouge/soil interaction and predict physical gouge characteristics. Several driving force models will be reviewed and the main characteristics are summarised in Table 2.2-1.

2.2.1 Chari Model

Chari (1975) presented the original model with extensions, refinements and validations of the model subsequently published including Chari (1980), Chari and Peters (1981) and Green (1984). The analysis is based on an energy balance between the driving force and soil resistance due to a sloping seabed. The mass of the iceberg, current and wind forces were considered.

2.2.2 FENCO Model

Two models based on a three-degree of freedom, kinematic, dynamic model and a single degree of freedom energy balance model were developed by FENCO (1975).

The dynamic, force equilibrium model considers the effects of wind, wave, current and pack ice driving forces. The ice feature is considered a rectangular prism with motions analyzed in a two-

dimensional plane (i.e. surge, heave and pitch). Hydrodynamic effects of added mass and moment of inertia are taken into account.

The energy balance approach only considers the forward motion (i.e. surge) of a rectangular ice feature and equates the initial kinetic energy plus current and wind drag forces to the work done on soil deformation. Hydrodynamic added mass effect is accounted for by an added mass coefficient.

2.2.3 COGLA Model

Been et al. (1990a) developed a model to calculate the energy of an advancing ice feature and the energy dissipated by work done on the seabed over prescribed displacement intervals. The model considered idealised pressure ridge geometry. Surge and heave motions, righting moment, and flexural strength of the surrounding ice field were considered. The environmental driving force was due to wind and current with an option for ice feature orientation.

2.2.5 AARI Model

The deterministic model is based on an energy balance approach similar to Chari (1975) (Stepanov et al., 1998). The ice gouge process considers the kinetic energy of the hummock field, which is expended by work due to soil resistance force. The analysis considered the hummock field geometry and drift velocity, which was based on current, tidal current and storm surge components.

2.2.6 C-CORE Model

The objective was to model iceberg gouge processes on the northeast Grand Banks (McKenna et al., 1999). A comprehensive assessment of the environmental driving forces, ice gouge forces, iceberg characterisation and hydrostatics was incorporated. The deterministic analysis was based

on a nonlinear iterative solution of the static equilibrium and was a subset within a Monte Carlo simulation framework to estimate gouge depth distributions. The environmental driving forces include the effects of wind, wave, tidal current, inertial current and wind-driven Ekman current.

2.2.6 Assessment of Driving Force Models

The FENCO and C-CORE models represent the most comprehensive treatment of driving forces. Although, based on a series of calibration and sensitivity analyses, Comfort and Graham (1986) question the algorithm validity as presented by FENCO (1975). The C-CORE model, however, considers more realistic iceberg geometry profiles.

2.3 Seabed Reaction Force and Soil Failure Models

A significant amount of work has been conducted to develop ice gouge models. The review presented can not be considered complete and examples of other work not explicitly discussed include Bea et al. (1985), Beloshapkov and Marchenko (1998) which is mathematically complex and Truskov and Surkov (1991) which is based on the Chari (1975) model. Walter and Phillips (1998) conducted an extensive review of ice gouge model formulations. The main parameters are discussed and the model characteristics are summarised in Table 2.3-1.

2.3.1 Chari Model

Soil resistance was based on a passive pressure mechanism at the face of the iceberg (Chari, 1975). The seabed interaction force was dependent on ice gouge length, depth, and width, developed surcharge due to ice gouging, effective unit weight of soil and soil shear strength. The iceberg was considered a rigid indentor with constant draught. The soil response was soft and yielding with no volume change. The frontal mound (i.e. surcharge) is assumed remoulded with negligible shear strength.

2.3.2 FENCO Model

FENCO (1975) modelled the soil response as an elastic medium and rigid plastic material. A limit equilibrium analysis is used to estimate the soil resistance. The model assumed Coulomb passive pressure mechanism and was restricted to cohesive soil. The frontal mound surcharge contributes to the passive resistance, with a ratio of surcharge height to gouge depth fixed at 1.4, and the soil is considered remoulded. The model considers a shear force as a function of the lateral earth pressure and ice/soil friction coefficent.

2.3.3 COGLA Model

The model is presented by Been et al. (1990a) and the soil resistance was based on a passive pressure rupture zone located in front of the advancing ice feature. The magnitude was determined by a modified Sokolovski stress field solution, which included the formation of a dead wedge. A Mohr-Coulomb failure criterion was adopted. The solution also considered ice keel failure. Effective strength parameters and drained soil conditions were considered.

2.3.4 Surkov Model

Surkov (1995) developed a model on a basis similar to the formulation presented by Chari (1975). The primary differences are that the Surkov model considers granular or frictional soil and assumes that all of the displaced soil remains in front of the gouging ice feature.

2.3.5 AARI Model

The gouge model is based on an energy balance approach similar to Chari (1975). The soil resistance force is variable in time and depends on gouge length, seabed topography, soil properties, hummock keel width and angle of inclination for the keel face in contact with the seabed (Stepanov et al., 1998). The equilibrium equations are defined by the tangential and

normal components of the dead wedge and stationary soil, weight of the soil wedge and friction on the sides of the soil wedge. Relating the kinetic energy to the soil resistance force per gouge length, the maximum gouge depth can be calculated. Details are presented in Appendix A.

2.3.6 Kioka and Saeki Model

The model was based on experimental investigations of an ice feature gouging a granular seafloor due to pack ice driving forces (Kioka et al., 1998). Passive resistance on the front (Coulomb) and sides (Rankine) of the ice gouge are incorporated. Subgrade reaction, dynamic friction acting on the base of the ice feature and buoyancy is considered. The gouge forces are determined by solving the equations of motion in the horizontal and vertical direction as well as ice stability conditions. Surge and heave motions of the ice feature are taken into account.

2.3.7 C-CORE Model

Walter and Phillips (1998) have documented the development of two numerical models, drained and undrained conditions, for steady state ice gouge events. The main assumptions for the development of steady-state gouge conditions are the horizontal and vertical gouge forces, gouge depth, gouge width, as well as the size of frontal mound and side berms remain constant over large distances (often kilometers). The displaced soil will create a mound in front of the ice feature with a steady state height and slope angle, where additional scoured soil is cleared to the sides. A passive pressure rupture zone is assumed to occur in front of the dead wedge during steady state conditions.

For cohesive (c'- ϕ') soil under fully drained conditions, soil resistance is generated by passive pressure in front of the gouging iceberg, shear resistance at the base of the dead wedge, and shear resistance on the two sides of the dead wedge.

For cohesive (C_u) soil under undrained conditions, no dissipation of pore pressure occurs during the gouge event. A virtual work analysis based on an assumed incremental mechanism is conducted. Horizontal resistance is determined through a balance of the work input to the system with energy dissipated from the system. The model considers shear resistance along the base and sides of the dead and passive wedges as well as the interface between the dead and passive wedges. A clearing mechanism for moving accumulated soil to the sides of the ice feature is also considered. The vertical bearing capacity of soil under the dead wedge limits vertical scour resistance. The model does not account for energy required to shear the soil as the direction of soil movement changes, nor does it consider the geometric distortion and restraint of the keel above the soil.

2.3.8 Assessment of Soil Failure Models

These models, based on Rankine and/or Coulomb theories of passive pressure, can reasonably predict the forces induced by an ice keel to the seabed during scouring, and they are the state of practice in ice-seabed interaction modelling. Within the limitations of underlying passive pressure theories and limit equilibrium theory, those models provide information on possible failure mechanisms and forces induced in the seabed. Ice scour features and sub-scour stresses can therefore be inferred. However, beside the shortcomings of each such model and inherent errors induced by the assumption of plane failure surfaces, two major limitations of the soil failure models are:

1. Inability to predict subscour deformations. Most of the models predict scour induced soil deformations for the soil above the keel elevation (zone 1), based on some soil volume balance. Owing to the assumptions of limit equilibrium methods, those models do not offer any information on scour induced soil deformations outside the assumed failure planes. Correct estimation of subscour deformations is a crucial step in analyzing the response of buried pipelines to ice scour. Some of these models are further developed to predict subscour deformations, as described in Section 2.4.

2. Assumption of flat, regular ice keels, as opposed to highly irregular and spiky real keel shapes, can be (1) overly conservative - with respect to predicted forces induced to the seabed, and (2) under-conservative in the case of energy balance models predicting ice scour lengths and depths.

In addition, further conclusions can be stated (see also Table 2.3.2):

1. AARI, Chari, Surcov and FENCO models use relatively crude assumptions and their validity from the viewpoint of ice-soil interaction mechanisms is questionable.

2. COGLA model has better assumptions and also has an extension for estimating subscour deformations (Section 2.4.3).

3. Kioka model is suitable for estimating ice-soil interaction effects.

4. C-CORE soil failure model is also fit for estimating ice-soil interaction effects when scour characteristics are known. It is mentioned that the series of ice-scour models proposed by C-CORE includes options both for driving force and subscour deformation calculations.

2.4 Subgouge Deformation Models

2.4.1 Experimental and Field Investigations

A number of small scale, physical modelling studies of ice gouge events have been conducted; for example Paulin (1992), Been et al. (1990a), Poorooshasb (1990), Golder (1989) and Abdelnour, R. and Graham, B. (1984). The investigations considered various shaped indentors (i.e. ice gouge geometries), as well as material and mechanical properties of the soil. Load cells and pressure transducers directly measured the horizontal and vertical gouge interaction forces.

Pore pressure transducers measured the stress response with soil depth. In addition, methods were employed to characterise the resultant soil topography, profile and global deformation field due to ice gouge processes.

In general, the major conclusion drawn from these empirical studies was that varying degrees of subgouge displacements, oriented predominantly in the direction of motion, have been observed below the indentor. This was attributed to a dragging mechanism and shear failure. The subgouge deformation profile and magnitude was dependent on a number of factors including soil properties (type, strength, density) and indentor geometry (width, depth, attack angle). Issues of geometric boundary conditions (e.g. trench surface) and soil strength (e.g. trench backfill) also influenced subgouge deformation and rupture surface.

For ice-soil/pipeline interaction events where subgouge deformations are significant, the value of experimental studies conducted at 1g are limited. The main constraint is due to the inherent uncertainty of extrapolating data to full scale in order to predict soil/pipeline response. This issue was addressed by Poorooshasb and Clark (1990). Consequently, centrifuge modelling techniques are a viable alternative (Paulin et al., 1995; Rizkalla et al., 1992).

Observations from a series of 1g indentor tests, centrifuge experimental studies, and full scale observations are summarised in Appendix D.

2.4.2 COGLA Model

The model was developed through extensive investigations conducted by Fleet Technology and Golder Associates for Canadian Oil and Gas Lands Administration (COGLA). The comprehensive work was presented in a series of reports and of direct relevance are Been et al. (1990a) and Comfort and Been (1990). The study findings were also summarized in the papers Been (1990), Been et al. (1990b), Palmer et al. (1989), Palmer (1990) and Palmer et al. (1990).

The analytical model assumed two independent large strain, soil failure mechanisms within Zone 2 (Figure 2.1-2) during ice gouge events. The potential for subgouge deformation was related to (i) a passive failure defined by an outer rupture surface and (ii) shearing stress developed by the ice keel dragging along the gouged seabed (Figure 2.4-1).

The extent of subgouge deformations due to passive failure mechanism was assessed through application of velocity field solutions based on upper bound plasticity methods (Been et al., 1990a). There were several disadvantages for this approach, first, the solutions are not unique and optimization techniques must be employed and, secondly, for large deformation there was considerable difficulty in finding a velocity field consistent with the boundary conditions. Furthermore, the solution must also be compatible with laws of equilibrium, stress field, and governing constitutive relationships. The analysis concluded that the extent of the rupture surface, due to passive failure, was probably not significant with minimal subgouge disturbance expected. Been (1990) states that the rupture surface does not extend below the maximum gouge depth except for cases of non-homogeneous soil where strength decreases with depth.

The study concluded that subgouge response (Zone 2) was most likely due to shearing stress mechanism and dependent on the soil stress-strain behaviour (Been et al., 1990a). The development of subgouge deformation has also been observed in experimental investigations. Comfort and Been (1990) state that the subgouge disturbance, based on shallow seismic records, was on the order of 1.5 times the gouge depth. The results, however, were not considered conclusive and further research was warranted to accurately define the large deformation regime within Zone 2. Experimental investigations addressing this issue will be discussed in a later section.

2.4.3 C-CORE Model

The significance of subgouge deformations was realised through the Pressure Ridge Ice Scour Experiment (PRISE) investigations (Clark et al., 1998). In PRISE, an engineering model was

developed to assess the influence of ice gouge events on buried marine pipelines (Woodworth-Lynas et al., 1996). Experimental evidence from small-scale ice gouge trials recognized the potential for subgouge disturbance; for example Been et al., 1990 and Poorooshasb, 1990. Comparison of field studies on relict gouge events with centrifuge modelling experiments has supported the importance of and extent of subgouge deformation (Woodworth-Lynas, 1998; Woodworth-Lynas et al., 1998).

A three dimensional, empirical subgouge deformation model, based on analysis of centrifuge experiments conducted during PRISE, was developed by C-CORE. Schematic illustrations of the subgouge deformation profiles are illustrated in Figures 2.4-3 and 2.4-4. The vertical profile (Figure 2.4-3) exhibits an exponential decay with increasing depth. The longitudinal distribution (Figure 2.4-4), perpendicular to the ice gouge track, is characterised by a bounded, peak central displacement with a cosine tail distribution. Relationships defining the subgouge displacement field are detailed in Appendix B.2. A discussion is also presented by Nixon et al. (1996) and Woodworth-Lynas et al. (1996). In addition, relevant issues on ice gouge research are also presented in Clark et al. (1998) and Clark et al. (1994).

2.4.4 Finite Element Analysis

The emerging trend in analysis of ice-soil interaction, inherently including estimation of the subscour deformations and scour forces, is the numerical approach, mainly by means of finite element analysis. However, this approach is still very expensive computationally, and therefore full 3D analyses are not common. In the finite element analyses reported so far, it is usually assumed that the ice mass moves horizontally at a constant speed in a level seabed. The driving forces are assumed large enough to advance the ice keel through soil. No provisions are taken for possible crushing of the ice. The effects of a buried pipeline on subscour deformations can also be assessed, as described in Section 2.5.4.

A series of 2D and 3D finite element analyses of ice scour have been carried out under PRISE, and compared to centrifuge experimental measurements. Such numerical simulations of ice scour have been relatively successful in compressible materials, such as soft clays, but analyses in dilatant materials have had limited success due to numerical instabilities that prevented approaching steady state scour conditions. Results of a few such studies are summarized below:

1. Yang et al. (1993) and Poorooshab and Yang (1993) used an elastically-perfectly plastic, non-dilatant Drucker Prager model. They performed 2D and 3D analyses of ice scour, and a 3D analysis including a buried pipeline represented by beam elements. The analyses were un-coupled, assuming either drained or undrained conditions. Small strain formulation was adopted. It was concluded that (1) the subscour deformations were very small at depths larger than three scour depths, and (2) presence of a pipeline did not significantly affect soil response.

2. Yang et al. (1994, 1996), back-analyzed centrifuge experiments of ice scour in a clayey seabed, described by Lach (1996). Two-dimensional, un-coupled analyses (undrained soil) were performed. Good qualitative results were obtained regarding the pattern and vertical extent of soil deformations. However, the predicted values exceeded recorded values. This fact was attributed to the limited range of horizontal displacements that was simulated. It was also concluded that a pipeline installed within scour depth could not withstand the scour forces.

3. Lach (1996) performed 2D plane strain finite element analyses of three centrifuge experiments of ice scour in a soft clayey seabed (Speswhite kaolin). He used a modified Cam-clay soil constitutive model, coupled solid-fluid equations, and large deformation - finite strain analysis. Reasonably close predictions were obtained for one of the centrifuge tests - performed in normally consolidated clay - in terms of excess pore pressures, resultant forces and soil displacements. Less satisfactory results were obtained for tests performed at higher overconsolidation ratios. Limitations of the numerical

analyses, mostly related to the 2D simplification and to numerical problems induced by finite element distortion, are discussed by Lach (1996).

4. Phillips and Popescu (C-CORE 1998) performed parametric studies of soil strength and dilatancy angle, for ice scour in a dilatant sandy seabed. A non-associated plasticity Mohr-Coulomb soil constitutive model was used to simulate the soil behaviour. Keel displacements in excess of 10 scour depths were achieved in some of the analyses. The magnitudes and extent of predicted sub-scour deformations supported some of the observations from centrifuge model tests (C-CORE 1995, 1997). The results of the analyses were however dominated by the effect of modelling too much elasticity by the soil constitutive model. This affected the predicted scour forces, vertical to horizontal force ratios and sub-scour deformation field.

A comprehensive review of ice-seabed interaction finite element models, and recommendations for future work were provided by A.H. Chan and A. Foreiro (Phillips, 1998). Some of their conclusions, as well as results of more recent work, are summarized below:

1. **Numerical vs. analytical approach:** Soil deformations, plastic dilatancy and changes in effective stress during scour cannot be captured by analytical models. Therefore, limit equilibrium type solutions are useful for estimating initiation of slippage, but not for predicting the loads acting on buried pipelines.

2. **2D vs. 3D:** Two-dimensional simplification seems to be acceptable for simulating the ice scour problem. The problem still unsolved is correct simulation of development of the frontal mound (bulldozed material in front of the ice keel) and of clearing mechanism. 3D discrete element analyses would be necessary for investigating these phenomena and calibrating the 2D continuum models.

3. **Seabed materials:** Relatively close simulation of experimentally observed behaviour was achieved for clayey seabeds in analyses using a modified Cam-clay constitutive model. Analyses of ice scour in sandy seabeds were less successful, apparently due to limitations of available soil constitutive models for granular soil materials.

4. **Soil constitutive models:** There are obvious limitations of soil constitutive models implemented in commercial finite element software (e.g. ANSYS, ABAQUS), especially for modelling sands and overconsolidated clays. These limitations as well as recommendations for future work will be discussed in Section 2.5.5.

5. **Pore pressures and drainage:** Relatively close predictions in terms of excess pore pressure have been obtained in two-phase coupled analyses for clay materials. Special care is recommended for the case of sand materials, in both modelling shear induced dilation, and prescribing the drainage boundary conditions.

6. **Ice-soil interface:** Most commercial software have capabilities for proper simulation of the ice-soil interface.

7. **Analysis options:** Finite strain and large deformation theories are the recommended options for numerical modelling of ice scour.

8. **Mesh distortions:** Element distortion is a significant problem in such large deformation analyses. The updated Lagrangian method combined with adaptive mesh refinement is recommended vs. Arbitrary Lagrangian Eulerian technique. More work is needed for improving re-zoning and re-meshing capabilities of commercial software (see e.g. Popescu 1999).

2.4.5 Assessment of Subgouge Deformation Models

The COGLA model was limited in the difficulty of finding appropriate velocity field solutions for the passive failure mechanism and the shearing stress analysis did not explicitly define a subgouge displacement field. The C-CORE model has a number of distinct advantages the empirical observations are substantiated by field surveys and the model implicitly accounts for ice gouge mechanisms. Furthermore, the utility and simplicity of incorporating subgouge displacement field in numerical algorithms modelling ice gouge/soil/pipeline interaction can be realised.

Finite element analysis of subscour deformations is an emerging approach. Though very promising due to more appropriate assumptions than those used by analytical methods, the result validity is still limited by a series of issues, such as: correct modelling of soil nonlinear behaviour, very large deformation analysis, ice soil contact. At this stage finite element predictions still need to be validated by empirical observations. The computational effort is much larger than required by analytical methods, however the cost of finite element simulations is significantly lower than that required by physical modelling. Finite element models can be used to enhance the experimental methods by performing parametric studies.

2.5 Buried Pipeline Response Models

Standard stress analysis of pipelines must satisfy minimum design requirements for factors such as internal pressure (MAOP), temperature, unsupported span length or restrained sections. For buried pipelines, additional parameters can include thermal gradients and external loads (e.g. live loads imparted through road or rail beds) or differential ground motion (e.g. slope failure, faulting). A significant threat to the structural integrity of buried Arctic marine pipelines is large, relative soil deformation caused by events such as thaw settlement, frost heave and ice gouge. The treatment of differential ground motion effects on buried pipelines is typically

analyzed numerically due to the complex nonlinear ice/soil/pipeline interaction process. Generic soil/pipeline interaction models are presented and issues addressing coupled ice gouge processes are considered.

2.5.1 ASCE Model

ASCE (1984) has developed guidelines for seismic analysis and design of oil and gas pipeline systems. Parameters to define a soil/pipeline interaction model are presented. The continuum behaviour is illustrated in Figure 2.5-1(a). The axial or longitudinal (x-axis), horizontal (y-axis) and vertical (z-axis) displacement components are represented. The term (H_s) represents the burial depth below the ground or seabed surface to the pipe springline. An idealised structural model, shown in Figure 2.5-1(b), can represent the continuum analysis.

The soil reaction is discretised by a series of springs with equivalent stiffness terms (k_a, k_h, k_v) per unit length for the respective orthogonal, displacement components (axial, horizontal and vertical). The nonlinear spring elements can be defined by bilinear or hyperbolic load-deformation relationships, which are schematically illustrated in Figure 2.5-2. The ultimate loads (t_u, p_u, q_u) and critical displacements (x_u, y_u, z_u) characterise the elasto-plastic soil constitutive behaviour. Formulations that define the nonlinear response for granular and cohesive soils are summarised in Appendix C and specific details are presented in ASCE (1984).

ASCE (1984) recommends numerical procedures such as Newmark-Hall and the finite element method for soil/pipeline interaction analysis. A number of numerical and analytical studies on soil/pipeline interaction have incorporated elements of the ASCE (1984) guidelines; for example, Bruschi et al. (1995), Kenny et al. (2000), Nixon et al. (1996), Woodworth-Lynas et al. (1996) and Zhou and Murray (1993).

2.5.2 AARI Model

For the AARI model, the indirect interaction of a drift ice feature with a pipeline is schematically illustrated in Figure 2.5-3a. Stepanov et al. (1998) also considered an alternative scenario for direct interaction between the ice feature and pipeline, as shown in Figure 2.5-3b. Direct contact was assessed by three-dimensional finite element analysis. An algorithm was developed to analyse the problem numerically. The general free body diagram for a pipeline buried at a depth (H) is shown in Figure 2.5-4. The external load, due to the ice gouge event, is characterised by distributed line intensities (p_x, p_z) along the longitudinal y-axis. The pipeline response is analysed using a Winkler type foundation model. The solution of a Fredholm integral equation defines the longitudinal bending moment and shear force distribution. Stepanov (1998) concluded that indirect interaction in any situation does not cause pipeline failure and direct contact should be avoided.

The main advantage for the proposed pipeline response model is that a complex three-dimensional problem is reduced to one dimension and the obtained system of equations has a relatively low order. In addition, the soil model was defined as an elastic semi-space in contrast to finite element methods with bounded domains and defined geometric boundary conditions. Consideration of an elastic continuum is the main disadvantage for this model. Typically, large deformation soil processes (e.g. thaw settlement, ice gouge events) must account for nonlinear geometric and material soil/pipeline interaction.

2.5.3 C-CORE Model

The numerical model developed by C-CORE to analyse buried marine pipeline response to large soil deformations has two un-coupled components:

- ice gouge-induced soil deformations
- soil/pipeline interaction

The first element considers the ice gouge/soil relationship. Based on analysis conducted during PRISE, an empirically derived, engineering model defined a three-dimensional subgouge displacement field, as described in Section 2.4.3. Specific details are addressed in Appendix B.2 and presented by Woodworth-Lynas et al. (1996).

Two main objectives qualify the second, soil/pipeline interaction, component. One, to define the global soil/pipeline response, and two, characterise soil load-deformation relationships. The C-CORE model incorporates the main elements of the ASCE (1984) guidelines. The analysis considers a two dimensional model in the horizontal *xy*-plane as shown in Figure 2.4-4. The soil media is discretized by a series of discrete springs of stiffness, k_a and k_h, for the axial (x-axis) and horizontal (y-axis) coordinate axes, respectively. The ultimate or yield soil behaviour for the axial (t-x) and horizontal components (p-y) are defined by an elastic, perfectly plastic load-deformation relationship. The soil response functions are schematically illustrated in Figure 2.5-2 as a bilinear relationship and details are presented in Appendix C.1.

The pipeline response is predicted in a finite element analysis. The estimated subgouge deformations at the depth of pipe axis (springline) are prescribed to the p-y spring representing the soil (k_h) as an initial displacement boundary condition (Figure 2.5-5). Axial loads and bending strains develop in the pipeline due to relative, differential ground displacement. Further discussion on the finite element model developed by C-CORE is presented in Appendix C.2.

2.5.4. Continuum Finite Element Models

The state-of-the-art in pipeline-soil interaction analysis is the full continuum representation of both the soil and the pipe. A discussion of the main issues involved in such analyses, including a review of significant work reported so far is presented hereafter.

1. **The contact between soil and pipeline:** is modeled with interface elements, that can account for relative displacements. Various types of interface elements have been used,

such as: zero-thickness elements (e.g. double nodes with allowable relative motion), thin layer elements, modified quadrilateral/brick elements. Ng et al. (1997) compared the performance of three such interface elements. They upgraded one of them, and performed 2D simulations of lateral pipe loading in an elastic-perfectly plastic soil, to test the ability of the interface element in simulating gapping. A similar plane strain analysis, involving large relative displacements and gapping, and using a three node contact element, is reported by Yin et al. (1993). Popescu (1999) used a finite sliding formulation for 2D and 3D finite element analyses of buried pipes subjected to lateral and moment loading. This formulation allows for separation and sliding of finite amplitude and arbitrary relative rotation of the contact surfaces, and considers Coulomb friction, with optional shear stress limit.

2. **Structural behaviour of the pipeline:** Continuum representation of the soil allows full representation of the pipeline by 3D shell elements (or by beam elements, in a cross section, for 2D plane strain analyses). Numerous two-dimensional studies of pipe-soil interaction, using continuum elements for the soil have been reported in the literature. In some cases, the pipe was assumed rigid, and only interface effects, including load transfer, were pursued. True three-dimensional analyses, using shell finite elements for representing the pipe are very demanding computationally. Only a few references could be found, and only for cases where the surrounding soil was not represented in the analysis domain, but was replaced by assumed loads or displacements: Lara (1987) studied formation of wrinkles due to differential soil displacements, internal pressure and thermal loads; Jacob et al. (1997) simulated 'pull-in' operations in submarine pipelines, involving severe nonlinear effects due to large displacements; finite element simulations of pipelines acted by known sleeper contact forces (DiBatista et al. 1998), and of pipe bends subjected to in-plane bending (Yoshizaki et al. 1998), performed using nonlinear shell elements, were validated by full scale tests. Results of a full 3D finite element analysis of a buried pipe subjected to moment loading are reported by Popescu (1999). The pipe was discretized with 9-node doubly curved thin shell elements, and the soil with

20-node quadratic brick elements. Both the pipe and the soil materials were assumed elastic. Pipe bending and ovalization could be reasonably predicted, even with a relatively coarse mesh imposed by computer memory restrictions.

3. **Constitutive models for the pipe:** Linear elastic behaviour of pipe material is the most common assumption in pipe-soil interaction analyses. Popescu (1999) performed parametric studies of a flexible buried pipe subjected to vertical soil pressure. Among other aspects, the effects of assuming linear vs. nonlinear material behaviour were analyzed. It was concluded that for ovalization factors below 2%, the differences between linear and nonlinear assumptions are within 5%. However, correct prediction of post-buckling behaviour and snap-through phenomena, with very large displacements inducing plastic yield, can only be obtained using nonlinear constitutive models (e.g. Ramberg-Osgood) and specialized solution procedures (e.g. Riks algorithm, damped static or damped dynamic analysis).

4. **Constitutive models for the soil:** The linear elastic assumption used by some researchers (e.g. Tohda et al. 1988, 1994, Fernando and Carter 1998) is only applicable to situations involving a relatively low strain level, such as compressor induced vibrations, or moderate vertical loads on the backfill. The next step was to assume elastic – perfectly plastic behaviour of the soil materials (referred here are studies reported by Bruschi et al. 1996, and C-CORE 1998b and 1998c, for bilinear elastic-plastic springs, and by Workman 1992 and Yin 1993, for soil as an elastic-plastic continuum). Studies using non-linear hyperbolic soil models are also reported (e.g. Javanmard and Valsangkar 1998). However, to correctly simulate the pipe-soil interaction in problems involving large deformations, use of an appropriate soil model, able to reproduce both strain hardening and softening is necessary. Also, in the case of saturated soil materials, coupled field equations capabilities are required to reproduce pore water pressure build-up and suction phenomena induced by pipe movements through soil. Examples of such finite element analyses are listed here:

- Altaee and Boivin (1995) and Altaee et al. (1996) conducted 2D plane strain analyses of pipes moved laterally through soil to investigate the performance of various nonlinear soil constitutive models. Cam-Clay models were deemed to provide satisfactory results for normally consolidated and slightly overconsolidated clays. A boundary surface soil constitutive model was recommended for overconsolidated clays. In those analyses, no special consideration was given to the soil-pipe interface.

- Studies on the effects of ice scour on buried pipelines are reported by Yang and Poorooshasb (1997). They conducted 3D finite element analyses to investigate the effects of ice scour on pipelines buried in a sandy seabed, using a Drucker-Prager soil model. The pipeline was modeled as an elastic beam, and no slip was allowed at the interface.

- Two-dimensional, nonlinear finite element analyses of large scale tests of lateral loading of a buried pipe were performed at C-CORE for four soil materials: stiff and soft clays, dense and loose sands (Popescu 1999). Two plastic constitutive models were used to describe the nonlinear behaviour of the soil materials: Modified Cam-Clay, with associated plastic flow rule - for clays, and Morh-Coulomb with non-associated plasticity - for sands. Comparisons between numerical predictions and full scale experimental results proved that the finite element model was able to closely simulate the observed phenomena in terms of both force-displacement relations (Figure 2.5.6) and failure mechanisms. More details on the numerical results and model calibration are presented by Popescu et al. (1999).

Some of the limitations of the isotropic plasticity soil constitutive models available in commercial finite element software are discussed by Popescu et al. (1999), based on the results of finite element simulations of large scale pipe-soil interaction tests:

1. *Sub-yield behaviour*: Too much elasticity is simulated prior to reaching the yield surface; a more realistic shear stress-strain behavior, including gradual reduction of the

deformation moduli, could be modeled with multi-yield plasticity or bounding plasticity models.

2. *Flow rule, and in particular plastic dilation*: The classical plasticity constitutive models allow no dependence of plastic dilation behaviour on the effective stress ratio (one of the most important characteristics of soil materials). Shear induced plastic compaction can not be simulated with the Mohr-Coulomb model (only positive values are allowed for the dilation angle), while the modified Cam-clay model simulates plastic compaction but only on the cap - i.e. induced by hydrostatic stresses. Also, too much dilation is simulated by the modified Cam-clay model on the "dry" side of critical state, at low stress levels.

3. *Hardening rule*: The isotropic shear hardening of the Mohr-Coulomb model is governed by a cohesion type parameter (probably inherited from metal plasticity) - not in accordance with the observed behavior of pressure sensitive soil materials, in which shear hardening is dependent on the effective stress ratio.

The study performed at C-CORE (Popescu 1999) showed that drained clay material behaviour could be reasonably simulated with the modified Cam-clay model. However, due to unrealistic modelling of plastic dilation, the modified Cam-clay model is deemed inappropriate for partially drained materials, involving pore pressure analysis. In sands, even under monotonic loading, plastic effects with corresponding volume changes are much more important than in clays, and simple application of critical state models is inadequate. It was shown that the non-associated plasticity models implemented in Abaqus (Mohr-Coulomb and Drucker-Prager) are far from predicting the real, experimentally observed dilatational behaviour of granular soil materials. However, when used in problems involving drained sands, they can produce reasonable predictions if are properly customized.

Hybrid 3D approaches, with the soil modeled as a 3D continuum, and the pipeline discretized into 1D beam-like elements, are also reported. Selvadurai (1991) represented the pipe as an 1D

Bernoulli-Euler beam. Given the nature of the problem analyzed, no special consideration was given to the soil-pipe interface. Yang and Poorooshasb (1997) performed 3D continuum computations with Abaqus to investigate the effects of ice scour on buried pipelines The pipeline was modeled as an elastic beam, and no slip was allowed at the interface. It is evident that such analyses cannot capture the details of soil-pipeline interaction.

There are also mentioned in the literature (e.g. Manolis et al. 1995, Tehrani-Zadeh 1995, Liolios et al. 1998) a series of solutions based on combined boundary element – finite element methods. The pipeline is discretized in finite elements. The loads at the pipe-soil interface are evaluated with boundary elements, using, for example, the cavity theory. Though boundary element solutions are less demanding computationally than corresponding finite element approaches, they are only appropriate for linear or mildly nonlinear problems. Moreover, such an analysis is not accessible with widely available commercial software.

2.5.4 Assessment of Buried Pipeline Response Models

AARI model is restricted to linear elastic response and therefore it is deemed inappropriate for analysis of ice-soil-pipe interaction involving large deformations.

For large, relative displacement processes (e.g. thaw settlement, ice gouge), coupled soil/pipeline response is governed by strain based mechanisms. The computational mechanics are complex and require iterative solutions that account for nonlinear geometric and material behaviour. Consequently, numerical methods (e.g. finite difference, finite element method) are a rational and robust method to analyse pipeline response to ice gouge events. The state of practice in pipe-soil interaction analysis is represented by the structural finite element models - in short *p-y* methods (ASCE 1984) - using specialized beam-type elements for the pipe and Winkler type representation of surrounding soil.

The C-CORE ice gouge/soil/pipeline interaction model represents a more comprehensive, engineering assessment tool for large deformation, ice gouge events. It is based on the *p-y* structural model recommended by ASCE, and brings as a new and valuable element use of experimentally observed subscour deformations. This hybrid approach accounts for ice gouge processes and subgouge soil displacements based on empirical relationships derived from centrifuge modelling tests. Furthermore, the coupled soil/pipeline response considers fully nonlinear geometric and material behaviour.

The *p-y* methods have a long history of development and application, especially in the area of pile-soil interaction. The advantage of this approach, versus a full continuum representation of the surrounding soil, resides in its computational efficiency that allows for modelling of a significant length of the pipeline to capture the effects of interaction in longitudinal direction. The two main disadvantages are:

- lack of physical significance of the soil representation, requiring extensive experimental data and/or use of questionable empirical formulas for calibration of *p-y* and *t-s* spring properties,

- impossibility of modelling interaction details in the transverse cross-section, including ovalization, collapse and post-buckling behaviour of the pipe. These aspects can be addressed in a finite element analysis with continuum representation of the soil/pipeline interaction.

At this stage, continuum nonlinear finite element analyses involving large relative deformations are considerably more expensive than structural finite element analyses. However, they can successfully be used as a complement to the structural approach for predicting ovalization and collapse, and as support for p-y spring parameter calibration. They can also provide a cost effective complement to physical modelling.

Table 2.2-1. Summary of driving force model characteristics.

Model / Reference	Method	Driving Force	Ice Feature
Chari Model Chari (1975)	Energy	▪ wind ▪ current	▪ iceberg ▪ idealised rectangular prism ▪ added mass ▪ constant draught ▪ surge motion
FENCO Model FENCO (1975)	Energy	▪ wind ▪ current	▪ iceberg ▪ idealised rectangular prism ▪ added mass ▪ constant draught ▪ surge motion
	Force	▪ wind ▪ wave ▪ current	▪ iceberg ▪ idealised rectangular prism ▪ buoyant righting moment ▪ surge and heave motions
COGLA Model Been et al. (1990a)	Energy	▪ wind ▪ current	▪ pressure ridge ▪ idealised rectangular prism ▪ flexural stiffness of ice cover ▪ surge, heave and pitch motions
AARI Model Stepanov et al. (1998)	Energy	▪ current ▪ tidal current ▪ storm surge	▪ hummock field ▪ idealised trapezoidal prism ▪ drift velocity
C-CORE Model McKenna et al. (1999)	Force	▪ wind ▪ wave ▪ inertial current ▪ tidal current ▪ Ekman current	▪ iceberg ▪ realistic geometry ▪ hydrostatics ▪ hydrodynamics ▪ added mass ▪ surge, heave and pitch motions

Table 2.3-1. Summary of soil failure model characteristics.

Model / Reference	Model Characteristics	Model Output
Chari Model Chari (1975)	▪ cohesive soil ▪ Coulomb passive pressure mechanism ▪ sloped seabed ▪ no volume change	▪ gouge length, depth ▪ frontal mound height ▪ horizontal soil resistance
FENCO Model FENCO (1975)	▪ cohesive soil ▪ Coulomb passive pressure mechanism ▪ side friction ▪ sloped seabed	
COGLA Model Been et al. (1990a)	▪ Cohesive or granular soil ▪ passive resistance based on modified Sokolovski stress field solution to include formation of dead wedge ▪ Mohr-Coulomb failure criterion ▪ sloped seabed	▪ gouge length, depth ▪ ice feature heave, kinetic energy ▪ passive pressure vertical component
Surkov Model Surkov (1995)	▪ granular soil ▪ passive pressure mechanism due to surcharge of frontal mound ▪ sloped seabed ▪ surge motion	▪ gouge depth ▪ horizontal soil resistance
AARI Model Stepanov et al. (1998)	▪ ▪ sloped seabed ▪	▪ gouge length, depth ▪ seabed reaction force
Kioka Model Kioka et al. (1998)	▪ granular soil ▪ Coulomb passive pressure ▪ Rankine passive pressure ▪ subgrade reaction ▪ dynamic friction ▪ sloped seabed ▪ surge motion	▪ gouge depth ▪ ice force, frictional force, subgrade reaction
C-CORE Model Walter and Phillips (1998)	▪ cohesive or granular soil ▪ level seabed	▪ horizontal and vertical seabed reaction force

Table 2.3.2 Comparison of ice-soil interaction models.

Features	Ice/soil interaction models				
	AARI	Chari[1]	COGLA	Kioka	C-CORE
Various keel angles	No	No	<30°	Yes	Yes
Effective stress analysis	partially	No		No	Partially
Passive pressure	Yes	???	Yes	Yes	Yes
Evolution of frontal mound	Partially	partially	Yes	partially	Partially
Edge effects	No	No	Yes	Yes	Yes
Side friction	Yes	FENCO			Yes
Ice-soil friction	Yes	No		Yes	Yes
Seabed soil properties	Yes	Clays - Chari Sands - Surkov		Sands only	Yes
Capabilities for subscour deformations	No	No	Yes	No	Yes

(1) Surkov and FENCO models are similar to Chari

Table 2.3.3 Summary of experimental results for vertical to horizontal scour force ratios.

Study	F_v/F_h - clay	F_v/F_h – sand
PRISE - centrifuge experiments (C-CORE, 1997b)	1.03 … 2.07	0.91 … 1.18
PRISE - centrifuge experiments (Paulin, 1992)		1.03 … 1.26
Results of 1g laboratory tests and centrifuge experiments (Appendix D)	≈2	≈1

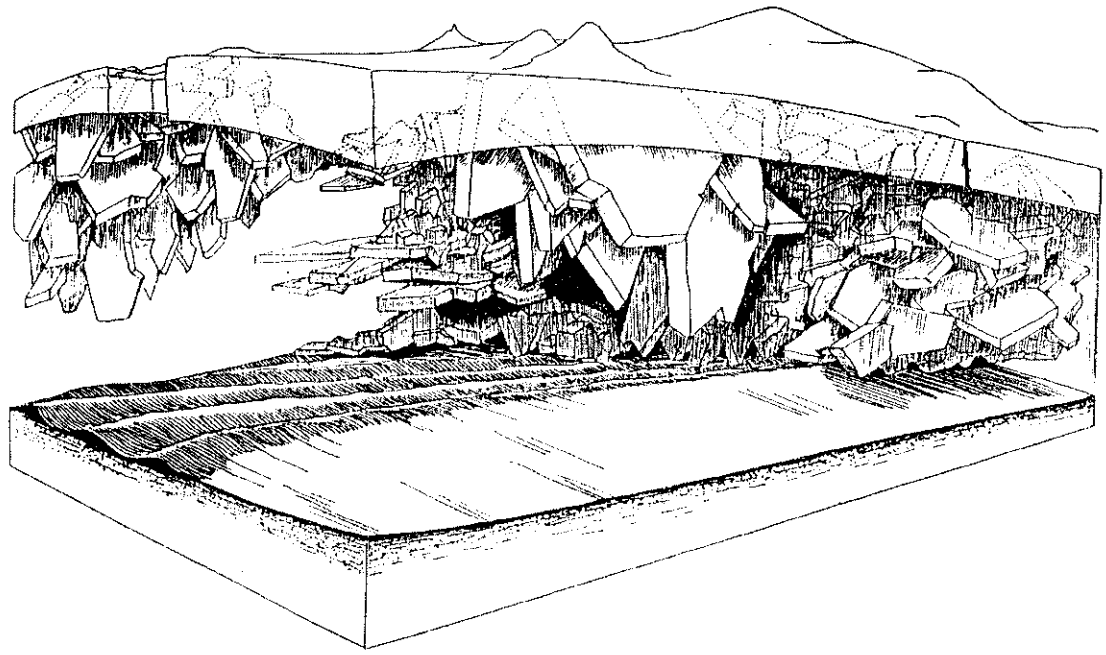

Figure 2.1-1. Illustration of a pressure ridge ice gouge event in the Russian arctic.

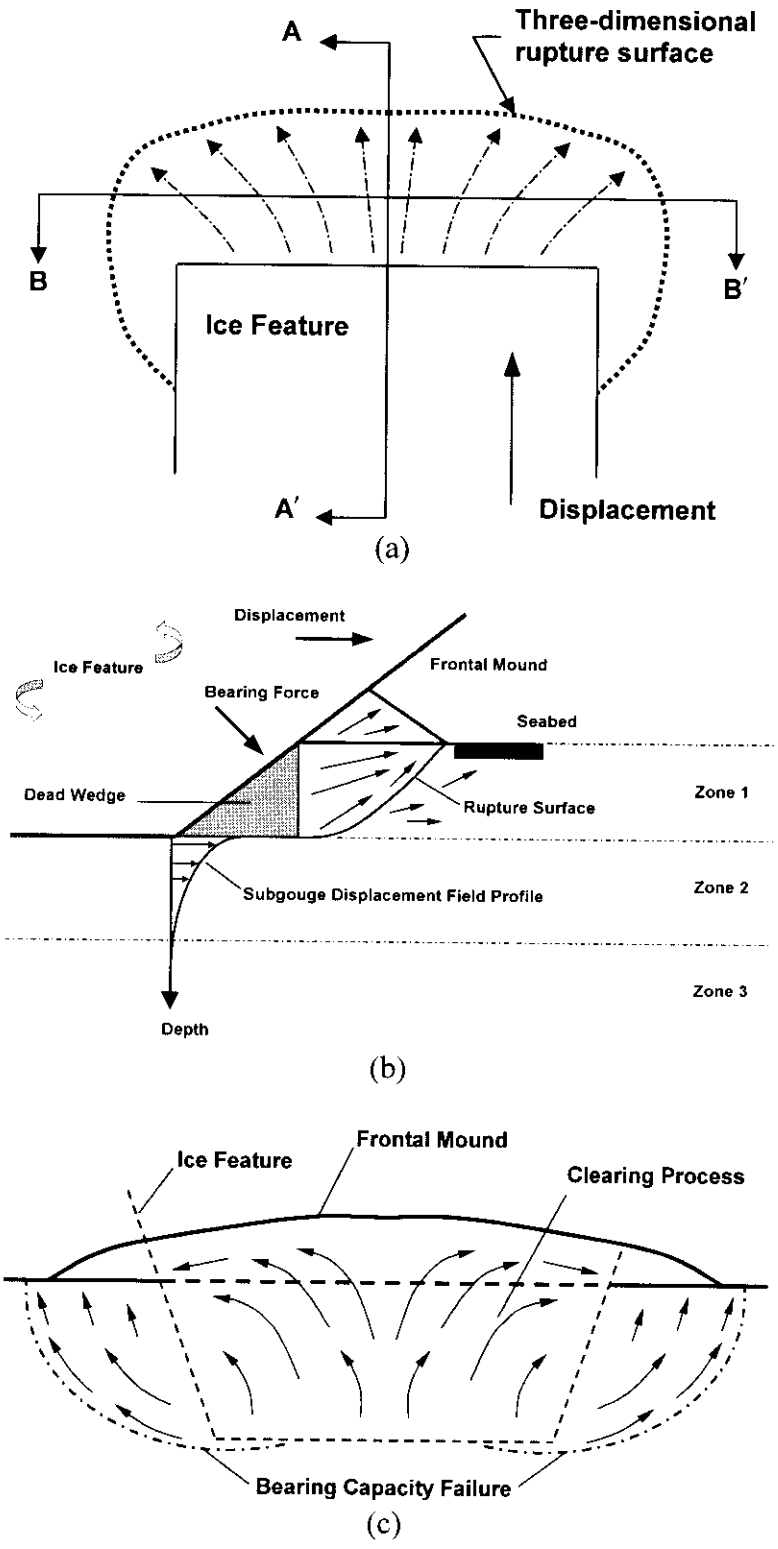

Figure 2.1-2. Ice gouge mechanisms (a) plan view, (b) section A-A′, (b) section B-B′.

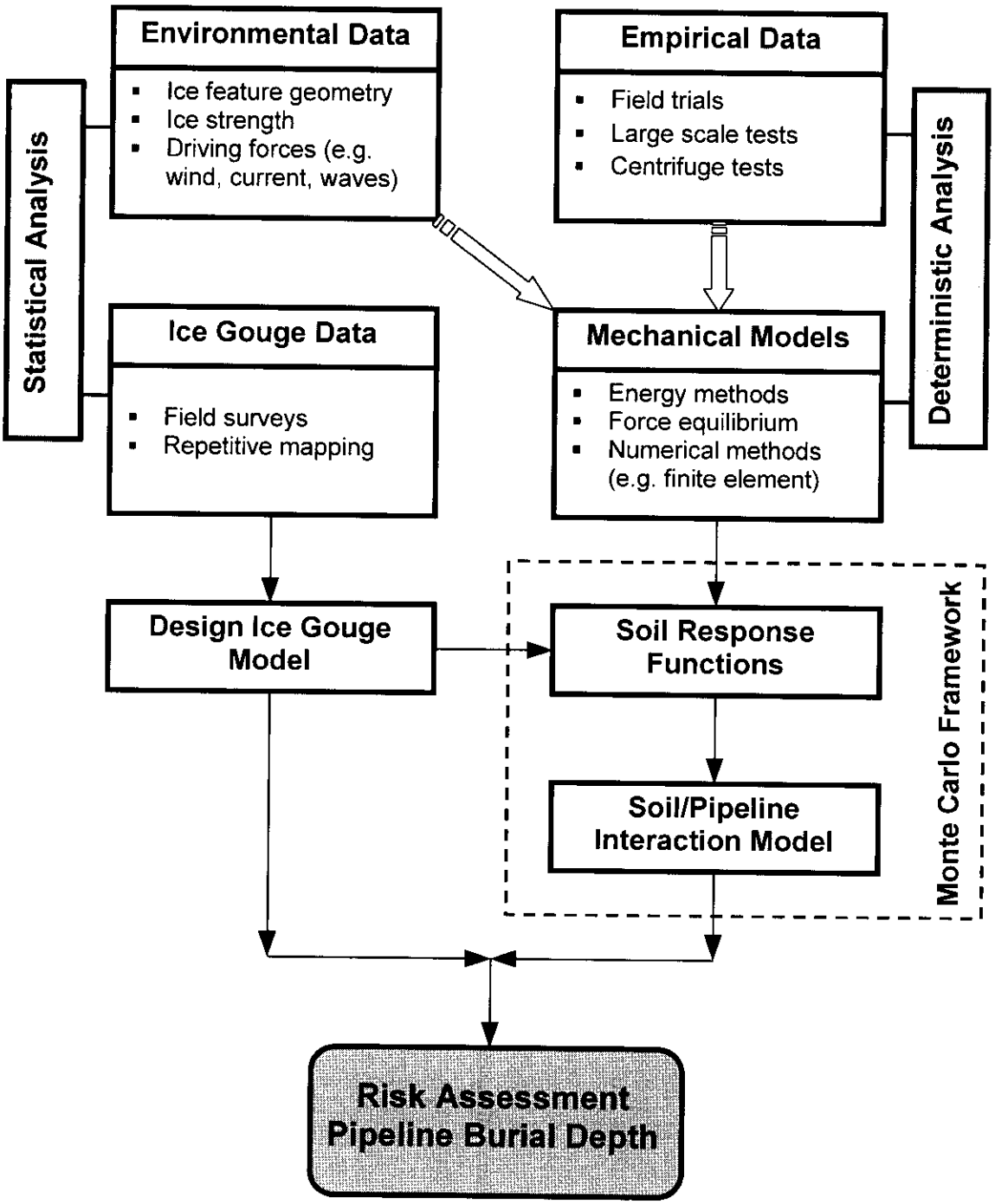

Figure 2.1-3. Engineering assessment tools for ice gouge/soil/pipeline interaction.

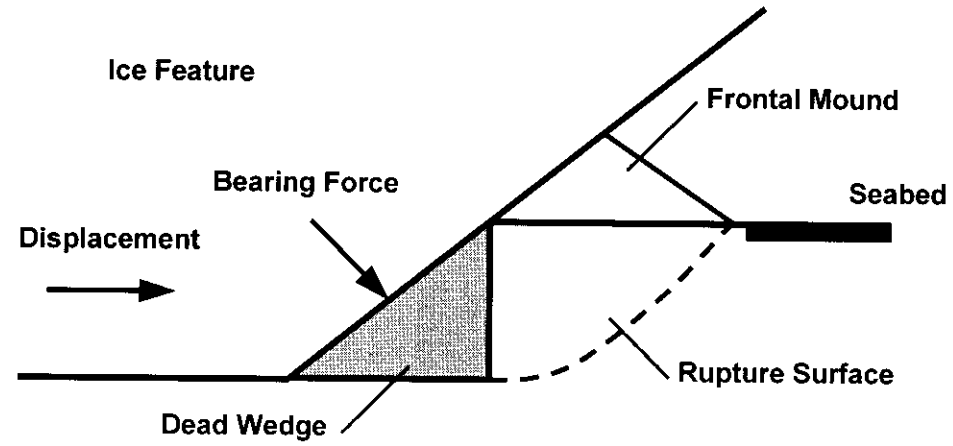

(a)

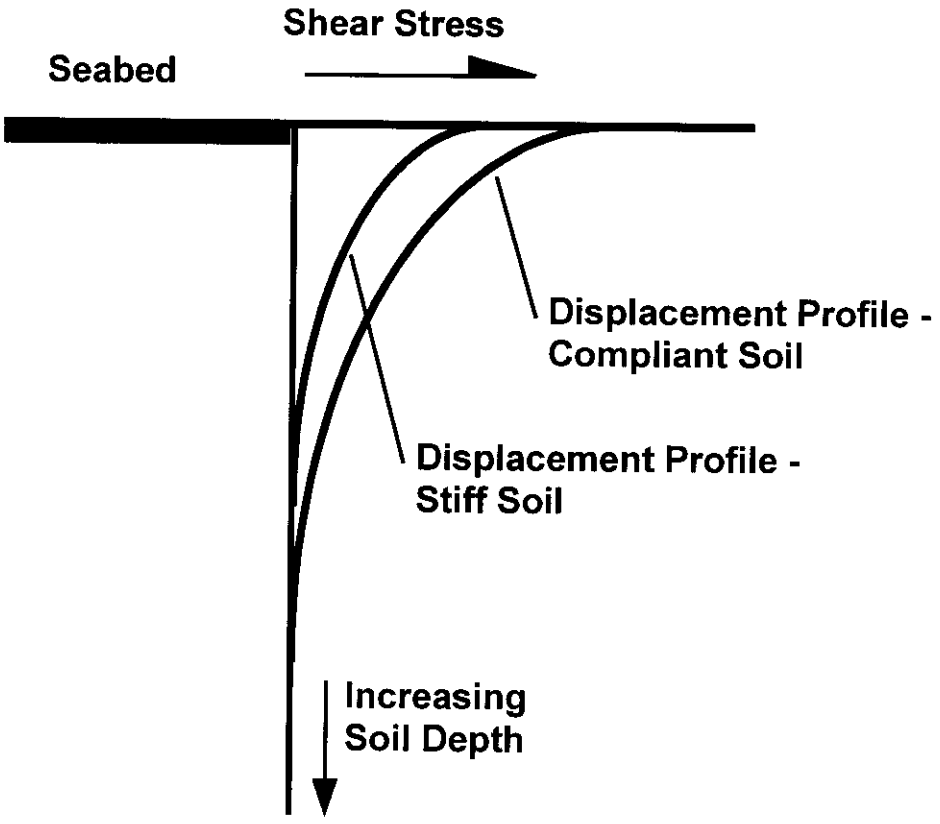

(b)

Figure 2.4-1. (a) Passive failure mechanism, (b) Shearing stress mechanism (Been et al., 1990b).

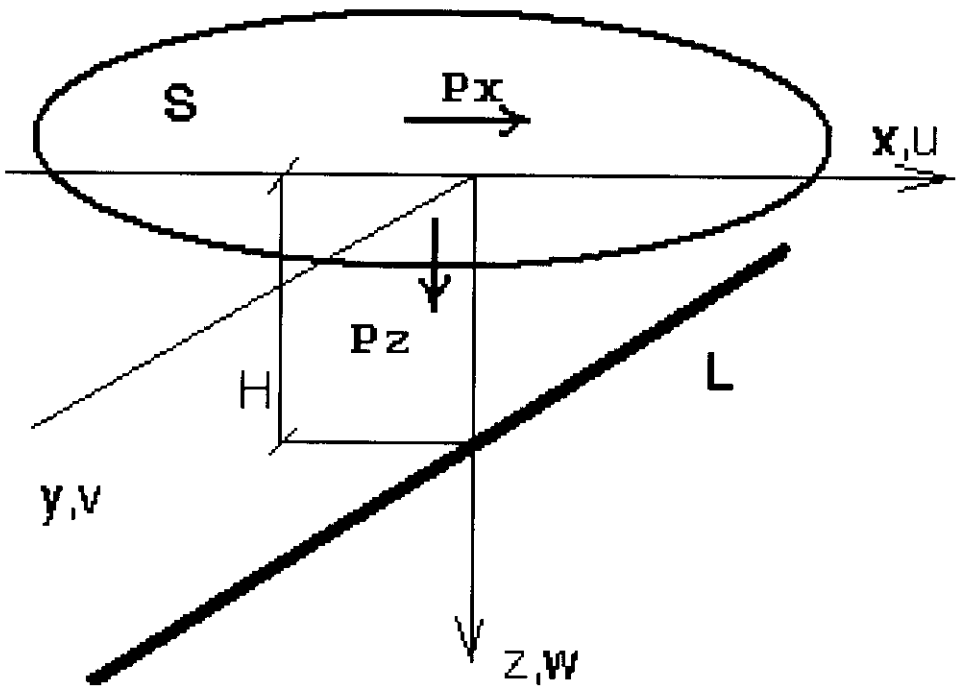

Figure 2.4-2. Schematic illustration of ice-soil-pipeline interaction model developed by AARI.

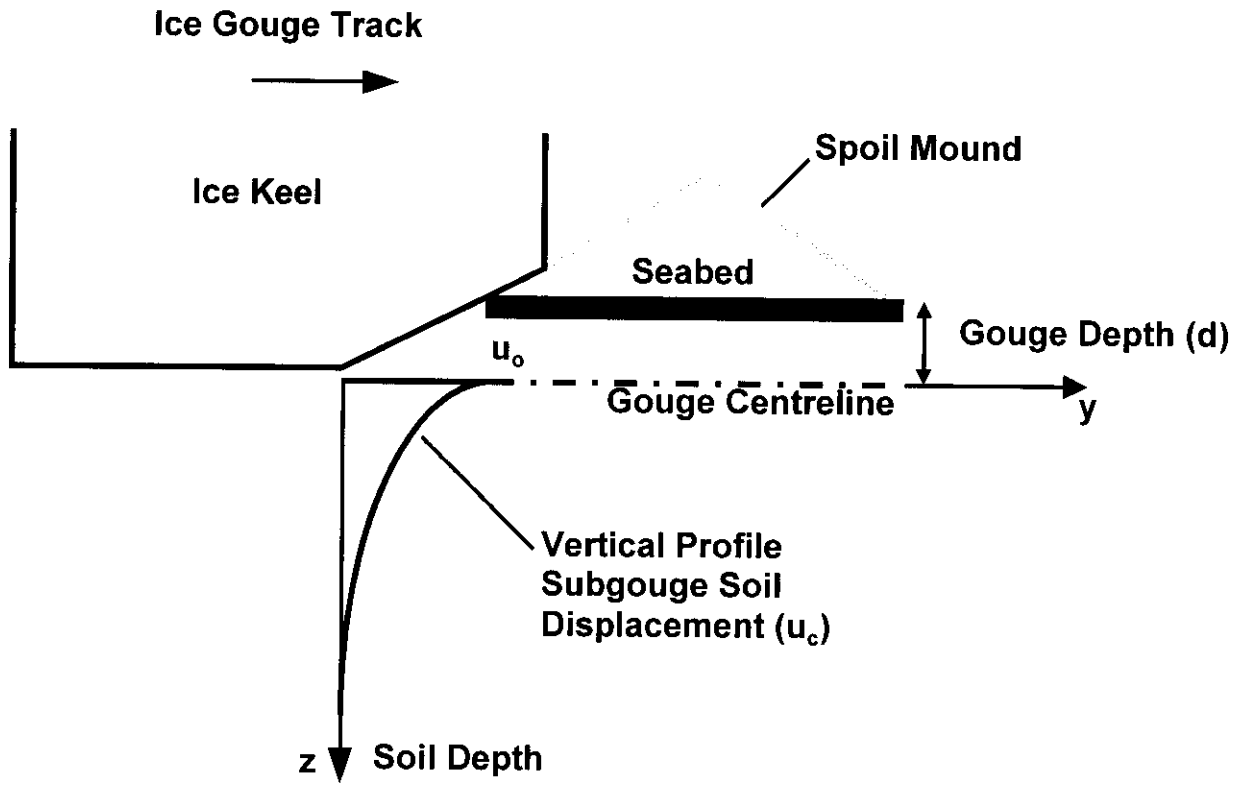

Figure 2.4-3. Schematic illustration of peak gouge displacement (u_o) and vertical distribution (u_c) of subgouge deformations for the C-CORE model.

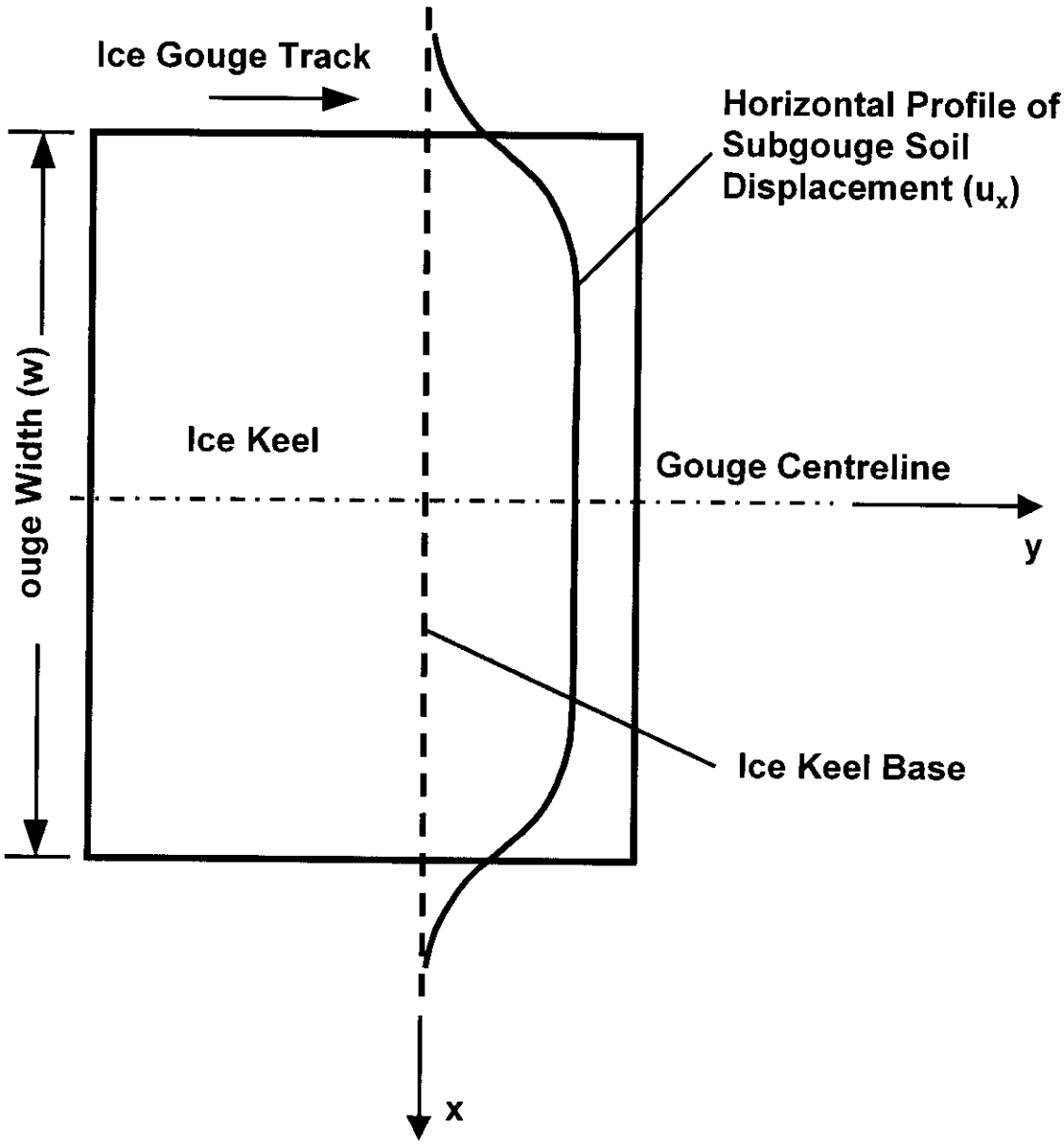

Figure 2.4-4. Schematic illustration of the longitudinal distribution and horizontal extent of subgouge deformations for the C-CORE model.

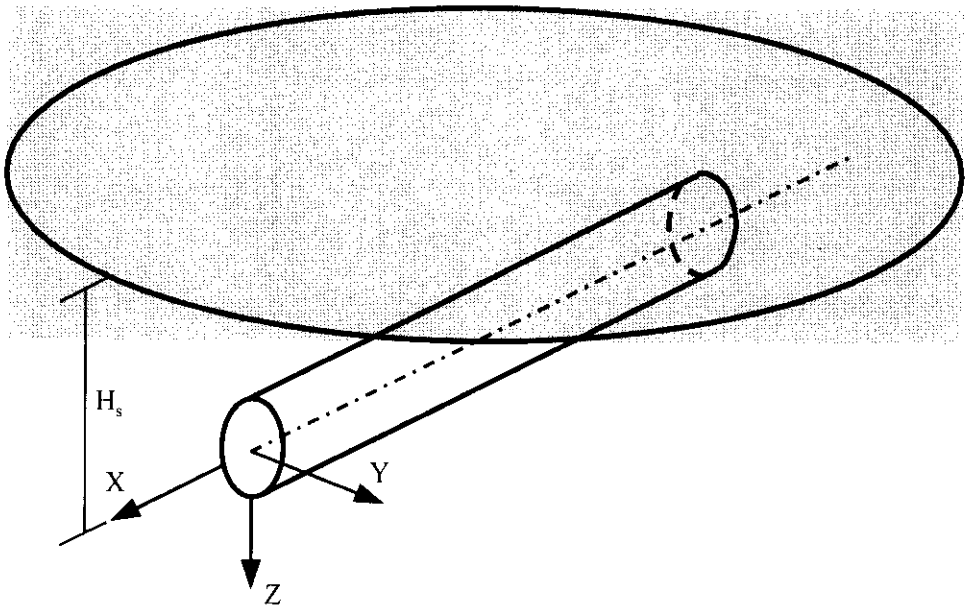

(a)

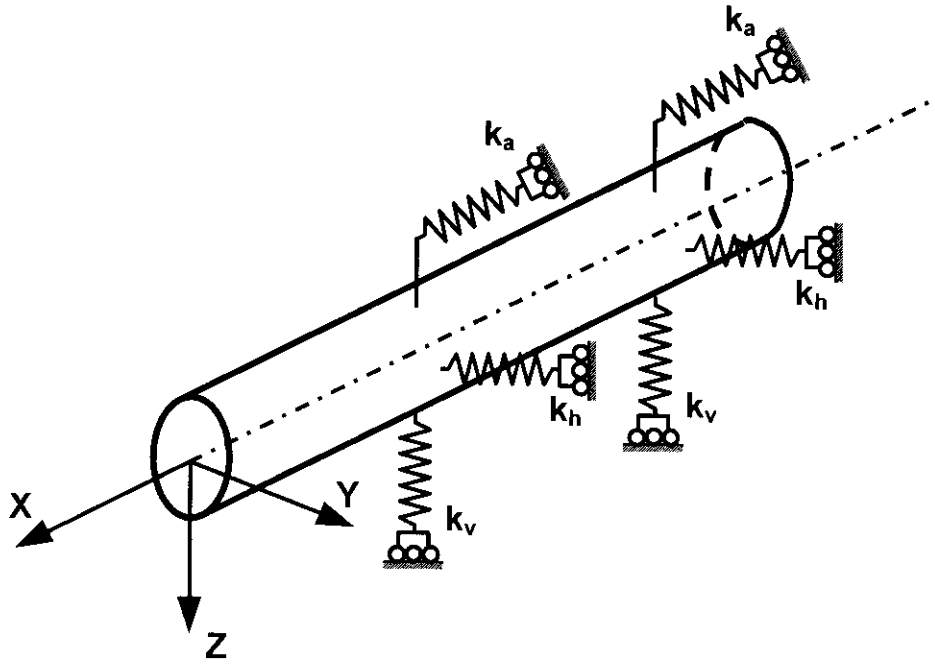

(b)

Figure 2.5-1. ASCE (1984) soil-pipeline interaction model. (a) Continuum analysis, (b) Idealised structural model.

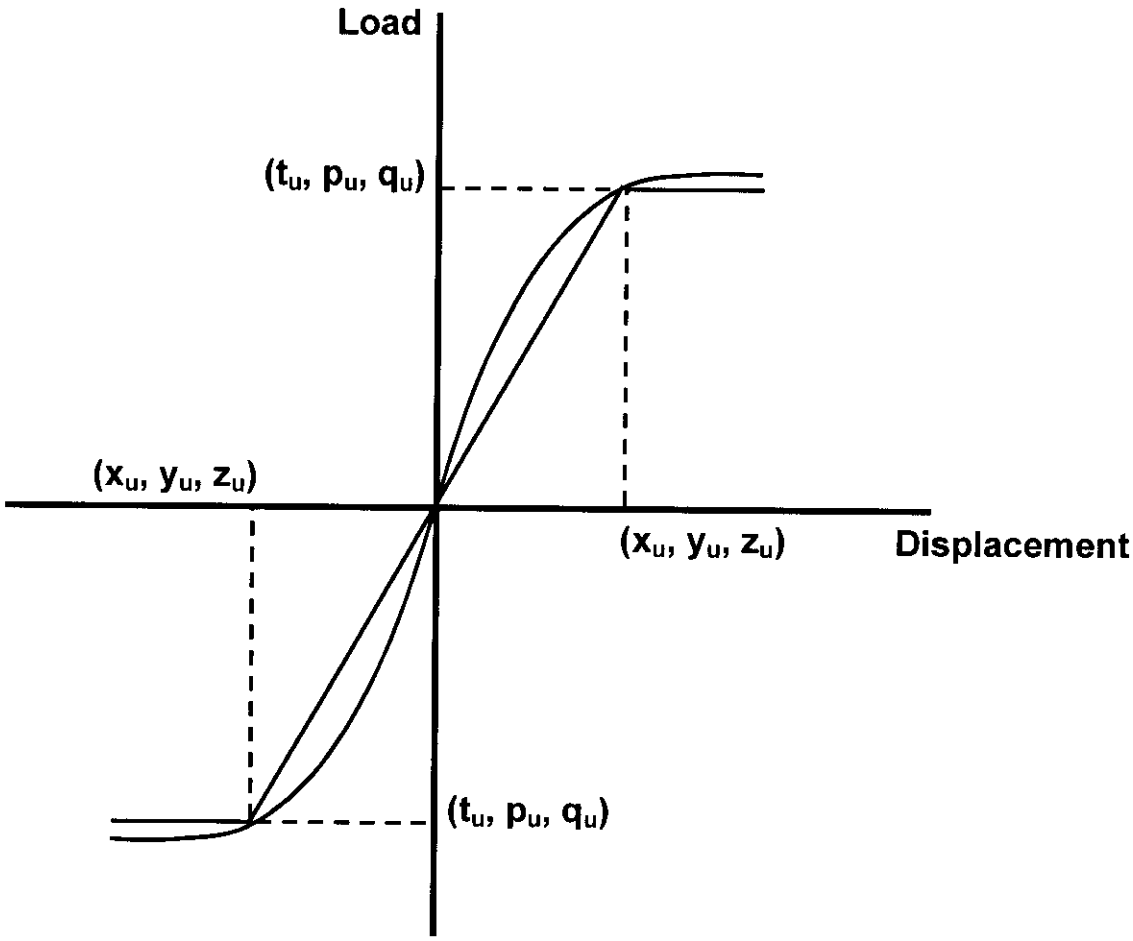

Figure 2.5-2. ASCE (1984) soil load-deformation relationships.

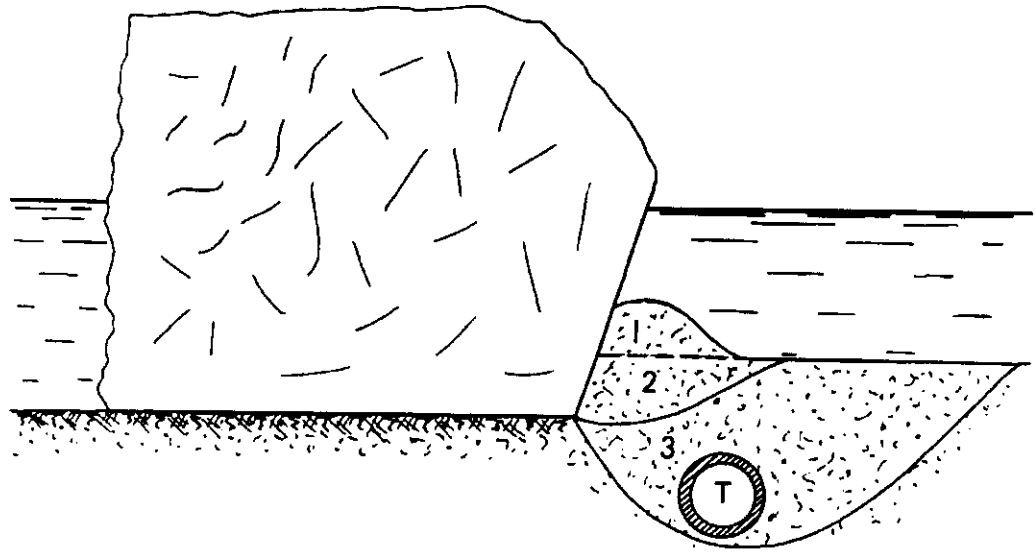

(a)

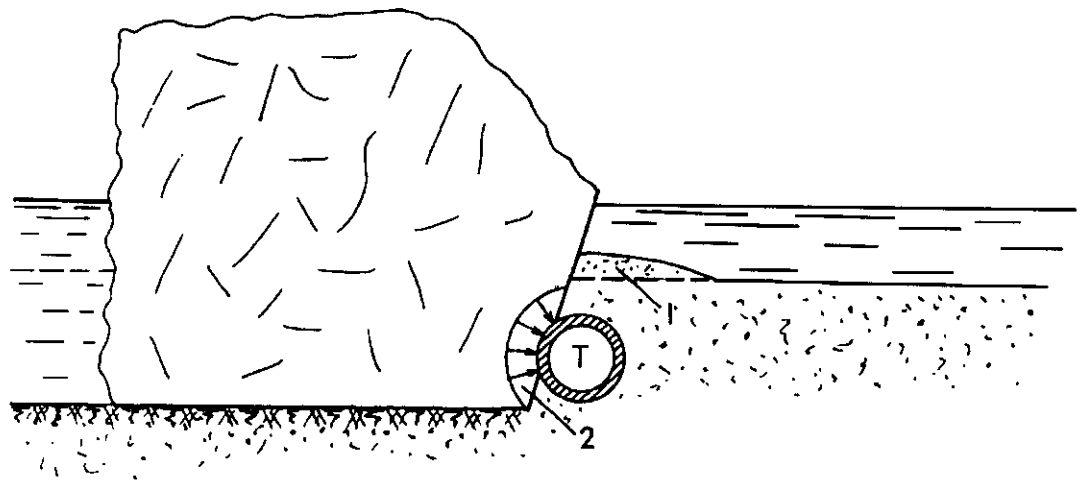

(b)

Figure 2.5-3. Schematic representation of ice-soil-pipeline interaction scenarios (a) indirect interaction of a drift ice feature with the pipeline, (b) direct impact against the pipeline.

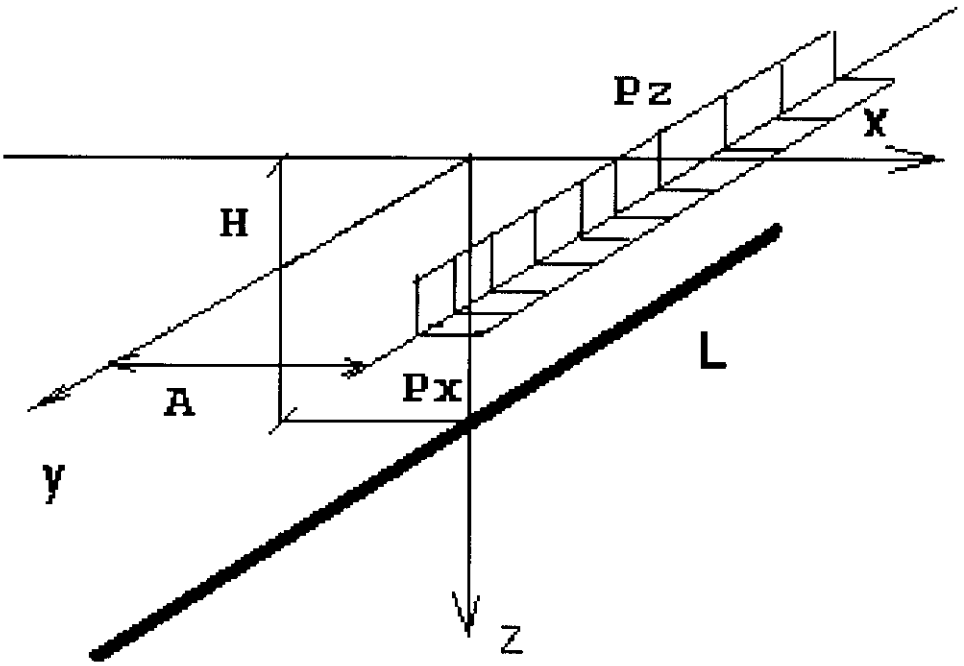

Figure 2.5-4. Schematic illustration of AARI approach of buried pipeline response to far-field soil deformation due to an ice gouge event.

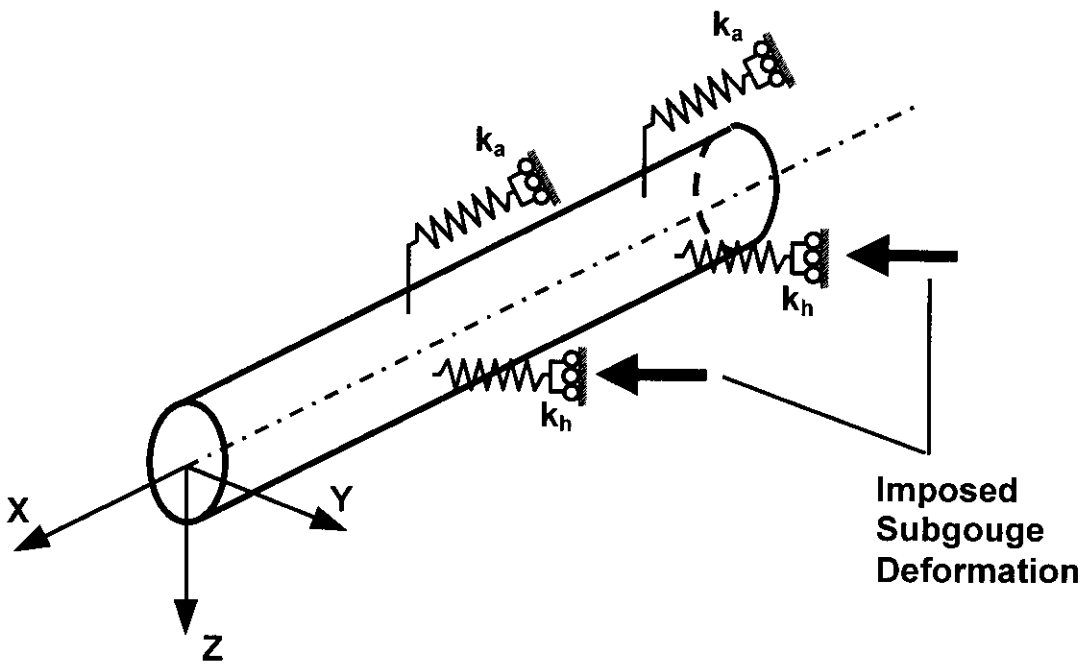

Figure 2.5-5. Representation of C-CORE soil/pipeline interaction model.

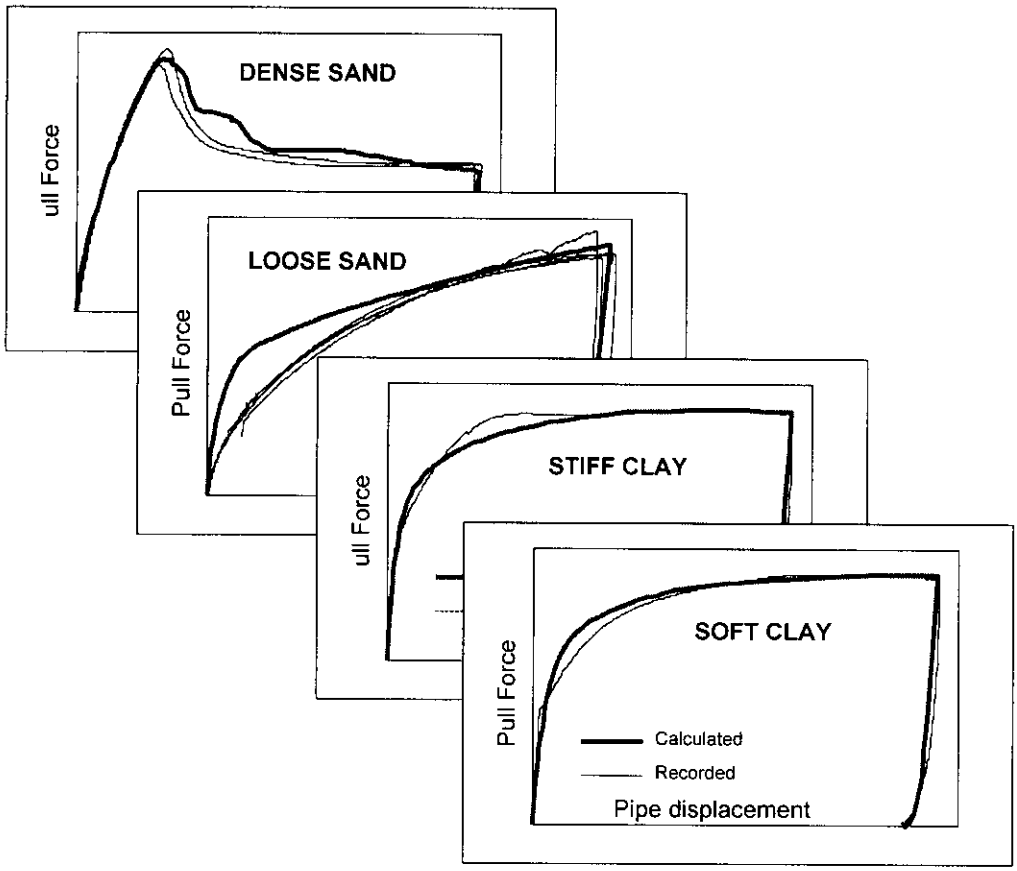

Figure 2.5-6. Comparison between results of full scale tests of lateral loading of a buried pipe (C-CORE 1998d) and predictions of 2D plane strain finite element analyses (Popescu 1999), in terms of force-displacement relations

3.0 Environmental and Physical Data

Ice gouge statistical analyses can be used as an independent tool to define pipeline risk where sufficient data exists. Design ice gouge models can be coupled with numerical ice/soil/pipeline interaction models for calibration or input parameters. Ice gouge statistics and supplementary environmental data for a number of geographic locations, including Grand Banks, Lake Erie, Sakhalin Island, and the Beaufort Sea, will be evaluated. The optimum method for determining the risk to marine pipelines is dependent on the available data and characteristics of the site.

3.1 General Framework for Assessing Pipeline Risk

3.1.1 Gouge Dimensions

When attempting to assess risk for a pipeline route in an ice environment, it is important to seek accurate physical data for that region. From the available data, it is necessary to obtain an estimate of the scour frequency and scour dimensions (width and depth) to conduct the risk assessment. Sometimes scour length is important for assessing risk, depending on how the scour data have been measured – along a linear track or over a given area.

3.1.2 Gouge Frequency

Scour density then may be defined as the number of scours per unit area or per unit length. For areal measurements of scour density, scour length then becomes an important piece of data. Typically, scour marks observed in a particular survey may vary considerably in age and the observed scour density does not in itself represent the rate at which scours occur.

To address risk issues, scour density has to be converted to annual frequency. Annual frequency can be expressed as the average number of new scours per year per unit area or as the number of new scours per year per unit length when considering survey lines or pipeline routes.

3.1.3 Age of Ice Gouges

Consider a particular area or line containing one scour mark 5 years old and two scour marks 10 years old. Assuming scour rate is constant over time, the average annual scour rate is the reciprocal of the average scour age, i.e. $(1 + 2) / (1 \times 5 \text{ yr} + 2 \times 10 \text{ yr}) = 3/(25 \text{ yr}) = 0.12 \text{ /yr}$.

Mathematically, scour frequency can be expressed

$$\eta = 1/T \tag{3.1}$$

where T is the average age of all scours marks present within the unit area or length. The actual age of individual features can be used if known and estimated if unknown. When many scours are considered, average age groups of scours can be made based on their physical appearance (e.g. infilling, berm characteristics). Maximum and minimum ages can be specified to obtain bounds on scour frequency.

Depending on the region of interest and thus which data are available, determination of annual scour frequency should result from following one of the paths presented in the flowchart, Figure 3.1. Each step in the process of analysing physical and environmental data to determine scour frequency will be explained by example for the four regions outlined above.

If a region has had repetitive mapping surveys of scour marks on the seabed, this data alone can be utilized directly to determine the annual scour frequency and scour dimensions (section 3.2 – Beaufort Sea). Lacking such complete information, one would then try to estimate infill rates and/or assess physical characteristics from visual surveys to, infer the age of scours and hence the annual scour frequency and scour dimensions for the region (section 3.3 – Lake Erie). If such information is still unavailable, the estimate of scour frequency should be inferred from

regional bathymetry, ice keel (or iceberg) shape, and areal density in order to determine a probability of exceeding a given draft. Then along with ice drift information (direction and speeds), infer the annual scour frequency (section 3.4 – Sakhalin Island). Failing all of these methods for determining annual scour frequency from physical and environmental data, the assessment must be based on any available scour dimensions, met ocean, and ice drift data for the region along with a mathematical model for simulating ice scour (section 3.5 – Grand Banks). The scour model is described in section 3.5.3. While it is best to use long-term measurements of environmental and physical data for statistical reasons, it is important to remember that measurements of occurrences a very long time ago may not be applicable to the present-day situation. For instance, relict scour marks made during the last ice age often give scour depths considerably deeper than could be possible considering the present-day environment and for this reason should not be included in such analysis. However, the historical data deemed useful must be assumed representative of present-day conditions up to the length of a pipeline's life.

It is important to note that as we move down this approach, more uncertainty is introduced in the annual scour frequency estimate (ie. preferably, we would always want to use scour data from repetitive mapping surveys to get the most accurate estimate of annual scour frequency).

3.2 Beaufort Sea

3.1.1 Geographic Region

The Beaufort Sea (Figure 3.2) is located within the southern part of the Arctic Ocean (contained within the Mackenzie Trough). Its shoreline is bound by Canada (to the east) the United States (to the west). Bathymetric studies of the Beaufort Sea show that the continental shelf portion of the seabed is relatively flat and moderately shallow (0 to 100m). The seabed slopes gently from the shoreline to the edge of the shelf after which it drops sharply to depths of about 1000m. The

Mackenzie Trough interrupts the continuity of the Western portion of the shelf where it extends to depths of 500m and eastward to the slopes of the Canada Basin (Gilbert and Pedersen, 1987).

Bounded by the Arctic Ocean to the north, ice pressure ridges drift into this region with keels often having depths of up to 50m (Weeks et al, 1983).

3.1.2 Available Data

Due to the considerable offshore activity in the Beaufort Sea in the past three decades, a great deal of effort has been expended in conducting seafloor repetitive mapping surveys of the area. Such information has provided extensive data on scour width, length, depth, areal density, and orientation. By comparing surveys from consecutive years, age of scours could also be found with reasonable confidence. Weeks et al. (1983) who present findings from seven years of seabed survey data which were collected between 1972 and 1979 (excluding 1974). This data was collected in the American Beaufort and represents a total trackline length of approximately 1500km. Gilbert and Pedersen (1987) present a database which contains computer-derived scour parameters for more than 37 100 scours measured in the Canadian Beaufort Sea using echo-sounder data and side-scan sonar data. These data were collected between 1970 and 1983 and represent a total trackline length of about 5000km.

During the fall (freeze-up) or the spring (break-up) seasons, the motion of thin or fragmented ice features can encroach on shallow sloping areas (e.g. coastline and artificial islands). The horizontal motion, known as ice ride-up, has to overcome the associated frictional and plowing forces. Increasing or discontinuous slope gradients, grounded ice features or frictional limits cause the moving ice to fracture into blocks build vertical features, which is called ice pile-up. Ice pile-up events are typically occur 10m (33ft) inland from the sea, whereas ice ride-up can extend 50m (165ft) inland (Cammaert and Muggeridge, 1988). Pile-up heights of 3 to 6m (9.8ft to 19.7ft) were reported for the seaward side of Seal Island and Stump Island, located within the Northstar project area (COE, 1999). INTEC (1998b) predicted an ice pile-up height of 17m (56ft) for a 100-year event at Seal Island. For regions throughout the Beaufort Sea, the

mechanisms have the potential to alter shorelines and nearshore bathymetry, which in the longer term may pose a threat to nearshore facilities with increased erosion (DNR, 1998).

The ice gouge process can be defined as the interaction of an ice feature, that can be characterized by a significant keel profile (e.g. pressure ridges, icebergs), and the seabed due to environmental driving forces (e.g. wind, current, wave loads). A schematic illustration of an ice gouge event is shown in Figure 3.5. The dominant features include a linear track depression or furrow with a gouge depth (d) and gouge width (w) referenced to the initial seabed datum. For steady-state gouge processes, a dynamic equilibrium is developed where the "plowed" soil is balanced with the creation of a frontal mound and side berms (lateral embankment, h), which are associated with clearing mechanisms.

Typically, engineering design parameters for ice gouge events is determined through statistical analysis of an ice gouge database. The information is compiled from site or route specific investigation employing echo sounder, side scan sonar or sub-bottom profiler surveys. A typical dataset, defining the gouge depth as a function of water depth, for the Alaskan Beaufort Sea and the Northstar project area is illustrated in Figure 3.6. Extensive statistical analysis conducted by INTEC (1998b), consider the 100-year ice gouge event for the Northstar project area to be on the order of 1.1m (3.5ft).

One measure to address the significance and potential for ice gouging is through gouge intensity. The parameter defines the number of ice gouge events per unit area multiplied by the maximum gouge width and depth (COE, 1999). The frequency (i.e. number of gouge events) and severity (i.e. gouge depth, width magnitude) of an ice gouge event is dependent on a number of factors including topography, climate, environmental driving forces, bathymetry, soil characteristics as well as ice regime, conditions and strength. For example, in sheltered areas of the landfast ice zone, ice gouging predominantly occurs during the transition break-up period when ice features are mobile. In the seasonal zone, first-year and multi-year pressure ridges as well as significant ice features such as icebergs and ice islands can gouge the seabed at any time during the year.

These characteristics are illustrated in a gouge intensity map for the Northstar project area (Figure 3.7).

Assessment and interpretation of the ice gouge dataset requires sound engineering judgement and experience. A number of factors must be considered in order to filter out spurious records, to account for seabed erosion and infilling rates with time, to separate relict from recent events and to determine recurrence rates (i.e. number of times per year the gouge event will occur in a particular region).

3.1.3 Method of Analysis

Based on the data available for the Beaufort Sea region, and the framework outlined above, an analysis of annual ice scour frequency would involve an examination of repetitive mapping survey data. From this, statistical descriptions of scour width, depth, and length (where needed) would be derived and age of scours could be estimated based on the appearance of scour marks from year to year.

Using the scour dimensions and annual scour frequency, a risk assessment could be performed to provide the design scour depth for the return period desired.

3.3 Lake Erie

3.3.1 Geographic Location

Lake Erie is a large body of fresh water, approximately 420 km long and 90 km across at its widest point, with its axis angled in a southwest/northeast direction. The international border between Canada and the United States lies along this axis (see Figure 3.3). The lake is relatively shallow and flat with maximum depths reaching only 24m in much of its area; the exception is the eastern basin where depths to 64m are recorded.

Gas wells and their gathering systems occupy significant areas of the Ontario sector of Lake Erie. Talisman Energy (formerly Pembina Resources) has published a map set with accompanying tables identifying the location of these features.

The routing for the proposed millennium pipeline was chosen specifically so as not to exceed 30m water depth and to have the least impact on existing gas field facilities. The selected route centerline reaches its maximum depth of approximately 29m below IGLD reference level some 20km from the United States landfall. The proposed route will cross three existing and possibly one future Talisman gas gathering lines in Canadian waters.

The lake floor along the pipeline route is generally smooth, with local relief rarely exceeding 2m above the surrounding elevations. Lake-floor slopes are generally less than 1% grade. Where significant features were encountered on the centerline of the survey route, whether natural or man made (e.g. shipwrecks, other archeological monuments, or debris), the route was modified to minimize the effects of these features.

3.3.2 Available Data

Geotechnical conditions of the lake were provided along the proposed pipeline route as measured in 1997 by Racal-Pelagos and two 1998 surveys Canadian Seabed Research and Trow International. These geotechnical surveys also provided ice scour measurements along the proposed pipeline route as well as an estimate of infill rates from sedimentation and erosion studies along the proposed pipeline route.

Considerable amounts of ice environment data were available for the Lake Erie region. Ice charts providing surface concentrations were available in various formats for more than a 20 year period, and aerial photography of the entire lake could be utilized to estimate ridge density. As

well, various publications giving anecdotal information about lake ice conditions were available in reference to the proposed Ontario Hydro cable crossing project.
Comprehensive environmental data were also available describing wind, and air temperatures of the Lake Erie region. These data were analysed to give the dominant wind directions and speed distributions to understand the major ice feature driving forces in the lake, the directions in which these forces should act, as well as the ice-forming environmental conditions.

3.4.3 Method of Analysis

Based on the data available for Lake Erie, and the framework outlined above, an analysis of annual ice scour frequency would involve an examination of scour measurements in relation to infill rates in order to estimate the age of scours identified.

Using the scour dimensions and estimated annual scour frequency, a risk assessment could be performed to provide the design scour depth for the return period desired.

3.4 Sakhalin Island

3.4.1 Geographic Location

Sakhalin Island is located in the Sea of Okhotsk off the eastern coast of Russia (Figure 3.4). Separated from the continent by a narrow 6km strait, the island is approximately 750 km long (north-south direction) but only 200km wide at its widest point (east-west direction). Offshore developments are occurring on the eastern side of the island, where local bathymetry shows a gradual increase in water depth from the shoreline to about 30m at a distance of 6 to 10km.

The seabed is predominantly well-sorted fine sand at the offshore installations, while coarser tills may be present at selected locations where significant current speeds occur. Due to tidal currents and ocean waves, there is considerable material transport in the nearshore zone which is expected out to 10m water depth.

Predominant ice features in this region are pressure ridges formed from first-year sea ice. These features tend to drift to the eastern coastal area and form tight ice packs during the winter season. Grounded ice features (stamukha) often refloat, drift with the ice pack, and are subsequently driven into the seabed. Keels of floating stamukha seldom reach a maximum depth of more than 20m.

3.4.2 Available Data

Field studies were carried-out on pack ice floes off the coast of Sakhalin Island during 1995, 1997, and 1998 by Vaudrey and Associates, Kvaerner Masa Yards, and the Arctic and Antarctic Research Institute respectively. These studies detailed the dimensions of primarily large, grounded ice features (stamukhas) and gave information about the upper bound of ice features which might be expected in this region. ASL Environmental Sciences Ltd in 1997 conducted a study of floating ice feature keels using upward looking sonar instruments positionednear the seabed at different sites. This data provided detailed information about ice keel shapes, ice drift speeds and directions. Also, ice floe sizes were available from a number of sources, and ice surface concentration data from standard ice charts made available by the National Ice Center for 1996-1998.

Environmental conditions were also available from the National Climatic Data Center which included long-term measurements of air temperatures which could help in determining the validity of recent ice condition measurements with weather conditions.

3.4.3 Method of analysis

Based on the data available for the Sakhalin Island region, and the framework outlined above, an analysis of ice scour frequency would involve an examination of ice keel and drift data in

conjunction with bathymetric data to estimate the number of contacts with the seabed. From this, annual scour frequency can be inferred.

Using annual scour frequency and limited information on scour dimensions, a risk assessment could be performed to provide the design scour depth for the return period desired.

3.5 Grand Banks

3.5.1 Geographic Location

The Grand Banks are one of the world's largest and richest natural resource areas, renowned for the commercial fishery and hydrocarbon potential. Illustrated in Figure 3.5, the Grand Banks is situated off the East Coast of Canada and on the Southeast coast of the province of Newfoundland and Labrador. The Grand Banks are a series of raised submarine plateaus on the edge of the North American continental shelf.

3.5.2 Available Data

A summary of the oceanographic and meteorological design criteria for the Terra Nova offshore development field, which is representative of the northeast Grand Banks, is summarised in Table 3.1-1 (Terra Nova, 1996). The site location (46°N 48°W) is situated in approximately 90m of water relative to the mean sea level (MSL). The Grand Banks water depth ranges from 36.5m to 185m. Seaconsult (1988) presents detailed information on environmental and physical data.

Geotechnical

The geotechnical properties for near surface strata (0-30m) on the northeast Grand Banks can be characterised as (C-CORE, 1997b)

Soil Type	*"Strength"*	*Soil Unit Weight*
Granular	$\phi = 40° \pm 2°$	$\gamma = 20.5 kN/m^3 \pm 0.5\ kN/m^3$
Cohesive	$C_u = 90kPa \pm 50kPa$	$\gamma = 17.0 kN/m^3 \pm 1.0\ kN/m^3$

The granular soil could be classified as fine to medium sand and between poorly and well graded material.

Ice Feature and Ice Gouge Characteristics

Iceberg waterline length is the main dimension for which there are reliable distributions on the Grand Banks. Several studies were conducted in the early 1980's, primarily for Mobil Oil, and include Hodgson et al. (1988), ICE Engineering Ltd. (1984,1985), Mobil Hibernia Development Studies (1982,1983,1984), Dobrocky (1984), and NORDCO (1980). The length and mass of individual icebergs were measured from stereo aerial photographs (mass being proportional to above water volume), and draft was measured using sonar profiling techniques.

Relationships between iceberg waterline length (L), width (W), draft (D) and height (H) have been established through examination of the available data sources (McKenna et al., 1999). The data were correlated using a principal component analysis and the mean ratios are $L/D = 1.38$, $W/D = 1.06$ and $H/D = 0.35$. Four characteristic iceberg shapes were defined based on digitised profiles. The shapes are listed in Table 3.1-2, with an estimate of the relative probability of occurrence, and are illustrated in Figure 3.6

The mean iceberg drift speed (0.28m/s) was evaluated primarily from Seaconsult (1988) with data derived from International Ice Patrol (IIP) iceberg sightings (PERD Iceberg Database, 1998) also considered. Parameters defining the iceberg feature and ice gouge characteristics are summarised in Table 3.1-3.

The values for iceberg areal density for the Terra Nova and Whiterose sites were determined from the most recent database of iceberg counts available (Jordaan et al, 1999). The iceberg

database covers 1960 to 1998 International Ice Patrol (IIP) iceberg counts. Iceberg numbers for each degree square were taken from IIP ice maps, which were issued approximately twice a month during the iceberg season. The areal densities given in the database reflect an annual average number of icebergs in each degree square covered. In Table 4.1, the areal density for Terra Nova was chosen to be the same as for the 46°N 48°W degree square since the Terra Nova site is approximately in the centre of the degree square. The areal density for Whiterose was determined based on the average areal density of the adjacent degree squares.

3.5.3 Method of Analysis

Based on the framework outlined in section 3.1 and the available data for the Grand Banks region (section 3.5.2), the method of estimating scour frequency is based on the incorporation of known environmental, bathymetric, and ice drift data into a Monte Carlo upslope ice scour model. The model is described in the following sections.

3.5.3.1 Iceberg Scour Model

The present Monte Carlo upslope iceberg scour model was built directly on the work of McKenna et al (1999). McKenna et al (1999) presented a Monte Carlo model in which iceberg scour depth distribution was estimated based on a balance between scour forces and environmental driving forces. Iceberg geometry and hydrostatic stability were also carefully characterized in this effort. The model assumed the seabed to be level and the ratio of vertical to horizontal scour forces equal to 1.25. This section will outline the additions to the model by McKenna et al. (1999) and will present the results obtained.

Scour Force model

Under the PRISE program, C-CORE developed a new model for computing horizontal and vertical scour soil forces (Walter and Phillips, 1998). The model is briefly described in section

X.X of this report. This soil force model was utilized in the present iceberg scour model and makes the following assumptions:

- Sandy and clay soils were evenly distributed (50% of icebergs generated scoured in sandy soil and 50% in clay).
- Scour width was sampled from a normal distribution with a mean of 25m and a standard deviation of 14m.
- Iceberg angle of attack was chosen as 15°.
- Undrained shear strength, Cu for the clay model was sampled from a gamma distribution with a mean of 105kPa and a standard deviation of 42kPa.
- Internal angle of friction, ϕ was sampled from a normal distribution with a mean of 40° and a standard deviation of 2°.
- Effective unit weight, γ_p was sampled from a normal distribution with a mean of 10.7kN/m^3 and a standard deviation of 0.5 kN/m^3.

Seabed Slope

To make reasonable comparisons with field data, it was deemed necessary to modify the McKenna et al (1999) model to also include seabed slope. By making this modification, it was possible to produce a distribution of scour lengths.

A distribution of seabed slopes (see Figure 3.7) was determined from bathymetric data for the Grand Banks region bounded by 48°W, 46°N to 49°W, 48°N (see Figure 3.8). This distribution appears to be exponential with a mean of 1.83m rise per 1000m run (1.83×10^{-3} m/m slope) and a standard deviation of 1.54m rise per 1000m run (1.54×10^{-3} m/m slope).

Solution to the scour problem was made in two steps; a free drift solution, and a solution for upslope scour. The second step (upslope scouring) was comprised of two sub-steps which were iterated to find the final solution - iceberg pitch and heave due to scour and the solution for

iceberg drift speed and direction under the action of environmental forces and resisting force from scour with a sloped seabed.

The first step, (free drift solution) was calculated according to McKenna et al (1999). Free drift occurred before icebergs made contact with the seabed and was based on a balance of the environmental driving forces (north-south and also east-west directions). Iceberg velocity and drift angle were varied to balance the forces through a nonlinear minimization scheme, and the resulting values were used to start the upslope scouring iteration routine.

When a free drift solution was found, the water depth for the sloping seabed was set equal to the iceberg draft (Figure 3.9) and the second step began (upslope scouring). With the first iteration of the upslope scouring routine, the iceberg was assumed to have moved a distance Δx in the horizontal plane. Hence, scouring began with the first iteration in this routine. The difference of the iceberg draft and water depth at this point provided an initial estimate of the scour depth and therefore the scour forces acting on the iceberg keel. Using the McKenna et al (1999) solution for equilibrium heave and pitch, an estimate of scour depth was made by adjusting the heave and pitch of the iceberg, which in turn reduced the scour depth and associated scour forces. The final solution for iceberg heave and pitch was reached when the hydrostatic forces were in balance with the scour forces.

At this point, the energy equation

$$KE_1 = KE_2 + \Delta PE_{h(1\text{-}2)} + \Delta PE_{p(1\text{-}2)} + E_{s(1\text{-}2)} - E_{e(1\text{-}2)} \qquad (3.2)$$

Where:

$KE_i = \frac{1}{2} MV_i^2$ = iceberg kinetic energy at the i^{th} iteration
$\Delta PE_{h(1\text{-}2)}$ = change in heave potential energy from previous to current iteration
$\Delta PE_{p(1\text{-}2)}$ = change in pitch potential energy from previous to current iteration

$|E_s|_{(1-2)} = \frac{1}{2}(F_{sh1} + F_{sh2})\cdot\Delta x$ = energy lost in scouring between the previous and current iterations

$|E_e|_{(1-2)} = \frac{1}{2}(F_{e1} + F_{e2})\cdot\Delta x$ = energy added from environmental forces between previous and current iteration

M = iceberg mass

V_i = iceberg velocity

$(F_{sh})_i$ = Horizontal scour force at the i^{th} iteration

$(Fe)_i$ = Environmental driving force at the i^{th} iteration

was minimized through a nonlinear minimization routine to find the iceberg velocity and drift angle for the current iteration. If the velocity was positive, and less than the previous iteration, the iceberg was moved the horizontal distance Δx and the next iteration was computed in the same fashion. Otherwise, the iceberg was assumed to have depleted its total kinetic energy and simulation of the next iceberg began.

Model Assumptions

Assumptions made in constructing the upslope scour model included:

- Scouring was always assumed to occur perpendicular upslope. Making this assumption implies that the iceberg always encounters the same slope, regardless of the heading angle change. Since the seabed slopes encountered were quite small, this assumption is justified.

- Iceberg length, width, draft, and height data from the eastern region of the Grand Banks (REF?) was used to conduct a principle component analysis of iceberg dimensions. Residuals of the analysis were plotted and shown to be close to normally distributed. Based on this, it has been assumed that iceberg dimensions are not correlated. Another check was performed to this end. The data was transformed to the log-log scale and a linear regression line fit. To remove the bias introduced in this type of fit, a smearing estimate was computed and included in the fit before the data were transformed back to the linear scale. The scatter about the log-log fit was then computed as numbers randomly sampled from a normal distribution and multiplied by the standard deviation of the residuals of the estimate. Plotting

the original data for width, draft, and height as a function of iceberg length on the same axes as the estimate using principle component analysis and smeared log-log regression shows the results to agree well (Figures 3.10 - 3.12). Based on this analysis, principle component analysis method has been assumed a reasonable method for generating the iceberg principle dimensions.

Results

<To be completed when model is run with seabed slope distribution and LWDH data>

Table 3.1-1. Summary of oceanographic and meterological design criteria for the Grand Banks.

Parameter		Return Period (Years)		
		1	10	100
Wind	1h mean wind speed at 10m above MSL	29m/s	32m/s	34m/s
	3s gust wind speed at 10m above MSL	39m/s	43m/s	46m/s
Tide	Maximum tidal range	1.04m	1.04m	1.04m
	Storm surge level above MSL	0.50m	0.61m	0.73m
	Storm surge depression below MSL	0.54m	0.66m	0.79m
Tsunami	Tsnuami level above MSL	0.00m	0.10m	1.20m
	Tsunami current	0.00m/s	0.00m/s	0.35m/s
Wave	Significant wave height	10.9m	13.2m	15.4m
	Peak period	14.1s	15.5s	16.7s
	Maximum individual wave height	20.7m	25.1m	29.3m
	Period of maximum wave	12.5s	13.5s	14.7s
Current	Maximum current speed 20m below surface	0.85m/s	0.89m/s	1.06m/s
	Direction (to) of near-surface current	W	W	W
	Maximum current speed 45m below surface	0.86m/s	0.97m/s	1.09m/s
	Direction (to) of mid-depth current	SW	SW	SW
	Maximum current speed 70m below surface	0.70m/s	0.83m/s	0.96m/s
	Direction (to) of near-bottom current	SE	SE	SE

Table 3.1-2. Characteristic iceberg shapes for the Grand Banks.

Shape	Description	Relative Probability	Reference Volume	Critical *W/D* for Stability
1	sculpted	0.18	1.01	1.0
2	tapered	0.30	0.62	0.8
3	ellipsoidal	0.29	0.97	1.1
4	tabular	0.23	0.89	1.0

Table 3.1-3. Characteristic iceberg and iceberg gouge parameters for the Grand Banks.

	Parameter	Magnitude	Reference
	Mean drift speed	0.28m/s	Seaconsult (1988)
	Area density	0.60/°/°	

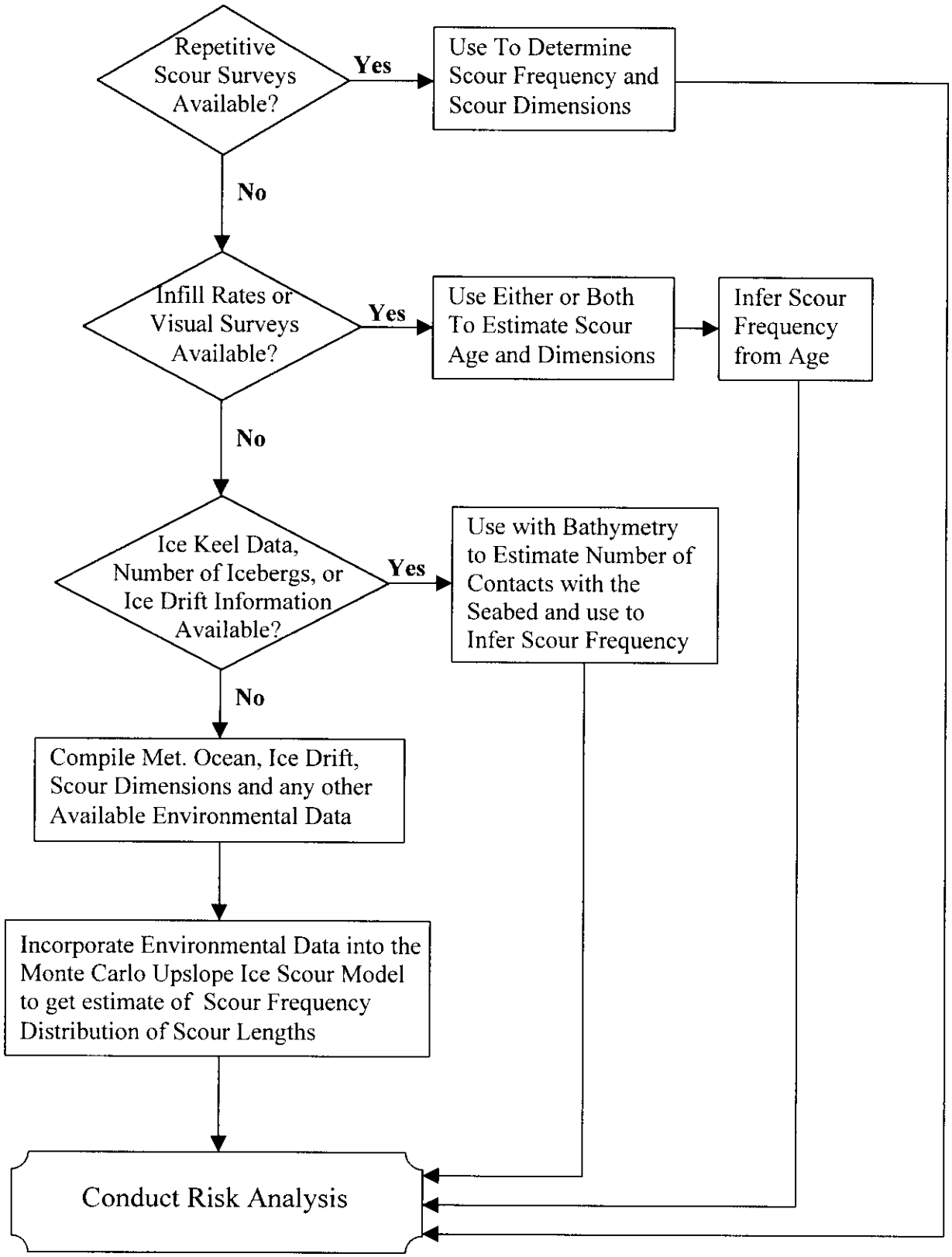

Figure 3.1 Flowchart outline of framework for analysis of ice risk based on available data.

(a)

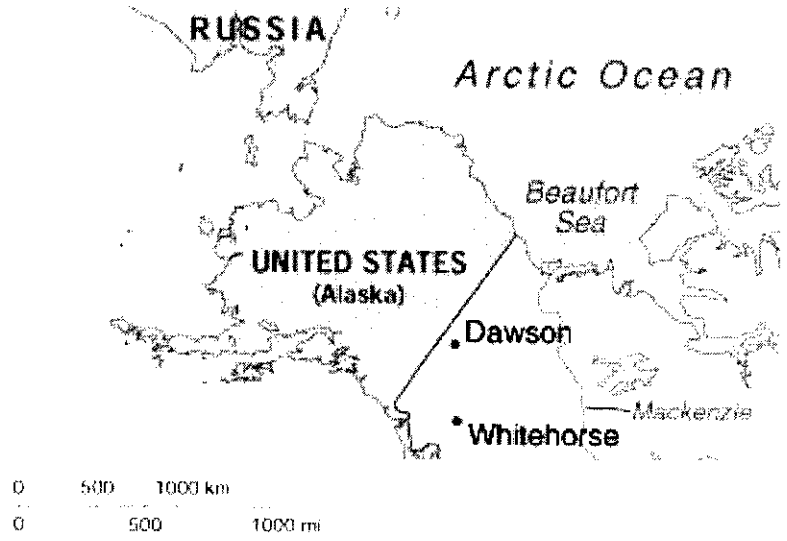

(b)

Figure 3.2 Geographic location of Beaufort Sea (a) world map, (b) local map.

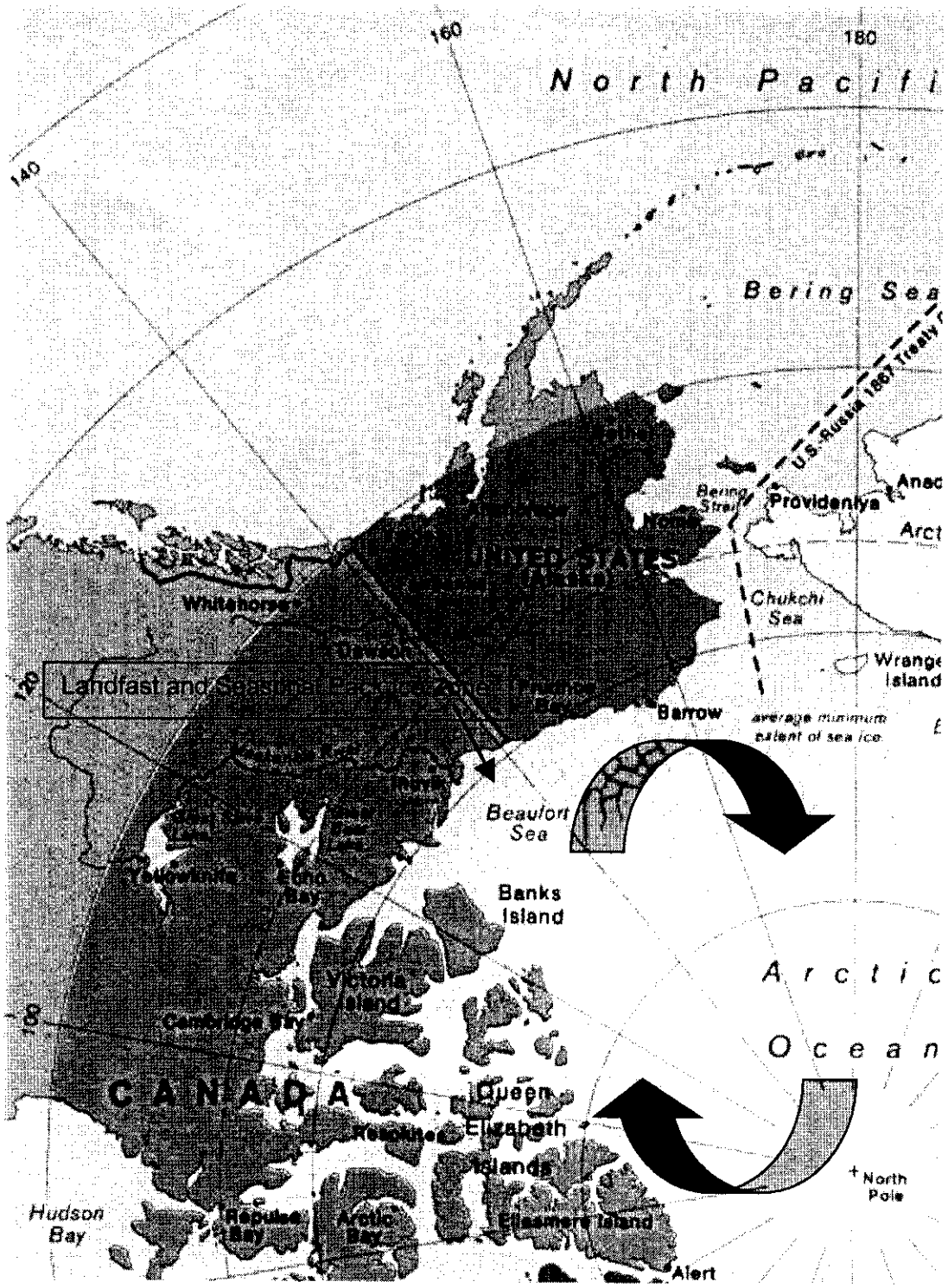

Figure 3.3. Average Minimum Extent of the Polar Pack and Major Drift Pattern for the Beaufort Sea Gyre.

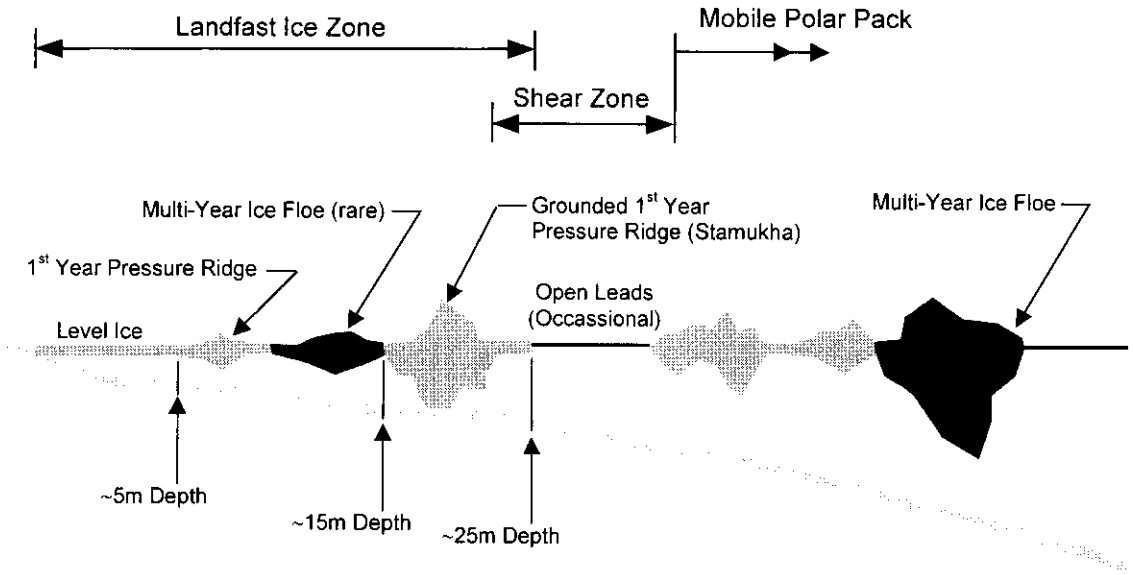

Figure 3.4. Typical Profile of Ice Zones and Conditions in the Alaskan Beaufort Sea.

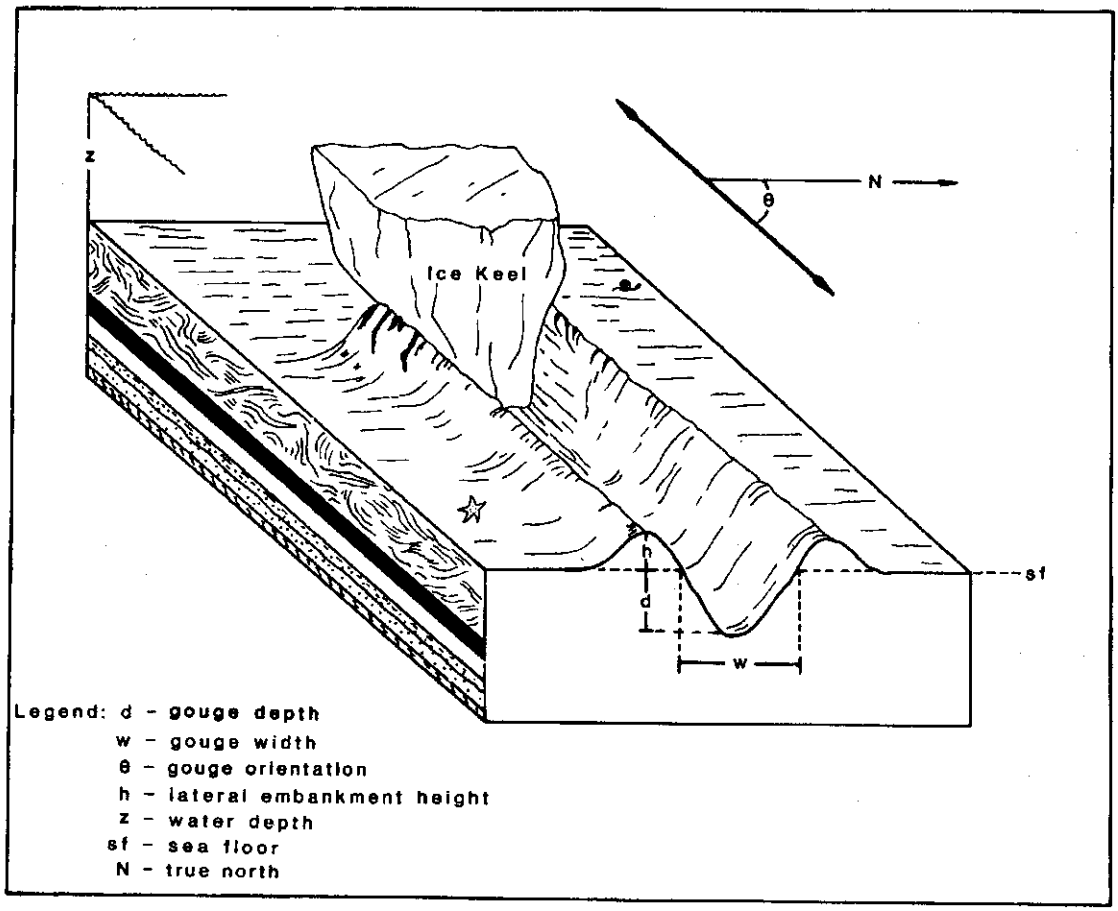

Figure 3.5. Schematic Illustration of an Ice Gouge Event (Weeks et al., 1983).

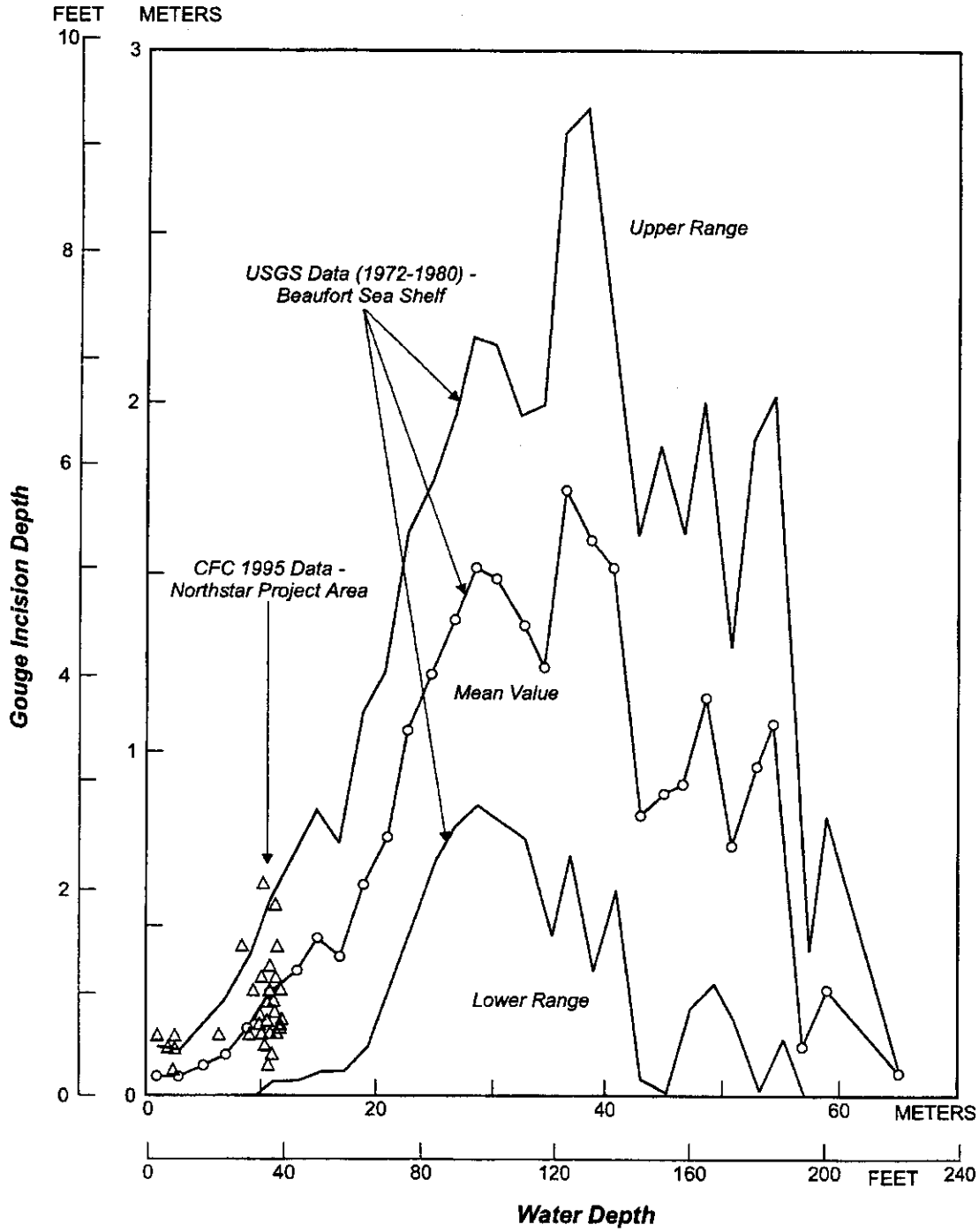

Figure 3.6. Gouge Depth Survey Measurements as a Function of Water Depth (COE, 1999).

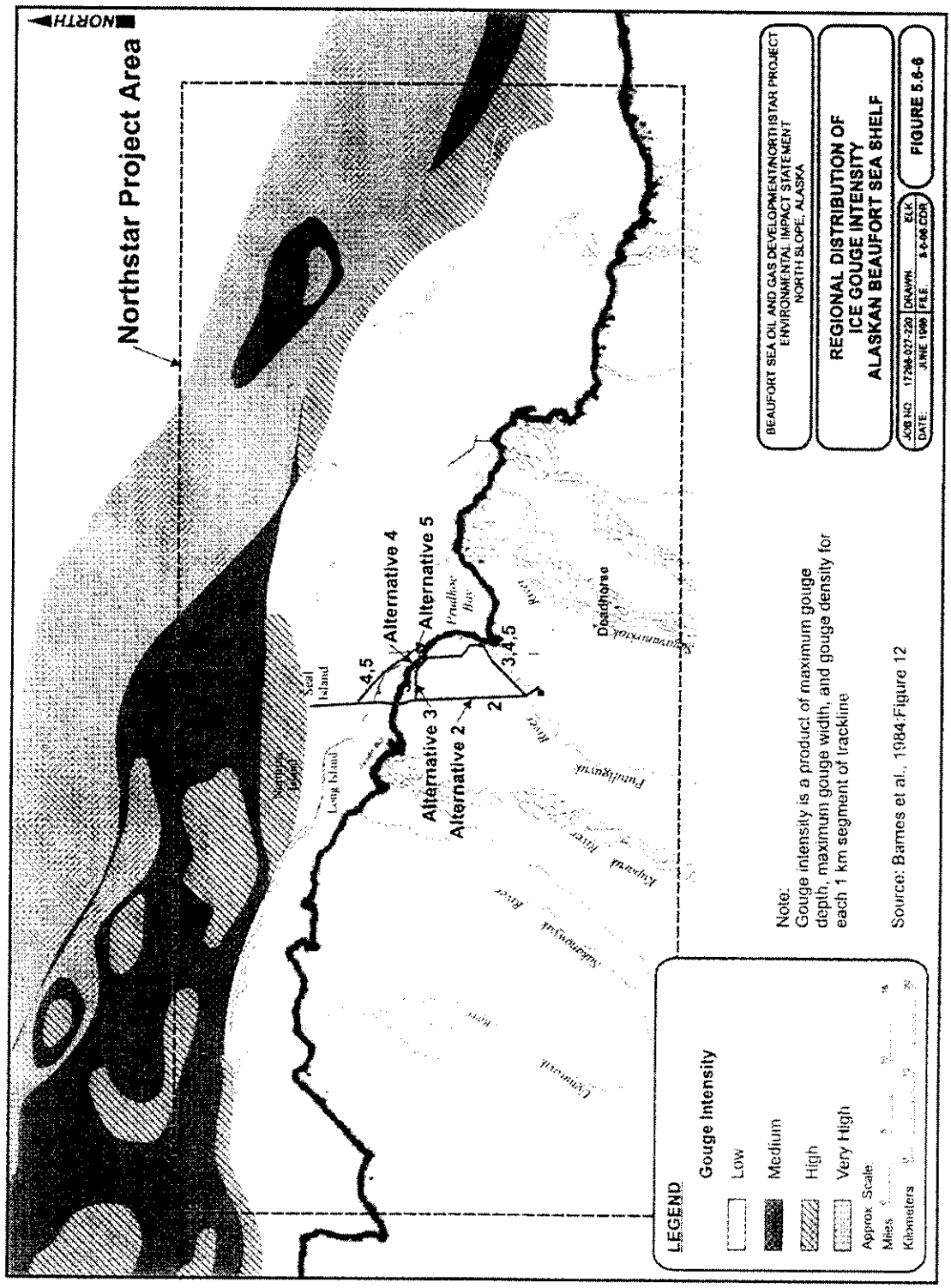

Figure 3.7. Regional Distribution of Ice Gouge Intensity for the Alaskan Beaufort Sea within the Northstar Study Area (COE, 1999).

(a)

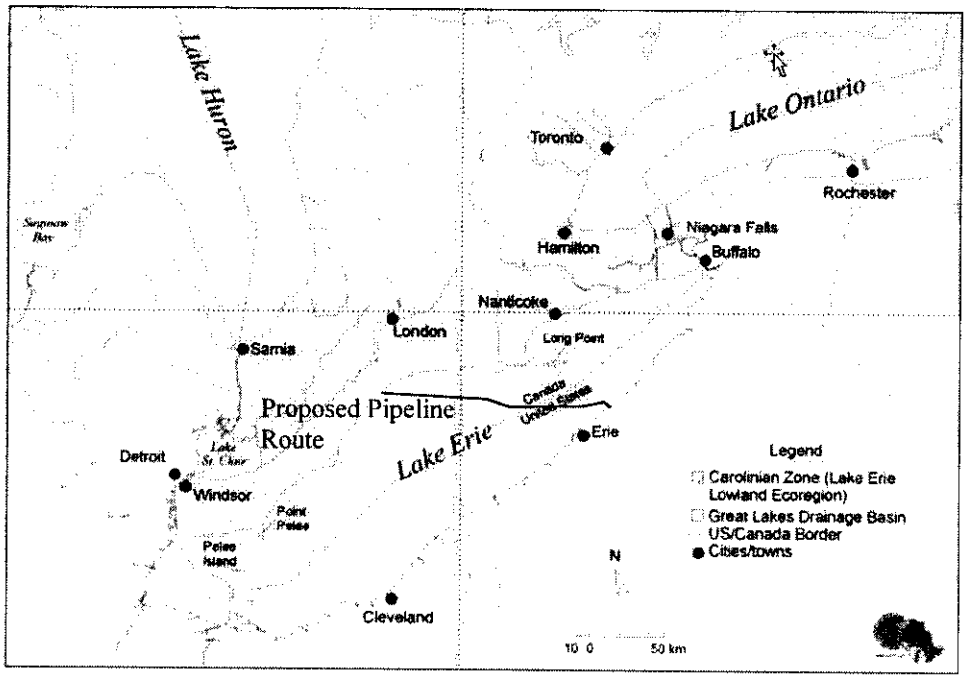

(b)

Figure 3.8 Geographic location of Lake Erie (a) world map, (b) local map.

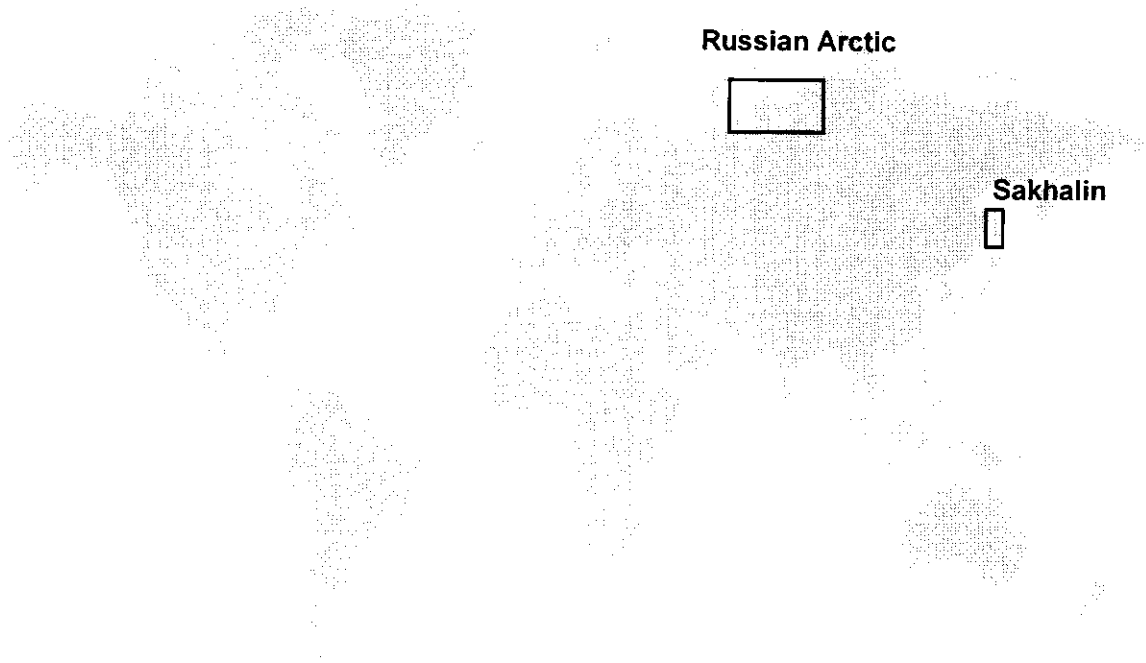

(a)

(b)

Figure 3.9 Geographic location of Russian Arctic and Sakhalin (a) world map, (b) local map.

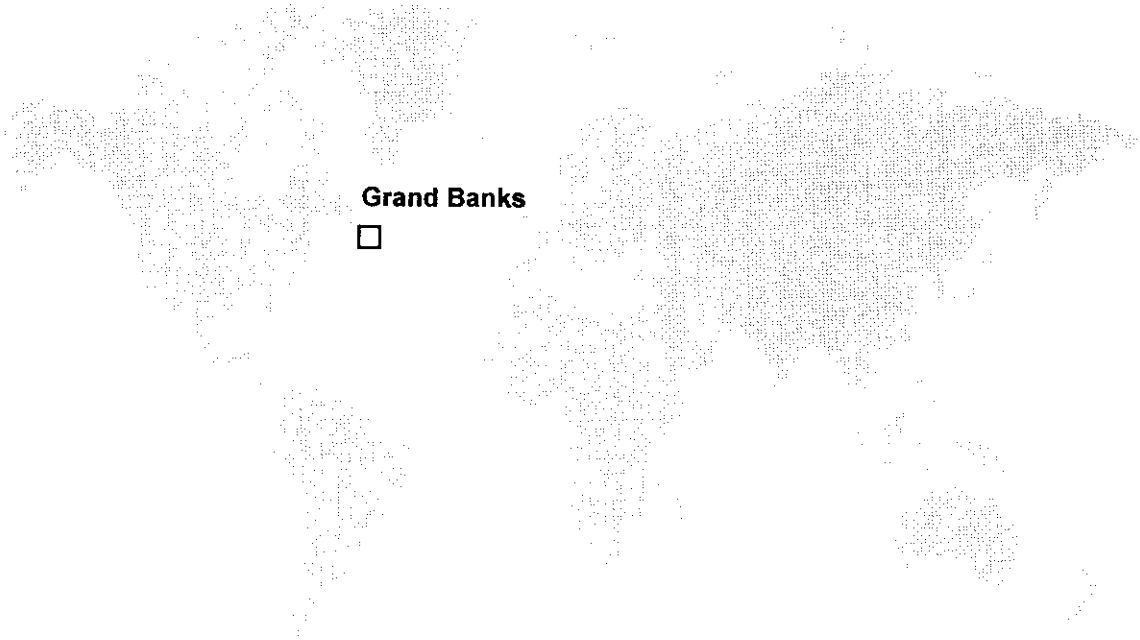

(a)

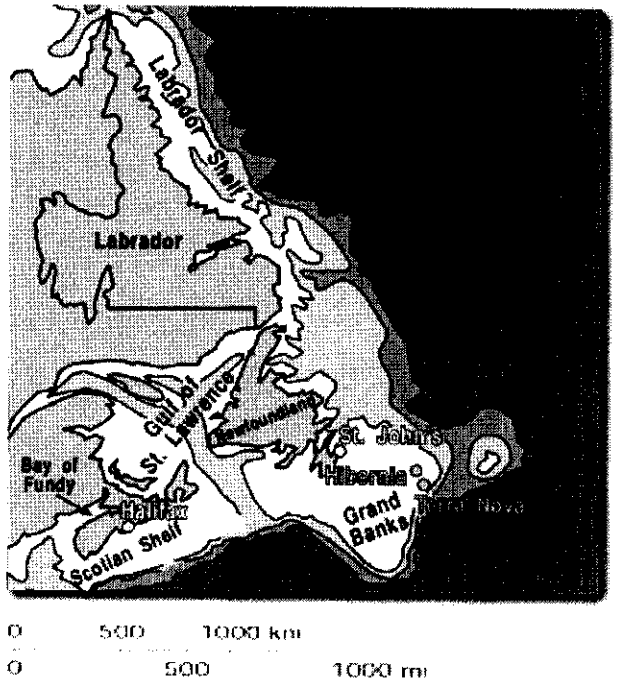

(b)

Figure 3.10 Geographic location of Grand Banks (a) world map, (b) local map.

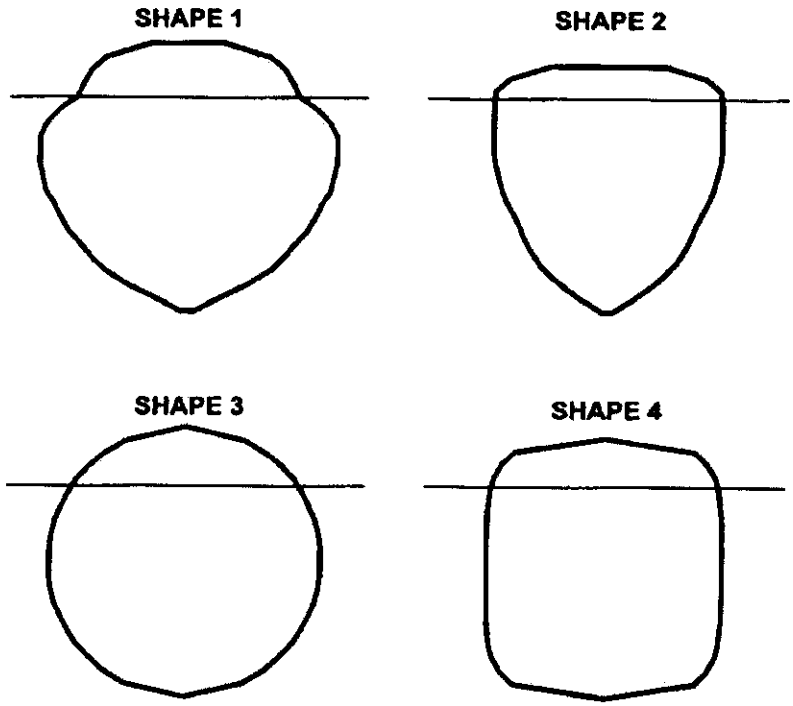

Figure 3.11 Normalised characteristic iceberg shapes for the Grand Banks.

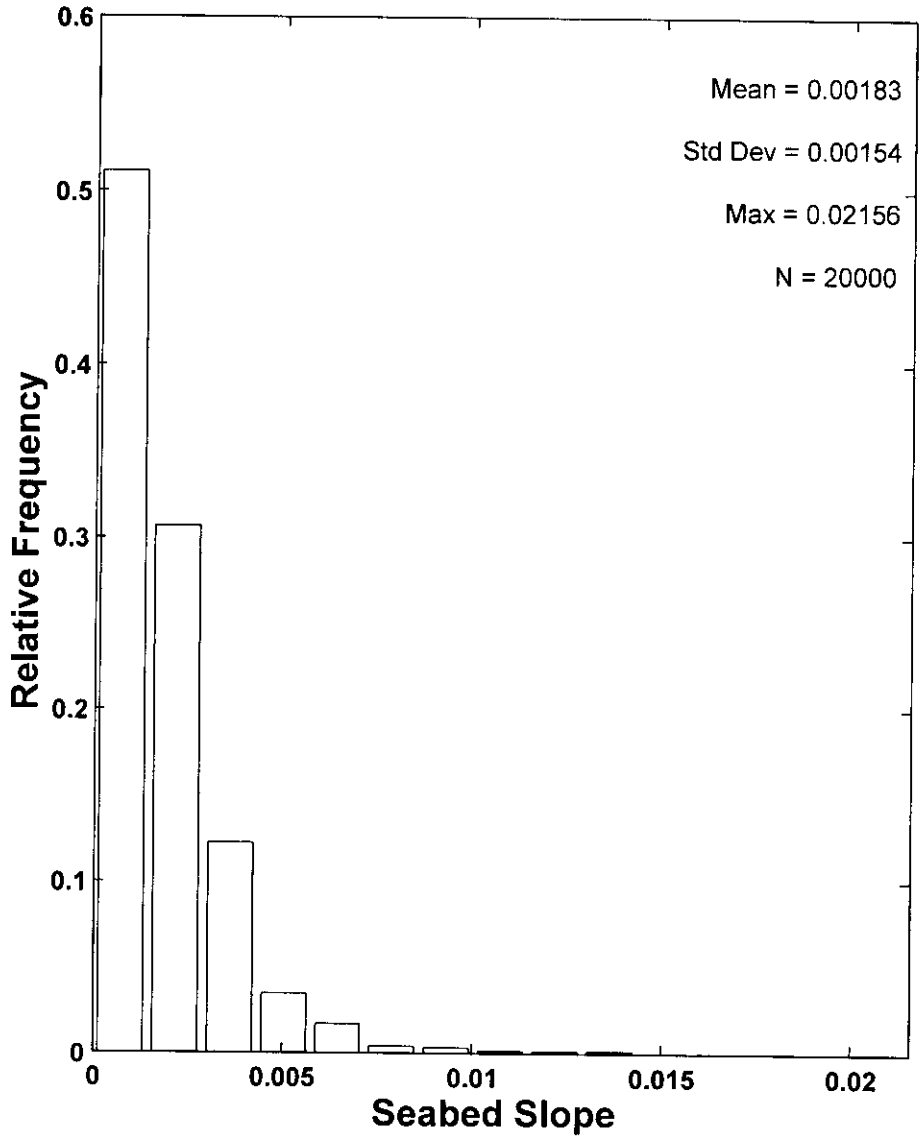

Figure 3.12 Distribution of seabed slopes on the Grand Banks.

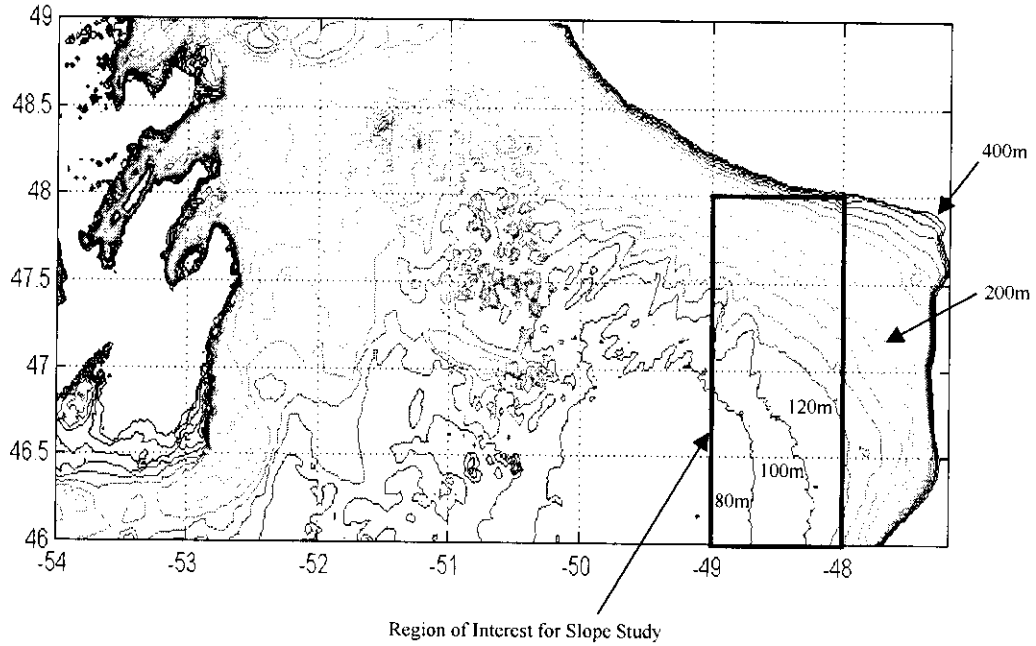

Figure 3.13 Region of Grand Banks used for seabed slope study.

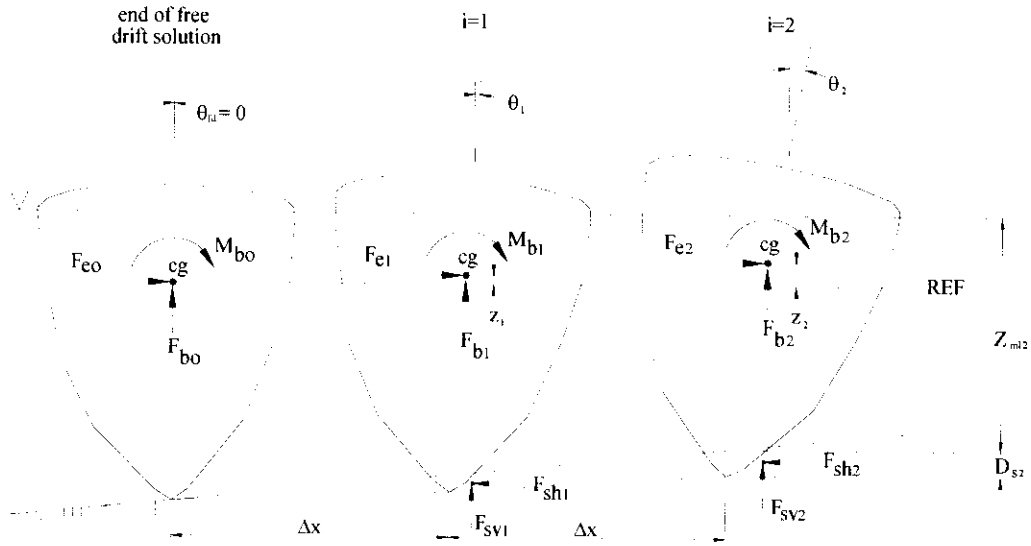

Figure 3.14 Schematic of upslope scour model variables.

4 ICE GOUGE RISK FRAMEWORK

4.1 Overview

4.1.1 Basis

For a marine pipeline subjected to ice gouge events, concerns include:

- minor damage to the pipeline without loss of containment; and
- major damage resulting in loss of containment.

The first concern may be seen as a serviceability issue, while the latter represents an ultimate failure issue. Although other factors such as corrosion or seabed mobility may lead to pipeline failure, focus in this chapter is exclusively on the ice gouge process.

4.1.2 Objectives and Constraints

A primary objective when designing a marine pipeline against ice gouges is to minimize the life cycle cost. For rare events such as ice gouges, the life cycle cost is determined for the most part by the development cost. Assuming trenching or burial to be the primary means of reducing the risk of ice damage, the main objective can be satisfied by minimizing pipeline burial depth.

The fundamental constraint is the satisfaction of target safety levels. Typically, target safety levels are defined on the basis of acceptable risk criteria such as the maximum failure probability level for a governing limit state. Additional constraints that can be considered include maximum burial depths based on trenching technology limitations or cost, as well as minimum burial depths based on upheaval buckling, trawl loads or accidental loads. Some of these issues are illustrated in Figure 4.1.

4.1.3 Approach

Typically, the design of onshore and offshore pipeline systems has been based on working stress or allowable stress design criteria; for example ASME B31.8 (1995) for gas and ASME B31.4 (1994) for liquid pipeline transportation systems. Stress based design defines the allowable stress as a fraction of the specified minimum yield stress (SMYS) in terms of design factors. The 'safety' factor accounts for variation in material properties, applied loads, structural defects and

model uncertainty. For particular design scenarios, the allowable stress criteria may be overly conservative or uneconomical. For example, the maximum allowable hoop stress check for high pressure pipelines with low diameter to wall thickness ratios (D/t) or deformation based mechanisms such as ice gouge events, respectively. In addition, the importance of limiting strain criteria has gained wider acceptance and interest (Dinovitzer et al., 1999; Walker and Williams, 1995; Zimmerman et al., 1995)

Consequently, the development of standards and practice based on a limit states design philosophy has gained increasing recognition; for example API RP 1111 (1999), CSA Z662 (1999) and DNV (1996). Although a complete treatment has not necessarily been developed for all limit states, for example provisions are made in several design rules to allow for the option of buckling design based on allowable stress methods. Recently, the engineering assessment conducted for the Northstar development project has incorporated limit state strain criteria as part of the pipeline design basis (INTEC, 1998).

Limit states is a reliability based design methodology that specifies the factored resistance to be greater than the factored loads with incorporation of a limited plastic response. To illustrate the difference between allowable stress and limit states design, the respective stress-strain regimes for typical pipeline response is schematically illustrated in Figure 4-2. The Ramberg-Osgood formulation is generally adopted to define the stress-strain pipeline response. The three zones can be defined as

A Allowable stress - maximum level for conventional analysis with typical design factors ranging from 0.72-0.90
B Limit states - typical upper limit for loads governed by stress based mechanisms (e.g. wave, current)
C Limit states - typical upper limit for loads governed by strain based mechanisms (e.g. frost heave, ice gouge)

There are two main limit states categories: (i) ultimate limit states and (ii) serviceability limit states. The limit states design methodology is outlined in Figure 4-3.

4.2 Target Safety Levels

4.2.1 Overall Target Safety Levels

In general, allowable stress design methods consider environmental loads based on a fixed 100-year return period. The specified target level is a single value for the entire pipeline system.

The limit states approach considers a variable annual probability of exceedence per unit pipeline length for loads based on environmental processes. For example, CSA Z662 (1999) specifies an annual target safety level for general environmental loads as 10^{-2} per kilometre and for rare events, such as earthquake, iceberg impact, the exceedence limit is 10^{-4} per kilometre.

Sotberg et al. (1997) present annual target safety levels for offshore pipelines and recommended the following:

Limit State	Target Safety Level	Reference Units
Serviceability	$10^{-2} - 10^{-3}$	/total pipeline length /year
Ultimate	$10^{-3} - 10^{-4}$	/total pipeline length /year
Fatigue	10^{-3}	/total pipeline length /life cycle
Accidental	10^{-6}	/unit pipeline length /year

In view of fatigue limit states or economic factors related to project development, the time frame for target safety levels should be considered in view of the pipeline life-cycle; that is from mobilization to decommissioning.

4.2.2 Apportioning Ice Gouge Risk

It is not practical to design a marine pipeline such that the risk of failure due ice gouge considerations is apportioned equally over each kilometre for the entire length. If a pipeline were trenched at a constant depth, the risk of failure would then vary according to the risk of ice gouging at each point along the length.

A more practical method is to divide a pipeline into discrete segments based on constant bathymetry (e.g. water depth, seabed slope), soil properties (e.g. strength), gouge characteristics (e.g. frequency) or sections expected to be trenched at a constant depth. The risk allocated to each segment is then assumed to be proportional to the length of the segment.

If the target annual probability of failure per kilometre is represented by p, the target probability of failure for segment i is pL_i, where L_i is the length of segment i. The annual probability of failure for the whole pipeline is the probability of failure for segment 1 or segment 2 ... or segment i ... or segment n, where n is the number of pipeline segments. When the probabilities

of failure for the different segments are independent of each other, the overall failure probability is

$$P = 1 - (1 - pL_i)\ldots(1 - pL_i)\ldots(1 - pL_n) \quad (4.1)$$

Conceptually, this is equivalent to the probability of segment 1 not failing and segment 2 not failing ... and segment n not failing.

Consider a pipeline of total length L, divided into two equal segments. The overall probability of failure is $P = 1 - (1 - pL/2)\,(1 - pL/2) = pL - p^2 L^2/4$. A quick numerical calculation will show that $P \approx pL$ for small values of pL. In a number of cases, this relationship between overall failure probability and per kilometre failure probability will apply. In general, however, relationship (4.1) should be used to relate overall and per kilometre failure probabilities.

4.3 Design Gouge Parameters

4.3.1 Gouge Depth

A design gouge depth can be determined for each pipeline segment to satisfy an overall pipeline target or a per kilometre target. The target probability of failure is pL_i, where p is the target annual probability of failure per kilometre and where L_i is the length of segment i. The relationship between the overall target (P) and per kilometre target (p) is given by Equation (4.1).

The relationship between the design gouge depth and the target failure probability for the pipeline segment pL_i is

$$f(D) = pL_i / \eta \quad (4.2)$$

where $f(D)$ is the probability of exceedence associated with gouge depth D and η is the annual frequency of gouges crossing over the pipeline segment.

The gouge depth distribution is typically exponential or similar form. Since many ice gouges are very shallow, gouge depth distributions may need to be corrected for the limited accuracy of the sensor. For an exponential distribution, the probability of exceedence associated with gouge depth D is

$$f(D) = \exp(-bD) \tag{4.3}$$

where b is the slope of the natural logarithm of the probability of exceedence versus gouge depth relationship. The measured gouge depths are usually sorted and assigned a probability of exceedence according to their rank. In certain cases, the gouge depth distribution is shifted at the origin and the shifted exponential distribution

$$f(D) = \exp[-a(D - D_0)] \tag{4.4}$$

where a is the slope of the natural logarithm of the probability of exceedence versus gouge depth relationship and D_0 is a cut-off gouge depth. The parameters b, a and D_0 can be estimated using a least squares or other technique.

While a number of techniques are used to estimate design gouge depth, they all have the same essential form described above. The above process is described schematically in Figure 4.4.

4.3.2 Gouge Width

Since gouge depth is generally more critical for pipeline distress than gouge width, it is sufficient to select an average gouge width in combination with the extreme gouge depth. Sometimes the gouge width causing the most pipeline distress is used in combination with the extreme depth, but this can lead to an overly conservative design feature. This assumption is also appropriate because there is seldom a distinct relationship between gouge depth and width.

4.3.3 Joint Distribution of Gouge Depth and Width

Where gouge width and depth are correlated or the pipeline response is sensitive to gouge width, a single gouge feature may not best represent design conditions. In this case, the joint distribution of gouge width and depth can be used to obtain a family of gouge widths and depths satisfying the target annual segment failure probability.

4.3.4 Limit States Approach

When applying a limit states approach, there is no design environmental event *per se*. The target levels are associated with the pipeline response criteria in terms of stress and strain measures. An extension of the above approach, as illustrated in Figure 4.5. Probability distributions for the

pipeline stress and strain responses are calculated directly from the distributions of the ice gouge dimensions.

The deterministic analysis incorporates discrete parameters of the statistical distributions (e.g. ice feature geometry, velocity) and the response is analysed to define functional relationships over the range of parameters to be investigated. For example, the developed expression could be of the form,

$$q = \phi(d, w, \theta, H_c) \tag{3.4}$$

where q is the pipeline response expression as a function of gouge depth (d), width (w), relative gouge-pipeline orientation (θ) and pipeline cover depth (H_c). Constant coefficients are evaluated independently for each parameter variation using a least-squares regression technique. The parameter (q) represents the maximum effective stress (σ_{e_max}), maximum compressive strain (ε_{c_max}) or peak tensile strain (ε_{t_max}) experienced by the pipeline due to the ice gouge event.

The peak pipeline response (q) must be compared to defined target levels of safety (TLS) in accordance with the appropriate design standard or recommended practice. For defined return periods, exceedence analysis can be applied to estimate optimum burial depths that satisfy the (TLS) criterion. Thus, through Monte Carlo simulations, the functional relationships (i.e. $\sigma(d,w,\theta,H_c)$, $\varepsilon(d,w,\theta,H_c)$) can be defined in terms of annual probability of exceedence for given cover depths; that is $P(\sigma,H_c)$ and $P(\varepsilon,H_c)$. The final step is an iterative process to determine the appropriate pipeline cover depth, where the computed pipeline response equals the target levels of safety.

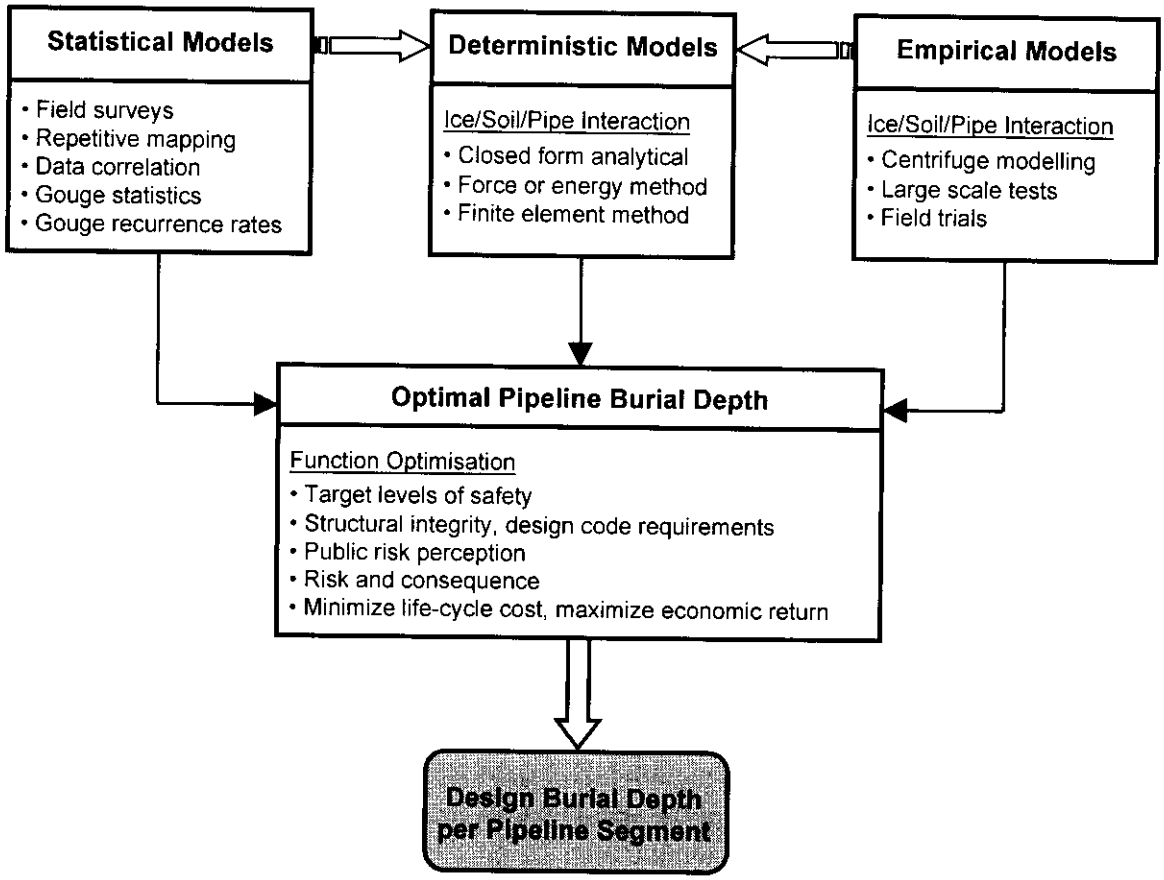

Figure 4-1. Pipeline burial depth optimisation strategies.

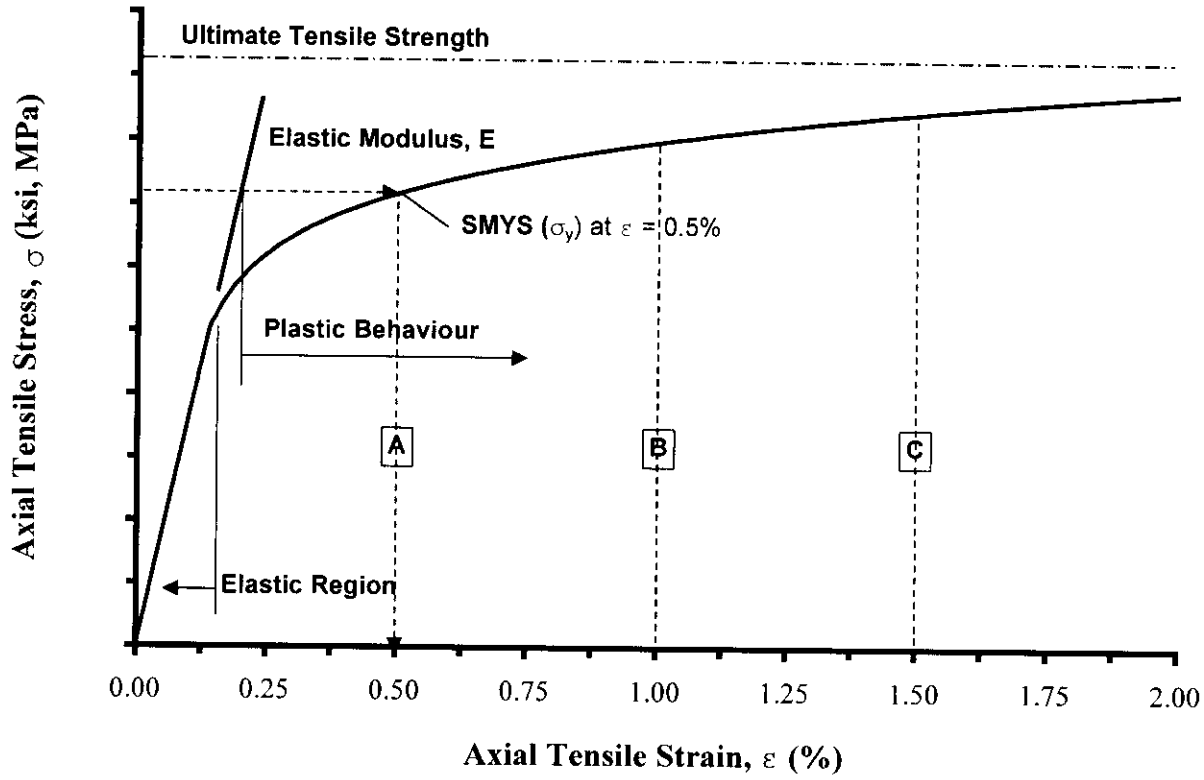

Figure 4-2. Typical pipeline stress-strain response and characterisation of upper limits for design methods.

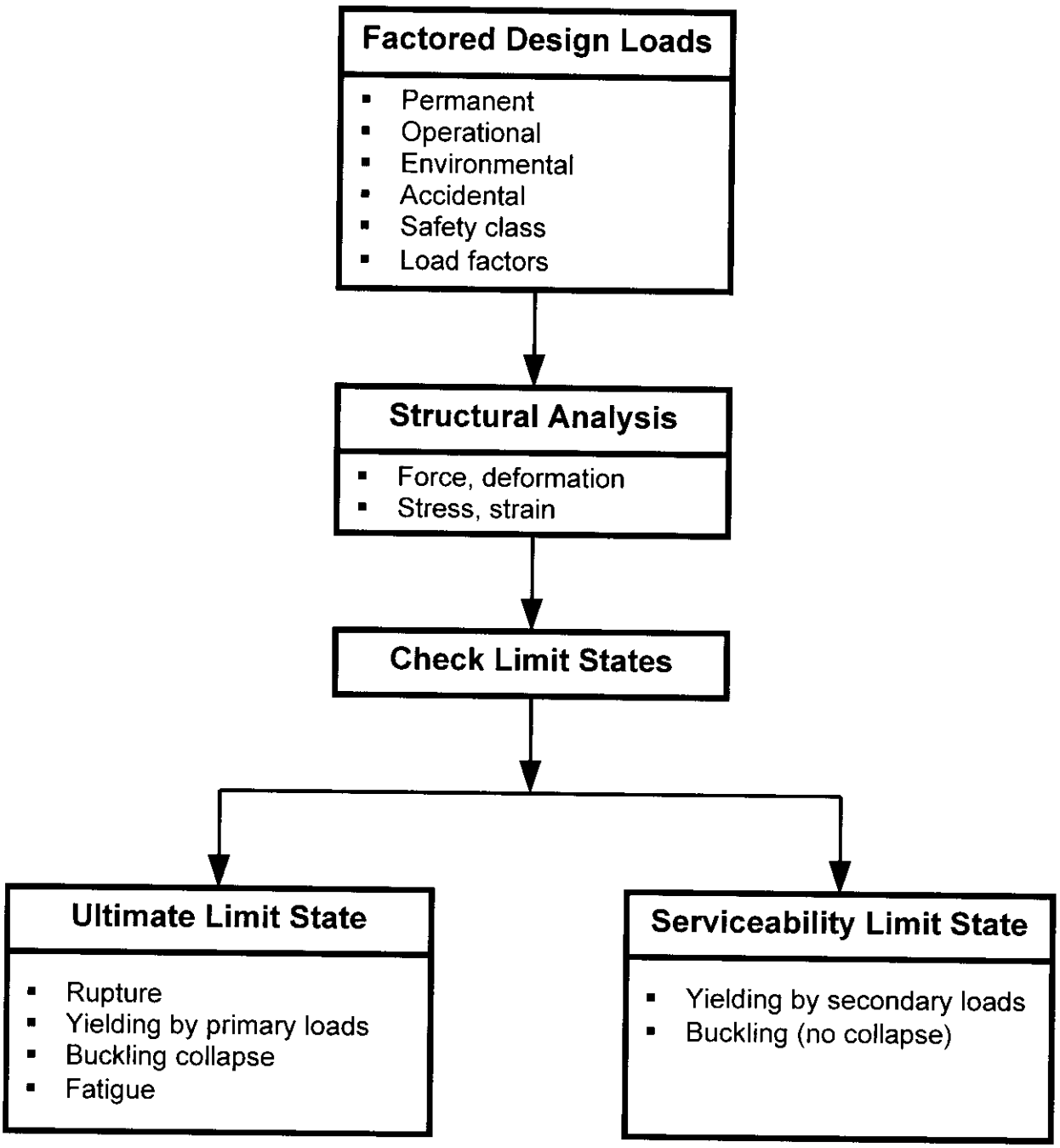

Figure 4-3. Summary of limit states design methodology.

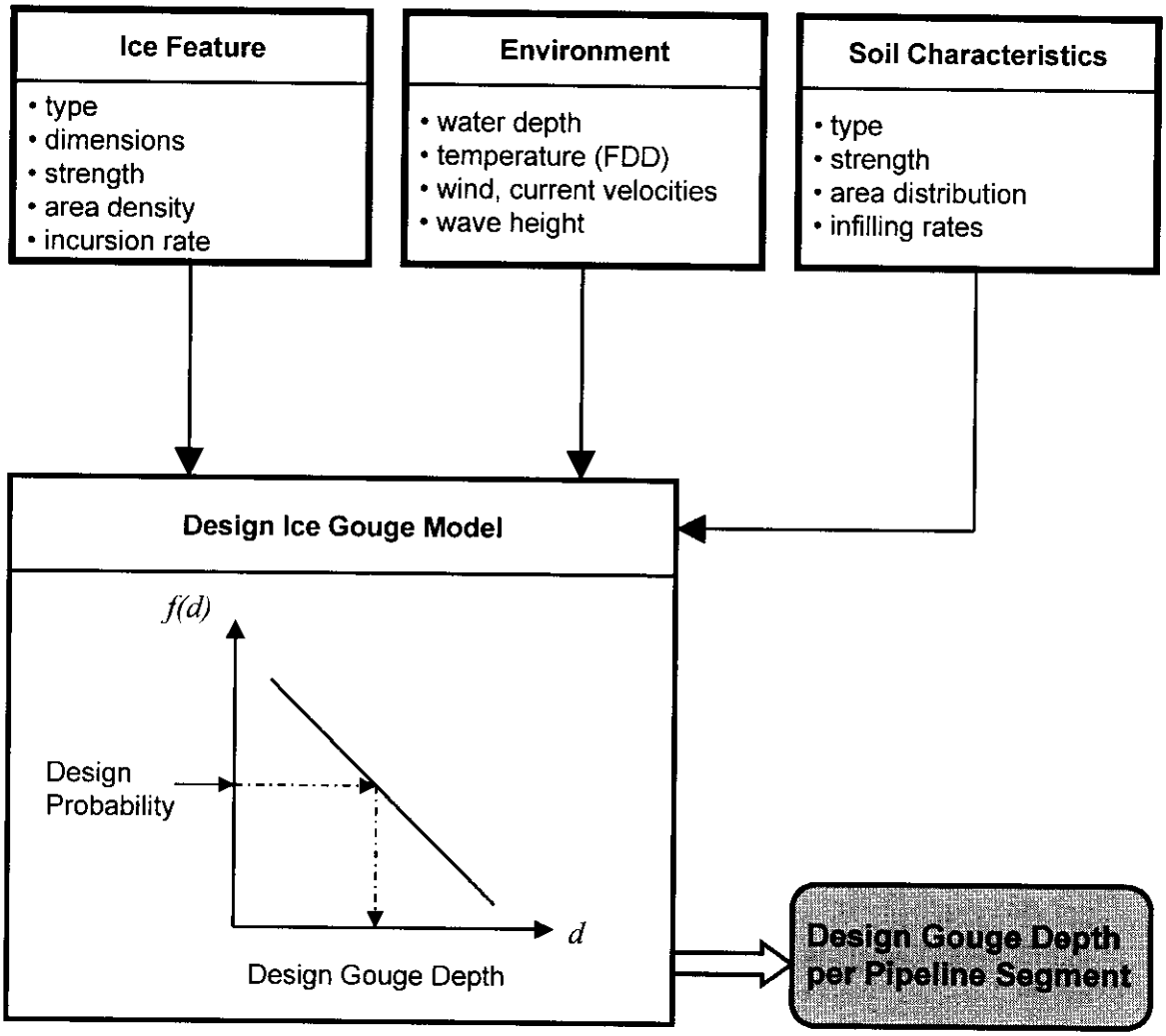

Figure 4.4 Schematic representation of design scour depth estimate per pipeline segment along a selected route.

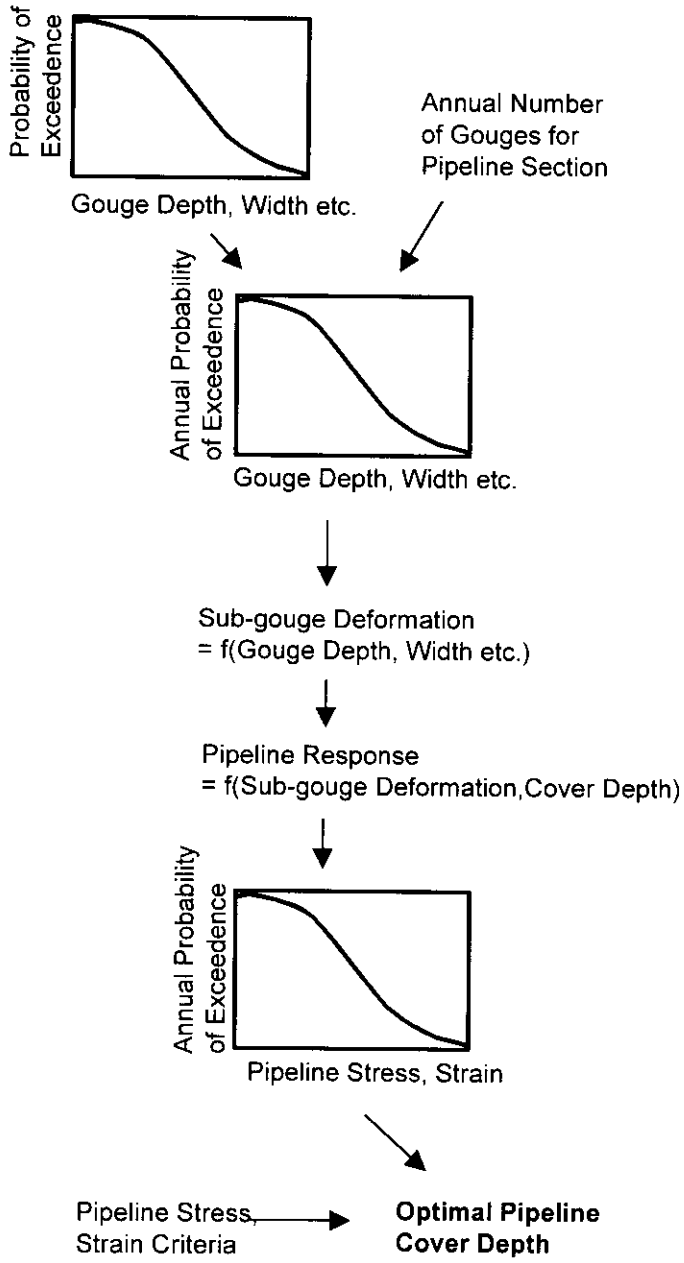

Figure 4-5. C-CORE approach for determining the optimal cover depth for pipeline risk model.

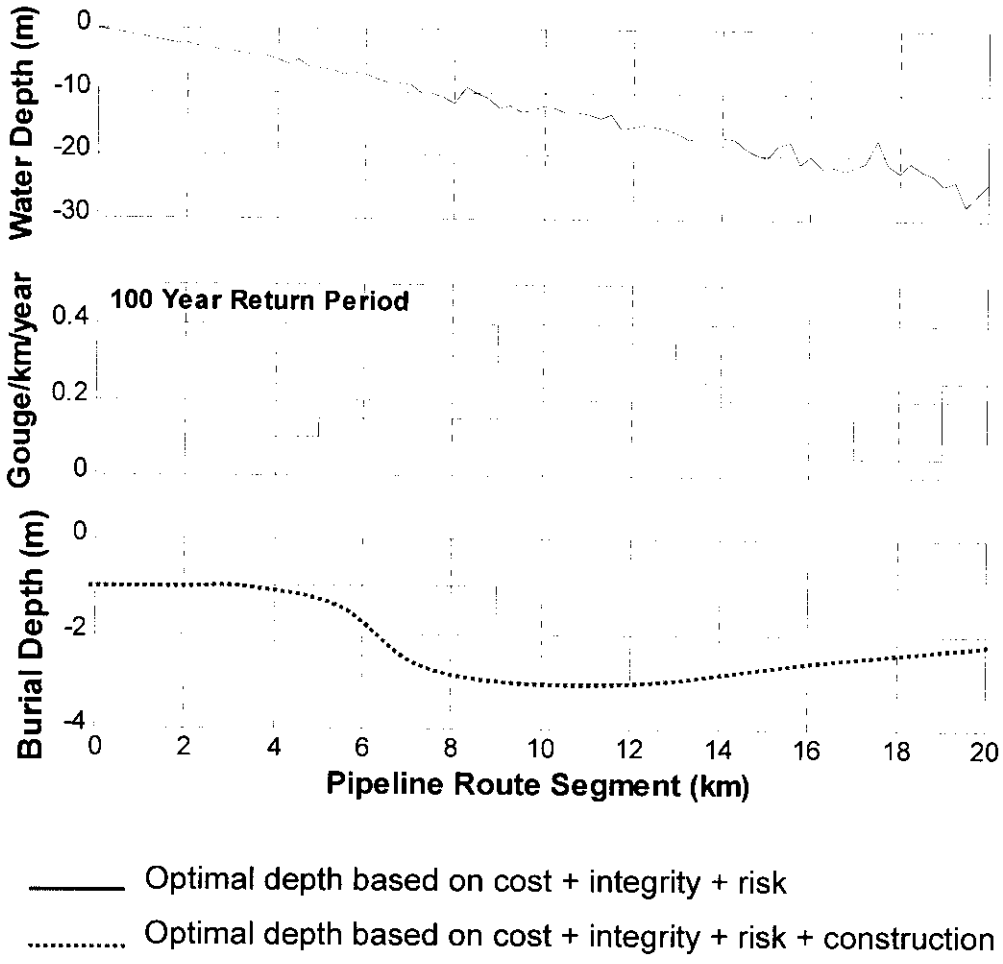

Figure 4.6 Optimal pipeline burial depth for fictitious resource development.

5.0 Assessment of Model Uncertainty

Pipelines are a practical and economic means for the development of many offshore oil and gas fields. For the arctic environment, in addition to other extreme design events (e.g. natural hazards such as earthquake, strudel scour, thaw settlement, etc.) ice gouging can be significant threat to the security of arctic marine pipelines. An assessment of the structural response to ice gouge events, with reference to recommended practice and design codes, is required to ensure pipeline integrity and environmental security.

Full-scale field trials and scaled model centrifuge tests are the best direct methods to measure pipeline response to ice gouge events. Although a parametric analysis would be time consuming and expensive. Consequently, numerical modelling is a viable alternative for conducting comprehensive investigations on ice gouge/soil/pipeline interaction.

A deterministic, parametric analysis has been conducted to examine the structural response of a buried marine pipeline to a design ice gouge scenario. Sensitivity analyses on defined variations of the baseline case were also considered. The numerical model established the fundamental characteristics that influence pipeline response. The numerical model employed for the study represents the current practice for analyzing pipeline response to large soil deformation fields; for example see INTEC (1998), Zhou and Murray (1993).

Based on the investigations conducted during the present study, issues associated with model uncertainty (e.g. related to inherent characteristics of the numerical method), input parameter uncertainty (e.g. soil properties, gouge geometry) and model limitations or constraints were addressed.

For parameter uncertainty, several key factors that must be addressed for marine pipeline design and risk assessment in terms of pipeline response to ice gouge events are:

- Parameter identification
- Uncertainty characterisation and modelling
- Influence and consequence

The first issue can be subdivided into *source*, *model* and *distribution* components. For example, consider ice gouge depth (*source*) statistics derived from field surveys. *Model* uncertainty can be propagated through both measurements (e.g. instrument resolution, technology limits) and methodologies (e.g. limits of technical knowledge, analytical methods or applied theory, human interpretation). Finally, model properties defining the statistic determine *distribution* uncertainty, which is typically insignificant for representative data sets. Parameter uncertainty characterisation can be accounted through error factors where model bias and scatter can be evaluated through sensitivity analysis of the probability distributions or stochastic processes. Fundamentally, the key parameters that influence uncertainty with respect to pipeline risk assessment are of primary importance. These issues will be addressed in context of the environmental and physical data sets.

5.1 Deterministic Model Analysis

The complex, nonlinear process of ice gouge/soil/pipeline interaction was analysed using the finite element method. The pipeline response model accounts for hoop stress due to internal pressure and bending strains due to the relative, differential ground displacement between the pipeline and soil. The soil load-displacement characteristics are defined in accordance with elements of the ASCE (1984) guidelines for the seismic design of oil and gas pipeline systems. The analysis considers a two-dimensional model where the continuum soil behaviour is discretized by a series of springs, attached to the pipe springline. Specific details on the ice gouge/soil/pipeline interaction model are discussed in Section ?? and Appendix ??. A summary of the baseline parameters and load case scenario variants is presented and further detailed discussion is documented in Appendix A5.

5.1.1 Baseline Model Parameters

Table 5-1 summarises the baseline model parameters considered for the ice gouge/soil/pipeline interaction analyses.

The pipeline selected was a 508mm (20″) outside diameter (D_o) with a 15.9mm (5/8″) wall thickness (t_w), which corresponds to a diameter-to-wall thickness ratio (D_o/t_w) of 32. The D_o/t_w ratio was based on a median value with respect to existing or proposed pipeline development projects. Some examples include Panarctic F-76 ($D_o/t_w \approx 15$), Colville River ($30 \leq D_o/t_w \leq 40$), Millennium ($D_o/t_w = 60$), Northstar ($D_o/t_w = 18$) and Sakhalin II ($40 \leq D_o/t_w \leq 48$). These projects encompass geographical areas as Lake Erie, Eastern Russian Arctic as well as the Canadian and Alaskan Beaufort Sea. The pipeline cover depth (H_c) represents the distance from the seabed surface to pipe crown. The selected pipeline grade was API 5L X52 and the mechanical properties are based on Walker and Williams (1995).

Two baseline cases as a function of soil strength, moderately stiff cohesive and moderately dense granular soil, were considered for the numerical analysis of a buried marine pipeline subject to an ice gouge event. The soil characteristics are based on moderately stiff undrained clay and moderately dense drained sand conditions with the yield response defined by ASCE (1984).

The ice gouge parameters were selected as representative values for a 100-year design event.

5.1.2 Variant Model Scenarios

Table 5-2 summarises the variant parameters on the baseline load case scenarios (Table 5-1) to be investigated. Scenarios were defined, as variations on the baseline load cases, to highlight and illustrate those parameters that exhibit a significant influence on pipeline response.

The issues addressed include internal pipeline material grade, pipeline diameter (D_o), gouge width (w), gouge depth (d), ice feature overburden stress (σ_v), subgouge displacement field, soil type (C_u,ϕ) and soil response functions (t_u–x_u, p_u–y_u). The influence of pipeline trench depth was indirectly incorporated through the cover depth (H_c) parameter, which was held at a constant depth of 0.5m below the modelled gouge depth (i.e. $H_c = 0.5m + d$). The specific combinations for the variant model analyses are summarised in Table 5-3.

5.2 Pipeline Response Analysis

Selected cases will be discussed to illustrate typical pipeline response characteristics and dominant parameters that influence pipeline behaviour. Further details of the finite element computations summarizing the longitudinal pipeline axial strain response are presented in Appendix A5.

5.2.1 Pipeline Strain Response

Ice gouging and the resultant soil/pipeline interaction is a complex and coupled process. For pipelines buried in the intermediate layer (Zone 2, Figure ?-?) subjected to extreme design ice gouge load cases (e.g. 100-year event), the structural response exhibits nonlinear material and geometric behaviour.

For the study parameters investigated, the analyses has shown that the computed pipeline response was governed by:

- factors that influenced longitudinal pipeline strain distribution (i.e. pipeline curvature response), and
- factors that influenced peak tensile strain levels

Analysis of tensile strains was considered, since this criterion represents a significant threat in terms of rupture and loss of product containment integrity for a pipeline. The consequence would be potential environmental damage and economic loss. Excessive compressive strain levels would most likely not cause rupture and probably only result in local wrinkling or sectional collapse due to ovalisation. This event would place restrictions on serviceability requirements and downtime loss.

For the investigated parameters, the main factors that influenced the longitudinal pipeline axial strain distribution (Appendix Figures A5-3 to A5-13) were:

- Pipeline diameter (D_o) for only cohesive soil (C_u)
- Gouge width (w)
- Cohesive soil strength (C_u)

The dominant parameters that governed pipeline axial strain magnitudes (Appendix Figures A5-14 to A5-19) were:

- Pipeline diameter (D_o)
- Pipeline grade for only granular soil (ϕ)
- Soil strength (C_u, ϕ)
- Gouge geometry (w, d) and subgouge soil displacement field $\left(u \propto \sqrt{wd}\right)$
- Ice feature bearing stress for only granular soil $\left(\sigma_v \equiv f\left\langle H_s^*, \phi \right\rangle\right)$

Characterisation of factors that dominate strain distribution and peak strain magnitudes should not be considered independent, since the ice gouge/soil/pipeline interaction event is a complex and coupled process. For example, consider the influence of the gouge width (w) on the pipeline strain distribution and peak strain level. Although the subgouge displacement field is proportional to the gouge geometry $\left(u \propto \sqrt{wd}\right)$, for the parameters investigated, the peak strain

level was associated with an intermediate gouge width, as illustrated in Figure A5-3. The pipeline curvature response for the wider gouge width ($w = 25m$) was moderated (i.e. lower strain level) due to the coupled interaction.

In summary, ice gouge/soil/pipeline interaction is a complex process, which is primarily dependent on the relative soil–pipe stiffness characteristics and mechanical properties, as well as the magnitude and distribution of the subgouge displacement field.

5.3 Pipeline Design Issues

The investigations have raised issues that have important implications on pipeline design. Although general characteristics on pipeline response have been identified, the analysis has demonstrated that detailed design and optimisation strategies are site specific and project dependent. Furthermore, variations on several parameters related to operational considerations have not been considered; for example diameter to wall thickness ratio (D_o/t), internal product pressure and thermal stress. These characteristics, in addition to the pipeline response to ice gouge events, impact structural integrity design issues.

For large deformation, loading mechanisms (e.g. frost heave, thaw settlement, ice gouge) strain based design criteria have to be employed, for economic design, to assess structural stability (i.e. compressive strain limits) and integrity (i.e. tensile strain limits) issues. The importance of adopting a limit strain criterion, in engineering practice and standards, has gained wider acceptance. For example, the pipeline industry (INTEC, 1998), engineering research community (Dinovitzer et al., 1999; Walker and Williams, 1995; Zimmerman et al., 1995) and standards agencies (API RP 1111, 1999; CSA Z662, 1999 and DNV, 1996) have recognized limit strain criteria. These issues were also addressed in Chapter 4.

Compressive strain limits are predominantly a function of the net pressure, residual stress/strain, initial ovality and D_o/t ratio; for example API RP 1111 (1999), CSA Z662 (1999). Product type and flow requirements may demand a large diameter pipeline system. Increasing pipeline diameter reduces the compressive strain limit, significantly at high D_o/t ratios, and, for soil displacement mechanisms, increases pipeline loading due to a greater projected area. The analysis presented in Appendix A6, however, illustrates that for certain load case scenarios, decreasing the D_o/t ratio does not necessarily commensurate with a decrease in compressive strain levels.

Tensile strain limits are normally established based upon consideration for the potential growth of the largest weld defect that satisfies the weld acceptance criteria; for example PD 6493 (1991), CSA Z662 (1999). Parameters such as weld toughness and notch ductility, maximum acceptable flaw size, misalignment and tensile strain limits can be established by engineering critical assessment (ECA) methods. ECA (i.e. fitness-for-purpose analysis) can be employed to evaluate pipeline integrity, with respect to the imposed tensile stress state, based on crack tip opening displacement (CTOD) values, which is dependent on the adopted welding procedure qualification. The weld toughness requirement increases and/or the maximum acceptable flaw size decreases with increasing applied tensile strain levels. Pipeline material grade and welding procedure can be selected to accommodate the tensile strain through considerations of material toughness (weld metal) and notch ductility (heat affected zone).

5.4 Pipeline Response Model Uncertainty

There are a number of factors that influence uncertainty with respect to the computed pipeline response related to inherent characteristics of the numerical model (e.g. theoretical basis) and fundamental assumptions of the ice gouge/soil/pipeline interaction model (e.g. soil response functions, subgouge displacement field).

5.4.1 Inherent Model Characteristics

The inherent model characteristics are constrained and limited by the specific numerical procedure employed for the ice gouge/soil/pipeline interaction analysis.

Modelled Pipeline Response

The simplicity afforded by beam theory, to readily develop numerical ice gouge/soil/pipeline interaction models, relies on the basic assumption that a one-dimensional approximation of a three-dimensional continuum is adequate. The fundamental constraint is that deformation of the cross-sectional area, in the same plane, is constant. This has significant implications for pipelines subjected to large combined strains (i.e. axial plus bending), since sectional collapse and/or post-buckling mechanisms are not considered at regions with a high radius of curvature. Furthermore, for the models employed during the current study, the pipe response was defined by the Timoshenko beam theory with a non-solid, closed, thin-wall section. This condition assumes that the transverse shear response is independent of the axial deformation and bending strain and that through thickness variation is negligible.

Modelled Soil Response

The main premise is that the soil continuum can be represented by a series of discrete springs representing independent, orthogonal soil deformation components.

5.4.2 Ice Gouge/Soil/Pipeline Interaction Model

The underlying assumptions incorporated in the model development also contribute to uncertainty, with respect to pipeline response, that can be addressed qualitatively.

Soil Response Functions

One area of significant importance demonstrated by the sensitivity analysis with respect to overburden stress, was the effective burial depth (H^*) and the defined load–displacement relationships (p_u–y_u) for cohesive soil. Based on the ASCE (1984) guideline, the soil stiffness term for clays decreases with increasing burial depth. This is illustrated in Figure A5-10 where the normalised stiffness is presented as a function of pipeline burial depth. This is contrary to the experimental observations of Paulin et al. (1995). For the finite element analysis conducted during the present study, a constant stiffness value for the p_u–y_u response of cohesive soil was adopted when the overburden stress was considered. The t_u–x_u curve for cohesive soil is not a function of burial depth and the stiffness response of granular soil increases with depth. Furthermore, the influence of dry and submerged conditions, displacement rates, confining stress, pipeline diameter, cover depth on the load–displacement response of soils has not been considered. For a limited range of test parameters, C-CORE (1999) has shown that, under submerged test conditions, the peak soil load and displacement response could be reduced by 50% in comparison with nominally dry state response.

Soil/Pipeline Interaction

The influence of soil variability (i.e. inhomogeneous distribution of soil properties and differential soil pressures) on pipeline response (i.e. pipe ovalisation, plastic hinge formation), are not accounted for in the model analysis.

The effect of an open trench or back-filled conditions for the buried pipeline significantly interacts with the resultant soil/pipeline response. Appropriate mechanical properties representing the combined response of native and remoulded soil, in addition to the development of an accurate numerical model must be further investigated.

Subgouge Displacement Field

Details of the empirical relationships defining the subgouge displacement field are presented in Nixon et al. (1996) and Woodworth-Lynas et al. (1996). The response functions were derived from analysis of centrifuge modelling tests conducted under PRISE. Further investigations are required to substantiate the relationships, particularly for granular soil, and investigate the influence of soil strength on the magnitude and distribution of subgouge deformation. The sensitivity analysis has demonstrated the significance of both the subgouge displacement field and soil strength on pipeline response.

Ice Gouge/Soil/Pipeline Interaction

Decoupling of the ice/soil and soil/pipe interactions may not be appropriate in some situations for several reasons:

- Gouge bearing stress influences the soil response functions (t_u–x_u, p_u–y_u) through an effective pipeline burial depth (H^*), pipeline strain response and initial ovalisation stress on the buried pipeline in addition to the non-uniform pressure distribution due to soil variability.
- The potential interaction between relative soil–pipeline stiffness, cover depth (i.e. free surface), pipeline diameter, subgouge displacement field and bearing stress need to be further investigated.

5.4.3 Addressing Uncertainty Issues

These issues concerning uncertainty directly impact pipeline burial depth optimisation strategies. The significance of the inherent model characteristics, in terms of influence on a realistic pipeline response analysis, can be determined through a systematic research effort. The development of two-dimensional and three-dimensional numerical models, which require more

computational resources, can be coupled with empirical studies (e.g. centrifuge, full-scale model test, and field trials) that investigate soil/pipeline response. The main objective would be to assess the current ice gouge/soil/pipeline interaction model.

Potentially, the models would address different objectives for pipeline design. The relatively simple, one-dimensional model could be calibrated, using the complementary numerical and empirical studies, and employed through the preliminary design phase to conduct parametric investigations. The more complex models would address issues relating to structural integrity and pipeline design optimisation.

Table 5-1. Baseline parameters for the finite element analysis to assess model sensitivity.

Feature		Parameter	Symbol	Magnitude	
				SI	Imperial
Pipeline (Grade 359 / API 5L X52)		Length	L	1000m	3280ft
		Outside Diameter	D_o	0.508m	20″
		Wall Thickness	t	0.0159m	5/8″
		Diameter/Thickness Ratio	D_o/t	32	
		Pressure	p	10MPa	1450psi
		Cover depth	H_c	1.5m	4.9ft
		Elastic Modulus	E	200GPa	29,000ksi
		Poisson's Ratio	ν	0.3	
		Yield Stress	σ_y	359MPa	52ksi
		Ultimate Tensile Strength	σ_u	455MPa	66ksi
		Plastic Yield Offset	α	1.79	
		Hardening Exponent	n	12	
Soil	Cohesive	Unit Weight	γ	19kN/m^3	120pcf
		Shear Strength	C_u	50kPa	7psi
		Yield Axial Load	t_u	70kN/m	4.8kips/ft
		Yield Axial Displacement	x_u	0.008m	0.3″
		Yield Horizontal Load	p_u	120kN/m	8.2kips/ft
		Yield Horizontal Displacement	y_u	0.080m	3.2″
	Granular	Unit Weight	γ	19kN/m^3	120pcf
		Friction Angle	ϕ	35°	
		Yield Axial Load	t_u	7kN/m	0.5kips/ft
		Yield Axial Displacement	x_u	0.004m	0.2″
		Yield Horizontal Load	p_u	55kN/m	3.8kips/ft
		Yield Horizontal Displacement	y_u	0.100m	3.9″
Gouge		Width	w	15m	49.2ft
		Depth	d	1m	3.3ft
		Bearing Stress	σ_v	0kPa	0psi

Table 5-2. Variant parameters for the finite element analysis to assess model sensitivity.

Feature		Parameter	Symbol	Magnitude	
				SI	Imperial
Pipeline		Diameter	D_o	0.273m	10.75″
Soil	Cohesive	Shear Strength	C_u	12.5kPa, 100kPa	288psf, 2160psf
		Soil Yield Response Functions (e.g. backfill conditions)	*t-x, p-y*	*f*(soil, gouge properties)	
		Maximum Subgouge Displacement	u_c	*f*(soil, gouge properties)	
	Granular	Friction Angle	ϕ	30°, 40°	
		Soil Yield Response Functions (e.g. backfill conditions)	*t-x, p-y*	*f*(soil, gouge properties)	
		Maximum Subgouge Displacement	u_c	*f*(soil, gouge properties)	
Gouge		Width	w	5m, 25m	16ft, 82ft
		Depth	d	0.5m, 1.5m	1.6ft, 4.9ft
		Bearing Stress	σ_v	50kPa, 100kPa	7psi, 15psi
		Subgouge Displacement Field	u_c	50%	

Table 5-3. Summary of specific parameter combinations employed for the finite element analysis to assess model sensitivity.

Variant Scenarios	Parameters		
	Pipeline	Soil	Ice Gouge
1	—	C_u = 12.5, 100kPa ϕ = 30°, 40°	w = 5, 25m
2	H_c = 1.0, 2.0m	—	d = 0.5, 1.5m
3	—	—	w = 5m 15, 25m σ_v = 50, 100kPa
4	—	—	$u \equiv 0.5$[a]
5	Grade 448 API 5L X65	—	—
6	D_o = 0.2731m, t = 8.7mm (D_o/t = 31)	—	—

[a] – Subgouge displacement field multiplied by a factor of 0.5.

REFERENCES AND BIBLIOGRAPHY

Abdelnour, R. and Graham, B. (1984). *Small Scale Tests of Sea Bottom Ice Scouring.* Proceedings, 7th **IAHR Ice Symposium**, Hamburg, Germany, Volume III, pp. 267-279.

Abdelnour R., Lapp D., Haider S., Shinde S.B. and Wright B. (1981). *Model Tests of Sea Bottom Scouring.* Proceedings, 6th International Conference on Port and Ocean Engineering Under Arctic Conditions, **POAC**, Volume II, Québec, QC, Canada, pp. 688-705.

Allan, D. (1986). *Risk Assessment for Iceberg-Scour Damage: Labrador Sea and Grand Banks.* Proceedings, **Ice Scour and Seabed Engineering**, Workshop on Ice Scour Research, Environmental Studies Revolving Fund, Report Number 49, Panel on Energy Research and Development (PERD), C.F.M. Lewis, D.R. Parrott, P.G. Simpkin and J.T. Buckley Editors, Ottawa, ON, Canada, pp. 240-248.

Allan, D. and Roggensack, W. (1986). *Engineering Applications and Risk Assessment: Summary and Discussion.* Proceedings, **Ice Scour and Seabed Engineering**, Workshop on Ice Scour Research, Experimental Studies Revolving Fund, Report Number 49, Panel on Energy Research and Development (PERD), C.F.M. Lewis, D.R. Parrott, P.G. Simpkin and J.T. Buckley Editors, Ottawa, ON, Canada, pp. 31-37.

Altaee, A. and Boivin, R. (1995). *Laterally Displaced Pipelines: Finite Element Analysis.* Proceedings, 14th International Conference, Offshore Mechanics and Arctic Engineering, **OMAE**, Volume V, Copenhagen, Denmark, pp. 209-216.

Altaee, A., B.H. Fellenius and H. Salem, (1996). Finite element modeling of lateral pipeline-soil interaction. *Proc. 15th Int. Conf. Offshore Mechanics Arctic Engrg*, vol.5, pp.333-341.

API 5L (1995). **Specification for Line Pipe.** API Specification 5L, 41st Edition, Exploration and Production Department, American Petroleum Institute, Washington, DC, USA, April 1995.

API RP 1111 (1999). **Design, Construction, Operation and Maintenance of Offshore Hydrocarbon Pipelines (Limit State Design).** API Recommended Practice 1111, 3rd Edition, American Petroleum Institute, Washington, DC, USA, July 1999, 45p.

API RP 2N (1995). **Design, Construction, Operation and Maintenance of Offshore Hydrocarbon Pipelines (Limit State Design).** API Recommended Practice 2N, 2nd Edition, American Petroleum Institute, Washington, DC, USA, December 1995, 82p.

ASCE (1984). **Guidelines for the Seismic Design of Oil and Gas Pipeline Systems.** Committee on Gas and Liquid Fuel Lifelines, Technical Council on Lifeline Earthquake Engineering, ASCE, New York.

Bea, R.G. (1986). *Engineering Aspects of Ice Gouging.* Proceedings, **Ice Scour and Seabed Engineering**, Workshop on Ice Scour Research, Experimental Studies Revolving Fund, Report Number 49, Panel on Energy Research and Development (PERD), C.F.M. Lewis, D.R. Parrott, P.G. Simpkin and J.T. Buckley Editors, Ottawa, ON, Canada, pp. 18-28.

Bea, R.G., Puskar, F.J., Barnes, P.W. and Reimnitz, E. (1985). *The Role of Ice Gouging in Determining Global Forces on Arctic Structures.* Proceedings, **Arctic '85**, Civil Engineering in the Arctic Offshore, ASCE, San Francisco, CA, USA, pp. 251-266.

Been, K. (1990). *Mechanisms of Failure and Soil Deformation During Scouring.* Proceedings, **Workshop on Ice Scouring and the Design of Offshore Pipelines**, Panel for Energy Research and Development (PERD), Canadian Oil and Gas Lands Administration (COGLA), Department of Energy, Mines and Resources, Calgary, AB, Canada, pp. 179-191.

Been, K., Palmer, A. and Comfort, G. (1990a). **Analysis of Subscour Stresses and Probability of Ice Scour-Induced Damage for Buried Submarine Pipelines, Volume II Deterministic Model of Ice-Soil-Pipe Interaction.** Panel for Energy Research and Development (PERD), Canadian Oil and Gas Lands Administration (COGLA), Department of Energy, Mines and Resources, Government of Canada, Ottawa, ON, Canada, 204p.

Been, K., Kosar, K., Hachey, J., Rogers, B.T. and Palmer, A.C. (1990b). *Ice Scour Models.* Proceedings, 9th International Conference, Offshore Mechanics and Arctic Engineering, **OMAE**, Volume V, Houston, TX, USA, pp. 179-188.

Beloshapkov, A. and Marchenko, A. (1998). *Mathematical Modeling of Ice Botom Scouring in Baydaratskaya Bay.* Proceedings, 14th International Symposium on Ice, **Ice in Surface Waters**, Hung Tao Shen Editor, Volume 1, Potsdam, NY, USA, pp. 345-352.

Braden, A., Mannikian, V., Rice, D., Swank, G., Hinnah, D., Monkelien, K., and Walker, J. (1998) *First Arctic Subsea Pipelines Moving to Reality.* Proceedings, 30th Offshore Technology Conference, **OTC**, Paper Number 8717, Houston, TX, USA, 20p.

Bruschi, R., Spinazzè, M., Tomassini, D., Cuscunà, S. and Venzi, S. (1995). *Failure Modes for Pipelines in Landslide Areas.* Proceedings, 14th International Conference, Offshore Mechanics and Arctic Engineering, **OMAE**, Volume V, Copenhagen, Denmark, pp. 65-78.

Bruschi, R., Monti, P., Bolzoni, G. and Tagliaferri, R. (1995b). *Finite Element Method as Numerical Laboratory for Analysing Pipeline Response Under internal Pressure, Axial Load, Bending Moment.* Proceedings, 14th International Conference, Offshore Mechanics and Arctic Engineering, **OMAE**, Volume V, Houston, TX, USA, pp. 389-401.

Bruschi, R., S. Glavina, M. Spinazze, D. Tomassini, S. Bonanni and S. Cuscuna, (1996). Pipelines subject to slow landslide movements structural modelling vs. field measurement. *Proc. 15th Int. Conf. Offshore Mechanics Arctic Engrg*, vol.5, pp.343-353.

C-CORE (1999). **Large Scale Modelling of Pipeline/Soil Interaction Under Lateral Loading.** Contract Report for Minerals Management Service, US Department of the Interior, C-CORE Publication No. 99-C25.

C-CORE (1998a). **Safety and Integrity of Arctic Marine Pipelines.** Contract Report for Minerals Management Service, United States Dept. of the Interior, C-CORE Publication 98-C15.

C-CORE, (1998b). **Large Scale Modelling of Soil/Pipe Interaction Under Moment Loading – Test GSC01.** Contract Report for Geological Survey of Canada, C-CORE Publ. No. 98-C20.

C-CORE, (1998c). **Large Scale Modelling of Soil/Pipe Interaction Under Moment Loading – Test GSC02.** Contract Report for Geological Survey of Canada, C-CORE Publ. No. 98-C21.

C-CORE, (1998d). **Large Scale Modelling of Soil/Pipe Interaction Under Axial or Lateral Loading.** DSS Contract 84084-50251/01-XSH.

C-CORE (1997a). **Pressure Ridge Ice Scour Experimental PRISE Phase 3c: Extreme Ice Scour Event Modelling & Interpretation.** Final Report, Prepared for BP Alaska, Chevron, Exxon Production Research, Petro Canada and Union Texas Petroleum. C-CORE Publication 97-C34.

C-CORE (1997b). **Behaviour of Icebergs Entering an Open Glory Hole.** Contract Report for Petro-Canada, March 1997, C-CORE Report 97-C11.

C-CORE (1995), Pressure Ridge Ice Scour Experiment (PRISE) Phase 3a: Centrifuge modelling of ice keel scour. Contract report 95-C12.

C-FER, (1993). Three-dimensional analysis of soil-pipeline interaction in a discontinuous heave zone. Contract Report for ESSO Res. Canada Ltd. And COGLA, Project 89-06 (proprietary to NEB).

Chari, T.R. (1975). **Geotechnical Aspects of Iceberg Scours on Ocean Floors.** Ph.D. Thesis, Memorial University of Newfoundland, St. John's, NF, Canada.

Chari, T.R. and Peters, G.R. (1981). *Estimates of Iceberg Scour Depths.* Proceedings, Symposium on Production and Transportation Systems for the Hibernia Discovery, St. John's, NF, Canada, February, 1981, pp.178-188.

Chouinard, L.E. (1995). *Estimation of Burial Depths for Pipelines in Arctic Regions.* **Journal of Cold Regions Engineering**, Volume 9, Number 4, pp. 167-182.

Clark, J.I., Phillips, R. and Paulin, M. (1998). *Ice Scour Research for the Safe Design of Pipelines: 1978-1998.* Proceedings, **Ice Scour and Arctic Marine Pipelines Workshop**, 13th International Symposium on Okhotsk Sea and Sea Ice, Mombetsu, Japan, February 1-4, 1998, pp. 1-7.

Clark, J.I., Paulin, M.J., Lach, P.R., Yang, Q.S. and Poorooshasb, H. (1994). *Development of a Design Methodology for Pipelines in Ice Scoured Seabeds.* Proceedings, 13th International Conference, Offshore Mechanics and Arctic Engineering, **OMAE**, Volume V, Houston, TX, USA, pp. 107-125.

Clark, J.I., Paulin, M.J. and Poorooshasb, F. (1990). *Pipeline Stability in an Ice-Scoured Seabed.* Proceedings, **First European Offshore Mechanics Symposium**, ISOPE, Trondheim, Norway, pp. 533-549.

Clark, J.I. and Poorooshasb, F. (1989). *Protection of Sea Bottom Facilities in an Ice Scoured Environment.* Proceedings, Annual Conference Canadian Society of Civil Engineers, **CSCE**, St. John's, NF, Canada, pp. 617-651.

Comfort, G. (1990). *A Case Study Analysis of the Probability of Ice Scour-Induced Damage for Submarine Pipelines.* Proceedings, **Workshop on Ice Scouring and the Design of Offshore Pipelines**, Panel for Energy Research and Development (PERD), Canadian Oil and Gas Lands Administration (COGLA), Department of Energy, Mines and Resources, Calgary, AB, Canada, pp. 145-162.

Comfort, G. and Been, K. (1990). **Analysis of Subscour Stresses and Probability of Ice Scour-Induced Damage for Buried Submarine Pipelines.** Summary Report. Submitted to Panel for Energy Research and Development (PERD), Canadian Oil and Gas Lands Administration (COGLA), Department of Energy, Mines and Resources, Government of Canada, Ottawa, ON, Canada, 30p.

Comfort, G., Gilbert, C. and Ferregut, C. (1990a). **Analysis of Subscour Stresses and Probability of Ice Scour-Induced Damage for Buried Submarine Pipelines, Volume Ia Database of Key Ice Scour Parameters, Main Report.** Panel for Energy Research and Development (PERD), Canadian Oil and Gas Lands Administration (COGLA), Department of Energy, Mines and Resources, Government of Canada, Ottawa, ON, Canada, 106p.

Comfort, G., Gilbert, C. and Ferregut, C. (1990b). **Analysis of Subscour Stresses and Probability of Ice Scour-Induced Damage for Buried Submarine Pipelines, Volume Ib Database of Key Ice Scour Parameters, Appendices.** Panel for Energy Research and Development (PERD), Canadian Oil and Gas Lands Administration (COGLA), Department of Energy, Mines and Resources, Government of Canada, Ottawa, ON, Canada, 324p.

Comfort, G. and Graham, B. (1986). **Evaluation of Sea Bottom Ice Scour Models.** Environmental Studies Revolving Funds, Report Number 37, Ottawa, ON, Canada, 71p.

CSA Z245 (1998). **CSA Z245.1-98 Steel Line Pipe.** 6th Edition, Canadian Standards Association, Standards Development, Etobicoke, ON, Canada, March 1998, 116p.

CSA Z662 (1999). **CSA Z662-99 Oil and Gas Pipeline Systems.** 3rd Edition, Canadian Standards Association, Standards Development, Etobicoke, ON, Canada, April 1999, 356p.

d'Apollonia, S.J. and Lewis, C.F.M (1986). *Numerical Model for Calculating Spatial Distribution and Mean Frequency of Iceberg Grounding Events.* Proceedings, **Ice Scour and Seabed Engineering**, Workshop on Ice Scour Research, Environmental Studies Revolving Fund, Report Number 49, Panel on Energy Research and Development (PERD), C.F.M. Lewis, D.R. Parrott, P.G. Simpkin and J.T. Buckley Editors, Ottawa, ON, Canada, pp. 221-232.

Davidson, S.H. and Simms, A. (1997). **Characterisation of Iceberg Pits on the Grand Banks of Newfoundland.** Environmental Studies Research Funds, Report Number 133, Calgary, AB, Canada, 99p.

Davidson, S.H., Collins, W.T. and Simpkin, P.G. (1991). **An Experiment to Monitor Four Iceberg Scours on the Grand Banks of Newfoundland.** Environmental Studies Research Funds, Report Number 107, Ottawa, ON, Canada, 110p.

DiBattista, J.D., J.J.R. Cheng, D.W. Murray and Z.J. Zhou, (1998). Laboratory tests and numerical modelling of sleeper-supported line pipe. *Proc. Int. Pipeline Conf.,* ASME, vol.2, pp. 789-796

DNV (1996). **Rules for Submarine Pipeline Systems.** Det Norske Veritas, December 1996, Høvik, Norway, 128p.

Dobrocky Seatech Ltd. (1984). **1984 Iceberg Field Survey**. Mobil Hibernia Development Studies.

Fernando, N.S.M. and J.P. Carter, (1998). Elastic analysis of buried pipes under surface patch loadings. *J. Geotech. Geoenv. Engrg.,* ASCE, 124(8):720-728.

Gaskill, H. (1986). *Report on a Non-Deterministic Model of Populations of Iceberg Scour Depths.* Proceedings, **Ice Scour and Seabed Engineering**, Workshop on Ice Scour Research, Environmental Studies Revolving Fund, Report Number 49, Panel on Energy Research and Development (PERD), C.F.M. Lewis, D.R. Parrott, P.G. Simpkin and J.T. Buckley Editors, Ottawa, ON, Canada, pp. 249-258.

Geonautics (1991). **East Coast Repetitive Seafloor Mapping 1979/1990.** Environmental Studies Research Funds, Report Number 128, Ottawa, ON, Canada, 49p.

Gilbert, G. and Pedersen, J. (1986). **Ice Scour Database for the Beaufort Sea.** Environmental Studies Revolving Funds, Report Number 55, Ottawa, ON, Canada, 99p.

Golder (1989). **Laboratory Indentor Testing to Verify Ice/Soil/Pipe Interaction Models.** Report, Gulf Canada Resources Limited and Golder Associates Limited, 42p.

Golder Associates Ltd., (1990). "Analysis of subscour stress and probability of ice scour-induced damage for buried submarine pipelines, volume II, Deterministic model of ice-soil-pipe interaction."

Goodwin, C.R., Finely, J.C. and Howard, L.M. (1985). **Ice Scour Bibliography.** Environmental Studies Revolving Funds, Report Number 10, Ottawa, ON, Canada, 99p.

Green, G.R. (1984). **Geotechnical Modeling of Iceberg-Seabed Interaction.** M.Eng. Thesis, Memorial University of Newfoundland, St. John's, NF, Canada.

Hodgson, G.J., Lever, J.H., Woodworth-Lynas, C.M.T. and Lewis, C.F.M. (1988). **The Dynamics of Iceberg Grounding and Scouring Experiment (DIGS) and Repetitive Mapping of the Eastern Canadian Continental Shelf.** Environmental Studies Research Funds, Report Number 94, Ottawa, ON, Canada, 315p.

ICE Engineering Ltd. (1984). **Iceberg Survey - Grand Banks - Hibernia.** Contract Report Prepared for the Bedford Institute of Oceanography.

ICE Engineering Ltd., (1985). **Iceberg Survey - Grand Banks - Hibernia.** Contract Report Prepared for the Bedford Institute of Oceanography.

Jordaan, I.J., Press, D., Milford, P. (1999). **Iceberg Databases and Verification**. PERD/CHC Report 20-41, March, 1999.

INTEC (1998). **Ice Keel Protection. Northstar Development Project Detailed Engineering.** Prepared for BP Exploration (Alaska), Inc., Anchorage, Alaska, USA, INTEC Project Number H-0660.03, Technical Note TN410, Revision 3, May 1998.

Jacob, B.P., N.F.F. Ebecken and M.G.F.M. Gomez, (1997). Numerical simulation of the 'pull-in' operation in submarine pipelines. *Engineering Structures,* 19(10):868-876.

Javanmard, M. and A.J. Valsangkar, (1988). Physical and finite element analysis of buried flexible pipelines. *Centrifuge '98,* Balkema, Rotterdam, pp.687-692.

Karadeniz, H., (1997). Interface beam element for the analyses of soil-structure interactions and pipelines. *Proc. 7th Int. Offshore and Polar Engrg Conf.*, vol.2, pp. 286-292.

Kenny, S., Phillips, R., McKenna, R.F. and Clark, J.I. (2000). *Response of Buried Arctic Marine Pipelines to Ice Gouge Events*. **OMAE** 2000, New Orleans, LA, USA, Paper Number OMAE00-5001, 8p.

Lach, P.R., (1996)."Centrifuge modelling of large soil deformation due to ice scour." Ph.D. thesis, Memorial University of Newfoundland.

Lanan, G.A., Niedorada, A.W. and Weeks, W.F. (1986). *Ice Gouge Hazard Analysis.* Proceedings, 18th Annual Offshore Technology Conference, **OTC**, Volume 4, Houston, TX, USA, pp. 57-66.

Lara, P.F., (1987). Revisiting the failure criteria of buried pipelines. *ASME – Petroleum Div. Publ..*, vol.6, pp143-154.

Liolios, A., K. Pitilakis and M. Yeroyanni, (1998). BEM-FEM convolutional approach to the unilateral contact problem of seismic soil-pipeline interaction. *Engrg, Analysis with Boundary Elements,* 22(1):77-81

Manolis, G.D., P.I. Tetepoulidis, D.G. Talaslidis and G. Apostolidis, (1995). Seismic analysis of buried pipeline in a 3D soil continuum. *Engrg, Analysis with Boundary Elements,* 15(4):371-394.

Marcellus, R.W. and Morrison, T.B. (1986). *Some Recent Studies Relating to the Determination of Pipeline Depths.* Proceedings, **Ice Scour and Seabed Engineering**, Workshop on Ice Scour Research, Environmental Studies Revolving Fund, Report Number 49, Panel on Energy Research and Development (PERD), C.F.M. Lewis, D.R. Parrott, P.G. Simpkin and J.T. Buckley Editors, Ottawa, ON, Canada, pp. 295-303.

Marcellus, R.W. (1980). *Interactions Between First-Year Grounded Ridge Keels and Trenched Pipelines.* Proceedings, **Workshop on Sea Ice Ridging and Pile-Up**, Snow and Ice Subcommittee, National Research Council of Canada, Calgary, AB, Canada, pp. 285-295.

McKeehan, D.S. (1986). *Marine Pipeline Design in Ice Environments.* Proceedings, **Ice Scour and Seabed Engineering**, Workshop on Ice Scour Research, Environmental Studies Revolving Fund, Report Number 49, Panel on Energy Research and Development (PERD), C.F.M. Lewis, D.R. Parrott, P.G. Simpkin and J.T. Buckley Editors, Ottawa, ON, Canada, pp. 9-17.

McKenna, R.F., Crocker, G, and Paulin, M.J. (1999). *Modelling Iceberg Scour Processes on the Northeast Grand Banks.* Proceedings, 18th International Conference, Offshore Mechanics

and Arctic Engineering, **OMAE**, Paper Number OMAE-99-1172, St. John's, NF, Canada, 10p.

Mobil Hibernia Development Studies, (1982). **Iceberg Field Survey.** Contract Report Prepared by ICE Engineering Ltd., St. John's, Newfoundland.

Mobil Hibernia Development Studies, (1983). **Iceberg Field Survey.** Contract Report Prepared by ICE Engineering Ltd., St. John's, Newfoundland.

Mobil Hibernia Development Studies, (1984). **Iceberg Field Survey.** Contract Report Prepared by ICE Engineering Ltd., St. John's, Newfoundland.

Mindlin R.D. (1953). *Force at a Point in the Interior of Semi-infinite Solid.* Proceedings, 1st Midwestern Conference on Solid Mechanics, University of Illinois, Urbana, IL, USA, p.111.

Murray, A., Ferregut, C. and Ritch, R. (1990). **Analysis of Subscour Stresses and Probability of Ice Scour-Induced Damage for Buried Submarine Pipelines, Volume III Probabilistic Modelling.** Panel for Energy Research and Development (PERD), Canadian Oil and Gas Lands Administration (COGLA), Department of Energy, Mines and Resources, Government of Canada, Ottawa, ON, Canada, 42p.

Myers, R.S., Blasco, S., Gilbert, G. and Shearer, J. (1996). **1990 Beaufort Sea Ice Scour Repetitive Mapping Program.** Environmental Studies Revolving Funds, Report Number 129, Ottawa, ON, Canada, 147p.

Nessim, M.A. and Jordaan, I.J. (1985). *Protection of Arctic Submarine Pipelines Against Ice Scour.* Proceedings, 4th International Conference, Offshore Mechanics and Arctic Engineering, **OMAE**, Volume V, Houston, TX, USA, pp. 610-617.

Ng, P.C.F., I.C. Pyrah and W.F. Anderson, (1997). Assessment of three interface elements and modification of the interface element in CRISP90. *Computers and Geotechnics,* 21(4):315-339.

Nordco (1980). **Iceberg Draft Measurement**. Labrador Sea, 1979.

Nixon, J.F., Palmer, A. and Phillips, R. (1996). *Simulations for Buried Pipeline Deformations Beneath Ice Scour.* Proceedings, 15th International Conference, Offshore Mechanics and Arctic Engineering, **OMAE**, Volume V, Houston, TX, USA, pp. 383-392.

Noble, P.G. (1980). *Interactions Between First-Year Grounded Ridge Keels and Trenched Pipelines.* Proceedings, **Workshop on Sea Ice Ridging and Pile-Up**, Snow and Ice Subcommittee, National Research Council of Canada, Calgary, AB, Canada, pp. 248-284.

Noble, P.G. and Comfort, G. (1980). *Damage to an Underwater Pipeline by Ice Ridges.* Proceedings, **Workshop on Sea Ice Ridging and Pile-Up**, Snow and Ice Subcommittee, National Research Council of Canada, Calgary, AB, Canada, pp. 248-284.

Palmer, A. (1998). *Alternative Paths for Determination of Minimum Burial Depth to Safeguard Pipelines Against Ice Gouging.* Proceedings of Ice Scour and Arctic Marine Pipelines Workshop, **13th International Symposium on Okhotsk Sea and Sea Ice**, Mombetsu, Hokkaido, Japan, pp. 9-16.

Palmer, A. (1990). *Design of Marine Pipelines in Seabed Vulnerable to Ice Scour.* Proceedings, **Workshop on Ice Scouring and the Design of Offshore Pipelines**, Panel for Energy Research and Development (PERD), Canadian Oil and Gas Lands Administration (COGLA), Department of Energy, Mines and Resources, Calgary, AB, Canada, pp. 167-178.

Palmer, A.C., Konuk, I., Comfort, G. and Been, K. (1990). *Ice Gouging and the Safety of Marine Pipelines.* Proceedings, 22nd Annual Offshore Technology Conference, **OTC**, Volume 3, Houston, TX, USA, pp. 235-244.

Palmer, A., Konuk, I., Love, J., Been, K. and Comfort, G. (1989). *Ice Scour Mechanisms.* Proceedings, 10th International Conference on Port and Ocean Engineering Under Arctic Conditions, **POAC**, Volume 1, Luleå, Sweden, pp. 123-132.

Paulin, M., Phillips, R. and Boivin, R. (1995). *Centrifuge Modelling of Lateral Pipeline/Soil Interaction – Phase II.* Proceedings, 14th International Conference, Offshore Mechanics and Arctic Engineering, **OMAE**, Volume V, Copenhagen, Denmark, pp. 107-123.

Paulin, M. (1992). **Physical Model Analysis of Iceberg Scour in Dry Sand and Submerged Sand.** M.Eng. Thesis, Memorial University of Newfoundland, St. John's, NF, Canada, 183p.

PD 6493 (1991). **Guidance on Methods for Assessing the Acceptability of Flaws in Fusion Welded Structures.** Bristish Standards Institution, London, UK, 115p.

Pilkington, R. (1986). *Estimating Ice-Scour Frequency and Risk to Buried Pipelines.* Proceedings, **Ice Scour and Seabed Engineering**, Workshop on Ice Scour Research, Environmental Studies Revolving Fund, Report Number 49, Panel on Energy Research and Development (PERD), C.F.M. Lewis, D.R. Parrott, P.G. Simpkin and J.T. Buckley Editors, Ottawa, ON, Canada, pp. 213-220.

Pilkington, G.R. and Marcellus, R.W. (1981). *Methods of Determining Pipeline Trench Depths in the Canadian Beaufort Sea.* Proceedings, 6th International Conference on Port and Ocean Engineering Under Arctic Conditions, **POAC**, Volume II, Québec, QC, Canada, pp. 674-687.

PIPLIN-III, (1991). Computer program for stress and deformation analysis of pipelines. Structural Software Development Inc., California, 94704.

Polomoshnov, A.M., Astafiev, V.N. and Surkov, G.A. (1999). *Method for Selecting Subsea Pipeline Route Under Ice Conditions (For the Sakhalin Offshore Case).* Proceedings of Ice Scour and Arctic Marine Pipelines Workshop, **14th International Symposium on Okhotsk Sea and Sea Ice**, Mombetsu, Hokkaido, Japan, pp. 130-136.

Poorooshasb, F. (1990). **Analysis of Subscour Stresses and Probability of Ice Scour Induced Damage for Buried Submarine Pipelines, Volume IV Large Scale Laboratory Test of Seabed Scour.** Panel for Energy Research and Development (PERD), Canadian Oil and Gas Lands Administration (COGLA), Department of Energy, Mines and Resources, Government of Canada, Ottawa, ON, Canada, 168p.

Poorooshasb, F. and Clark, J.I. (1990). *On Small Scale Ice Scour Modelling.* Proceedings, **Workshop on Ice Scouring and the Design of Offshore Pipelines**, Panel for Energy Research and Development (PERD), Canadian Oil and Gas Lands Administration (COGLA), Department of Energy, Mines and Resources, Calgary, AB, Canada, pp. 193-235.

Poorooshab, H.B. and Q.S. Yang (1993), Finite element analysis of seabed subscour deformation. *Pressure Ridge Ice Scour Experiment (PRISE) - Phase II*, Progress Report, C-CORE Contract Report No 93-C4.

Popescu, R. (1999), Finite element analysis of pipe-soil interaction; Phase I - two-dimensional plane strain analyses. Contract Report for Geological Survey of Canada, C-CORE Publication No. 99-C23.

Popescu, R., R. Phillips, I. Konuk and D. Deacu (1999), "Numerical and Physical Analysis of Pipe-Soil Interaction", *Proc. 52nd Canadian Geotech. Conf.*, Regina, Sask., pp.437-444.

Rajani, B.B., Robertson, P.K. and Morgenstern, N.R. (1993). *A Simplified Design Method for Pipelines Subject to Transverse Soil Movements.* Proceedings, 12th International Conference, Offshore Mechanics and Arctic Engineering, **OMAE**, Volume V, Houston, TX, USA, pp. 157-165.

Rinawi, A.M. (1993). *Wrinkling Evaluation of Straight Pipe-Sleeve Configuration.* **Pipeline Engineering**, ASME, Volume 55, Houston, TX, USA, pp. 1-6.

Rizkalla, M., Poorooshasb, F. and Clark, J.I. (1992). *Centrifuge Modelling of Lateral Pipeline/Soil Interaction.* Proceedings, 11th International Conference, Offshore Mechanics and Arctic Engineering, **OMAE**, Calgary, AB, Canada, 13p. Insert.

Seaconsult (1988). **Terra Nova Development Studies, Physical and Environmental Data for Production Systems at Terra Nova**. Contract Report for Petro-Canada, prepared by Seaconsult Limited, August 1988.

Selvadurai, A.P.S. (1985). *Soil-Pipeline Interaction during Ground Movement.* Proceedings, **Arctic '85**, Civil Engineering in the Arctic Offshore, ASCE, San Francisco, CA, USA, pp. 251-266.

Selvadurai and Assoc., (1991). Three-dimensional modelling of soil-pipeline interaction in a discontinuous heave zone. Contract Report for C-FER.

Shearer, J, Laroche, B. and Fortin, G. (1986). **Canadian Beaufort Sea 1984 Repetitive Mapping of Ice Scour.** Environmental Studies Revolving Funds, Report Number 32, Ottawa, ON, Canada, 43p.

Skurihin, V.A, Surkov, G.A. and Truskov, P.A. (1992). *Selection of the Subsea Pipeline Route for the Offshore Chaivo Field.* Proceedings, 2nd International and Offshore Polar Engineering Conference, **ISOPE**, Volume II, San Francisco, CA, USA, pp. 801-806.

Stepanov, I.V., Timofeyev, O.Y., Klepikov, A.V. and Malek, V.N. (1998). *An Approach to the Optimisation of the Burial Depth of Underwater Pipelines on the Arctic Offshore.* Proceedings of Ice Scour and Arctic Marine Pipelines Workshop, **13th International Symposium on Okhotsk Sea and Sea Ice**, Mombetsu, Hokkaido, Japan, pp. 59-69.

Surkov, G.A. and Truskov, P.A. (1992). *Probability Estimation of Moving Pressure Ridge Contacts with Pipelines.* Proceedings, 2nd International and Offshore Polar Engineering Conference, **ISOPE**, Volume II, San Francisco, CA, USA, pp. 797-800.

Tehrani-Zadeh, M., (1995). Three dimensional seismic behaviour of pipelines buried in backfill trenches. *Proc. Dev. Computer Aided Design Modell. Struct. Engrg.*, Civil-Comp Press, pp. 295-299.

Terra Nova (1996). **Development Plan and Environmental Impact Statement**.

Timmerman, W.J. (1983). *Design of Offshore Pipelines for Ice Environments.* **Design for Ice Forces**, Cold Regions Engineering, ASCE, Stan R. Caldwell and Randy D. Crissman Editors, pp. 69-99.

Tohda, J., M. Mikasa and M. Hachiya, (1988). Earth pressure on underground rigid pipes: Centrifuge model tests and FEM analyses. *Centrifuge '88,* Balkema, Rotterdam, pp.395-402.

Tohda, J., L. Li and H. Yoshimura, (1994). FE elastic analysis of earth pressure on buried flexible pipelines. *Centrifuge '94,* Balkema, Rotterdam, pp.727-732.

Trautmann, C.H., and O'Rourke, T.D. (1983). **Behaviour of Pipe in Dry Sand under Lateral and Uplift Loading.** Geotechnical Engineering Report 83-6, Cornell University, NY, USA.

Walker, A.C. and Williams, K.A.J. (1995). *Strain Based Design of Pipelines.* Proceedings, 14th International Conference, Offshore Mechanics and Arctic Engineering, **OMAE**, Volume V, Copenhagen, Denmark, pp. 345-350.

Walter, D. and Phillips, R. (1998). **PRISE – Force Models for Drained and Undrained Steady State Ice Scouring.** Contract Report, C-CORE Publication 98-C33, 60p.

Wang, A.T. (1990). *Design Ice Gouge Depth Computation through Computer Simulations.* Proceedings, **Workshop on Ice Scouring and the Design of Offshore Pipelines**, Panel for Energy Research and Development (PERD), Canadian Oil and Gas Lands Administration (COGLA), Department of Energy, Mines and Resources, Calgary, AB, Canada, pp. 237-246.

Weeks, W.F., Tucker, W.B. and Niedoroda, A.W. (1985). *A Numerical Simulation of Ice Gouge Formation and Infilling on the Shelf of the Beaufort Sea.* Proceedings, 8th International Conference on Port and Ocean Engineering Under Arctic Conditions, **POAC**, Volume 1, Narssarssuaq, Greenland, pp. 393-407.

Woodworth-Lynas, C.M.T., (1992). "The geology of ice scour." Ph.D. thesis University of Wales 269p.

Woodworth-Lynas, C., Nixon, D., Phillips, R. and Palmer, A. (1996). *Subgouge Deformations and the Security of Arctic Marine Pipelines.* Proceedings, 28th Annual Offshore Technology Conference, **OTC**, Volume 4, Houston, TX, USA, pp. 657-664.

Woodworth-Lynas, C.M.T., (1998). "Sub-scour soil deformation and the development of ideas from field work in the last decade." Proceedings of ice scour and arctic marine pipelines workshop, 13th international symposium on Okhotsk sea & sea ice Monbestu, Hokkaido, Japan p33-42.

Woodworth-Lynas, C.M.T. and J.Y. Guigne. (1990)."Iceberg scours in the geological record: examples from glacial Lake Agassiz." In, Glacimarine environments: processes and sediments (J.A. Dowdeswell and J.D. Scourse, eds.). Geological Society Special Publication No. 53: 217-233.

Woodworth-Lynas, C.M.T., R. Phillips, J.I. Clark, F. Hynes and X. Xiao (1998). "Verification of centrifuge test results against field data: results from PRISE". Proceedings of ice scour and arctic marine pipelines workshop, 13th international symposium on Okhotsk sea & sea ice Monbestu, Hokkaido, Japan pp.123-138.

Woodworth-Lynas, C.M.T., Bass, C.W. and Bobbitt, J. (1986). **Inventory of Upslope and Downslope Iceberg Scouring.** Environmental Studies Revolving Fund, Report Number 39, Ottawa, ON, Canada, 103p.

Workman, G.H., (1992). Design study of submerged sidebend response. *Proc. 11th Int. Conf. Offs. Mech. Arctic Engrg.*, Calgary, Alberta, vol. 5, pp. 367-373.

Yang, Q.S., Poorooshasb, F. and Poorooshasb, H.B. and (1991). *Analysis of Subscour Deformation by Finite Element Method.* **4th Canadian Conference on Marine Geotechnical Engineering**, Volume 2, St. John's, NF, Canada, pp739-754.

Yang, Q.S., Poorooshab, F. and Poorooshab H.B. (1993), Analysis of subscour deformations by finite element method. *Proc. 4th Canadian Conf. on Marine Geotech. Engr.*, St. John's, NF, pp.739-754.

Yang, Q.S., Lach, P.R., Clark, J.I. and Poorooshab H.B. (1994), Comparisons of physical and numerical models of ice scour. *Proc. 8th Int. Conf. Comp. Meth. Adv. Geomech.*, Morgantown, WV, pp.1795-1801.

Yang, Q.S., Poorooshab H.B. and Lach, P.R. (1996), Centrifuge modelling and numerical simulation of ice scour, *Soils and Foundations*, 36(1):85-96.

Yang, Q.S. and H.B. Poorooshasb, (1997). Numerical modeling of seabed ice scour. *Computers and Geotechnics,* 21(1):1-20.

Yin, J-H., Paulin, M.J., Clark, J.I. and Poorooshasb, F. (1993). *Preliminary Finite Element Analysis of Lateral Pipeline/Soil Interaction and Comparison to Centrifuge Model Test Results.* Proceedings, 9th International Conference, Offshore Mechanics and Arctic Engineering, **OMAE**, Volume V, Houston, TX, USA, pp. 143-155.

Yoon, K.-Y., Choi, K. and Park, H.-I. (1997). *A Numerical Simulation to Determine Ice Scour and Pipeline Burial Depth.* Proceedings, 7th International and Offshore Polar Engineering Conference, **ISOPE**, Volume II, Honolulu, HW, USA, pp. 212-219.

Yoshizaki, K., H. Ando and N. Oguchi, (1998). Large deformation behavior of pipe bends subjected to in-plane bending. *Proc. Int. Pipeline Conf.*, ASME, vol.2, pp. 733-740.

Zhou, Z. and Murray, D.W. (1993). *Behaviour of Buried Pipelines Subjected to Imposed Deformations.* Proceedings, 12th International Conference, Offshore Mechanics and Arctic Engineering, **OMAE**, Volume V, Houston, TX, USA, pp. 115-122.

Zhou, J.Z and D.P. Harvey, (1996). A model for dynamic analysis of buried and partially buried piping systems, *Pressure Vessels and Piping Systems,* PPV, vol. 331, ASME, pp. 21-29.

APPENDIX A

AARI Ice/Seabed Interaction Model

The model developed by AARI was originally created with reference to the design of pipelines crossing Baydaratskaya Bay. It replaces the actual shape of the scouring hummock by a simple shape (Figure A.1) by assuming that small irregularities of the hummock shape should not influence the process of scouring (i.e. the simple geometric shape is a dynamically equivalent body).

The deterministic model of scouring is based on an energy balance approach similar to that of Chari (1975). It is assumed that before scouring begins, the hummock has some kinetic energy, E which is expended by work of the soil resistance force, P. The force P is variable in time and depends on the topography of the seabed, soil properties, geometry of the hummock's keel, and other factors. The following assumptions are made about the interaction process:

- the hummock keel has the form of a parallelepiped with an inclined front side,
- during the hummock's movement a wedge of soil is pushed out, and
- the surface that separates the wedge and stationary soil (surface of failure) is a segment of a plane.

Up to this stage in the development, seabed slope angle has been considered constant. A more general solution applicable to arbitrary bottom topography is introduced below.

Force P is found from two equations of the wedge equilibrium. These equations are deduced for cohesive soils and include (Figure A.2) the forces N and S which are normal and tangent respectively to the plane of failure, the weight of the wedge W_s and the friction force S' along the sides of the soil wedge. The equations of the soil wedge's equilibrium follow.

For the projection of the forces on the horizontal axis:

$$P = S\cos\theta + N\sin\theta + 2S' \qquad (1)$$

For the projection of the forces on the vertical axis:

$$N\cos\theta = W_s + 2S' + S\sin\theta \tag{2}$$

$$\theta = \frac{\pi}{4} + \frac{\varphi}{2}$$

where:

φ angle of internal friction of the soil;

P the resistance force (P is considered as a motion velocity independent value);

N force normal to the front plane of the soil wedge;

S the force tangent to the front plane of the soil wedge;

W_s weight of the soil wedge;

S' the force of friction at the sides of the soil wedge.

The angle θ is always greater $\pi/4$ and φ should be less than $\pi/4$.

$$W_s = B \times \gamma \times C_B \tag{3}$$

where:

γ → specific weight of the soil in water;

B → width of the wedge (coincides with width of the keel of the model hummock);

C_B → area of the lateral side of the wedge i.e. of a triangle with sides $(d + h)/\cosh$ and X_1 and angle $\frac{1}{2}p\text{-}q\text{-}h$ between them.

$$X_1 = \frac{(d+h)(1+tg\eta \times tg\varphi)}{\cos\theta \times tg\varphi + \sin\theta} \tag{4}$$

$$\begin{aligned} CB &= \frac{1}{2}\frac{(d+h)}{\cos\eta}\frac{(d+h)\times(1+tg\eta\times tg\varphi)}{\cos\theta\times tg\varphi+\sin\theta}\cos(\theta+\eta) \\ &= \frac{(d+h)^2(1+tg\eta\times tg\varphi)(\cos\theta - tg\eta\times\sin\theta)}{2\cos\theta\times tg\varphi+\sin\theta} \end{aligned} \tag{5}$$

$$Ws = \frac{\gamma B(h+d)^2}{2} \frac{(1+tg\eta \times tg\varphi)(1-tg\eta \times tg\varphi)}{tg\varphi + tg\eta} \quad (6)$$

The friction force:

$$S = \frac{\tau}{\sqrt{2}} C'_A \quad (7)$$

where:

τ tangent stresses in the soil, t= $s \cdot t \cdot g \cdot f + C$;

σ normal stresses (it is assumed that these stresses are zero on the sides of the wedge);

C cohesion of the soil;

C'_A area of the triangle with sides $d/cosf$ and X_1 with angle $\frac{1}{2}p-q-f$ between them.

$$\begin{aligned} C'_A &= \frac{1}{2} \frac{d}{\cos\varphi} X_1 \sin(\pi/2 - \theta - \varphi) \\ &= \frac{1}{2} \frac{d}{\cos\varphi} \frac{d(1-tg\beta \times tg\varphi)}{(\sin\theta - \cos\theta \times tg\beta)} \cos(\theta + \varphi) \\ &= \frac{d^2}{2} \frac{(1-tg\beta \times tg\varphi)(1-tg\theta \times tg\varphi)}{tg\theta - tg\beta} \end{aligned} \quad (8)$$

$$S' = \frac{\tau}{2} \frac{d^2}{\sqrt{2}} \frac{(1-tg\beta \times tg\eta)(1-tg\theta \times tg\eta)}{tg\theta - tg\beta} \quad (9)$$

The force tangent to the surface of failure is equal to:

$$S = X_1 \tau B = \frac{\tau d B(1-tg\beta \times tg\eta)}{\sin\theta - \cos\theta \times tg\beta} \quad (10)$$

The force normal to the surface of failure is equal to:

$$N = \frac{1}{\cos\theta}\left(W_s + 2S' + S \times \sin\theta\right)$$
$$= \frac{1}{\cos\theta}\left[\frac{\gamma B(h+d)^2}{2}\frac{(1-tg\eta \times tg\varphi)(1-tg\eta \times tg\theta)}{tg\varphi + tg\theta} + \right. \quad \textbf{(11)}$$
$$\left. + \frac{\pi d^2}{\sqrt{2}}\frac{(1-tg\beta \times tg\eta)(1-tg\theta \times tg\eta)}{tg\theta - tg\beta} + \sin\theta \times \frac{\pi dB(1-tg\beta \times tg\eta)}{\sin\theta - \cos\theta \times tg\beta}\right]$$

Thus the resistance force P:

$$P = S\cos\theta + N\sin\theta + 2S' \quad \textbf{(12)}$$

Inserting expressions for S, N, and S' obtained above after simple transformation we arrive at the following:

$$P = dp_1 + d^2 p_2 + (h+d)^2 p_3 \quad \textbf{(13)}$$

where:

$$p_1 = \frac{B\tau(1-tg\beta \times tg\eta)}{\cos\theta \times (\sin\theta - \cos\theta \times tg\beta)} \quad \textbf{(14)}$$

$$p_2 = \frac{T(1-tg\beta \times tg\eta)(1-tg\theta \times tg\eta)(1+tg\theta)}{\sqrt{2}(tg\theta - tg\beta)} \quad \textbf{(15)}$$

$$p_3 = \frac{\gamma \times B}{2}\frac{(1+tg\varphi \times tg\eta)(1-tg\theta \times tg\eta)tg\theta}{tg\varphi + tg\theta} \quad \textbf{(16)}$$

Where:

$$d = kl$$

$$L = k_l l$$

$$k = tg\beta$$

$$k_l = \frac{tg\varphi + tg\beta}{1 + tg\varphi \times tg\eta}$$

l and l_0 are the length of furrow behind the ice hummock and the length of the berm in front of the ice hummock respectively.

Hence P depends on the variables l and l_0 in the following way:

$$P = lq_1 + l^2 q_2 + ll_l q_3 + l^2 q_4 \quad \textbf{(17)}$$

$$q_1 = p_1 k\,,\; q_2 = (p_2 + p_3)k^2 \quad \textbf{(18)}$$

$$q_3 = 2p_3 k k_l\,,\; q_4 = p_3 k_l^2 \quad \textbf{(19)}$$

Thus, the forces normal and tangent to the surface of failure depend on normal and tangential stresses in the soil. In accordance with the theory of limit equilibrium, these stresses in turn are functions of such soil characteristics as cohesion and the angle of internal friction. Solution of the system of two equations of soil wedge equilibrium in relation to the force P results in non-linear dependence of P on both variables l and l_l. Where l is the length of the furrow (angle of the seabed inclination is assumed a constant value here) and l_l the length of the berm in front of hummock.

In order to exclude one of these variables i.e. to determine the function $l_l = f(l)$, it is necessary equate the soil volume taken from the furrow with the soil located on the side and front berms. Berm shape is assumed as shown in Figure A.3.

The equating the volumes gives:

$$V_{HBCMIA} = V_{HIJL} + V_{JILK} + V_{IADLKE} + V_{ADGE} + V_{BDAG} \quad (20)$$

Taking into consideration the geometric correlations:

$$l_{AB} = \frac{l}{\cos\beta} \quad (21)$$

$$l_{AC} = \frac{d}{\cos\eta} = \frac{l\,tg\beta}{\cos\eta} \quad (22)$$

$$S_{ABC} = \frac{1}{2} l_{AB} l_{AC} \sin(\beta+\eta) = \frac{l^2}{2} \frac{tg\beta \times \sin(\beta+\eta)}{\cos\beta \times \cos\eta} \quad (23)$$

$$S_{ADE} = \frac{l_1^2}{2} \frac{tg(\varphi+\beta)}{\cos\beta \times (tg(\varphi+\beta) \times tg(\eta+\beta)+1)} \quad (24)$$

$$V_{ADGE} = V_{JILK} = \frac{1}{3} h F_{AEG} = \frac{l l_1^2}{6} \frac{1}{\cos\beta} \frac{tg(\varphi+\beta)}{tg(\varphi+\beta) \times tg(\eta+\beta)+1} \quad (25)$$

$$V_{ABCD} = V_{HIJL} = \frac{1}{3} h F_{ABG} = \frac{l l_1^2}{6} \frac{1}{\cos\beta} \frac{tg(\varphi+\beta)}{tg(\varphi+\beta) \times tg(\eta+\beta)+1} \quad (26)$$

$$V_{IADLKE} = B F_{ADE} = \frac{B l_1^2}{2} \frac{1}{\cos\beta} \frac{tg(\varphi+\beta)}{tg(\varphi+\beta) \times tg(\eta+\beta)+1} \quad (27)$$

$$V_{HBCMIA} = B F_{ABC} = \frac{B l_1^2}{2} \frac{tg\beta \sin(\eta+\beta)}{\cos\beta \cos\eta} \quad (28)$$

Where:

$F_{AEG}, F_{ABG}, F_{ADE}, F_{ABC},$ are areas of the corresponding triangles.

The equation of equal volumes is reduced to the solution of the corresponding triangles.

$$l_1^3 \frac{Y}{3} + ll_1^2 \frac{Y}{3} + l_1^2 \frac{BY}{2} = l^2 \frac{BZ}{2} \quad \textbf{(29)}$$

$$Z = \frac{tg\beta \sin(\eta + \beta)}{\cos\beta \cos\eta} \quad \textbf{(30)}$$

$$Y = \frac{tg(\eta + \beta)}{\cos\beta(tg(\varphi + \beta)tg(\eta + \beta) + 1} \quad \textbf{(31)}$$

The result of the equation solution is the function $l_1 = f(l)$.

Thus, we obtain the expression, which determines P as a function of the length of the furrow. The integration of this function gives the work of the soil resistance force A_p. The length of the furrow is determined by the condition that $A_p=E$, where E is initial kinetic energy of the drifting hummock. This equation implies that the total kinetic energy is expended in the work of the soil resistance force, after which the ice hummock stops moving. The depth of scour is easily determined from the length of the furrow (at the constant angle of seabed inclination), as they are connected by a simple geometric relationship.

The following algorithm for the calculation of the scour depth is used:

1. Calculate the coefficients $p_1, p_2, p_3, q_1, q_2, q_3, q_4$.
2. With the step Δl, the resistance force $P(l)$ for the current length of a furrow l is estimated as the solution of the following system of non-linear equations:

$$\begin{cases} P = P(l_1 l_2) \\ l_1 = f(l) \end{cases} \quad (32)$$

3. The work of the resistance force is calculated by the integration:

$$A_p = \int_0^l P(l)dl \quad (33)$$

If $A_p < E$, where E is the initial kinetic energy of an ice feature, then previous steps of the algorithm are repeated. If $A_p = E$, then the obtained length of the furrow l is used for calculating the depth of the furrow d.

4. Scour depth, then is written as:

$$d = l \cdot t \cdot g \cdot \beta \quad (34)$$

where β is the angle of seabed slope.

The algorithm described assumes that the seabed slope and the properties of the soil are constant along the whole length of a furrow. However, this is hardly the case for natural conditions. A more general version of this algorithm was developed to take into consideration the non-uniformity of the soil properties and seabed slope. The bottom profile along the line of the hummock motion is expressed as a sequence of the line segments specified by their nodal points. In this case the algorithm described earlier can be consecutively applied to each segment. The kinetic energy of the hummock after movement within the range of the previous segment is equal to the initial kinetic energy, E_b, before movement within the boundary of the segment being examined.

Four possible cases of hummock-seabed interaction can take place within each segment:

- the hummock interacts with the seabed at the initial point of the segment and scours the bottom along entire segment length;
- the hummock starts interacting with the seabed at an intermediate point of the segment and scours the bottom along the remainder of the segment length;

- the hummock interacts with the seabed at the initial point of the segment and exits the seabed at an intermediate point;
- the hummock starts interacting with the seabed at an intermediate point of the segment and exits the seabed at another intermediate point.

In all these interaction cases, the scour parameters at the segment are calculated using the known 3D co-ordinates of the segment and the kinetic energy, E_b of the hummock before entering the segment. The properties of the soil are assumed to be constant within the segment. If $E_b < A_p$ the ice hummock is considered to stop moving due to total expenditure of its kinetic energy.

An additional analysis was conducted to determine the influence of soil failure surface curvature on scour depth. The analysis showed that the insertion of this factor resulted in not more than 1.5 % difference of scour depth estimation within the considered range of seabed slopes, while, computer processing time increased considerably. Due to this reason curvature of the boundary surface was not accounted for in further calculations.

Analysis of the influence of hydrodynamic and aerodynamic forces acting on the hummock during its interaction with the soil has also been carried out. The simplified estimations showed that in the case of drift of a single hummock, the accounting for the influence of these forces gave an increase in scour depth of not more than 8 %. These estimations were based on the presentation of these forces as:

$$C(\rho V^2/2) \qquad \textbf{(35)}$$

Where:

- C drag coefficient (for the ridge sail when calculating aerodynamic force and for the ridge keel when calculating hydrodynamic force),
- ρ air/water density, and
- V relative wind/current velocity.

Drag coefficient was estimated assuming a parallelepiped hummock with dimensions equal to those of the ridge. For the case where the interaction of a vast ridged ice field with the seabed is considered, the hydrodynamic and aerodynamic drag forces would cause overall interaction forces to be greater.

1.2.3.1 Recommended directions of further work

1. The energy balance approach under predicts scour depths and is not applicable if considering the interaction of a vast ridged ice field with the seabed (rather than a separate hummock). A more general approach is based on the solution of ordinary differential equations of ice feature dynamics. Hydrodynamic and aerodynamic forces (including drag forces) may be introduced in these equations.

2. Finite element analysis of ice feature/seabed soil interaction seems the most promising way to get more reliable theoretical estimations of maximum scour depths. In fact, the prediction of scour depth and evaluation of soil and pipeline response is recommended for consideration as one problem. Taking into account that the finite element method is very computer time consuming, it is advisable to get simplified regression (parametric) dependencies by processing numerical simulation results. This is required for performing Monte Carlo modelling, since thousands of interaction events could be simulated.

3. Model and field tests of ice/soil interaction are an important source of knowledge on the mechanics of scour processes. These tests provide both input information for theoretical models and necessary data for validation of the models.

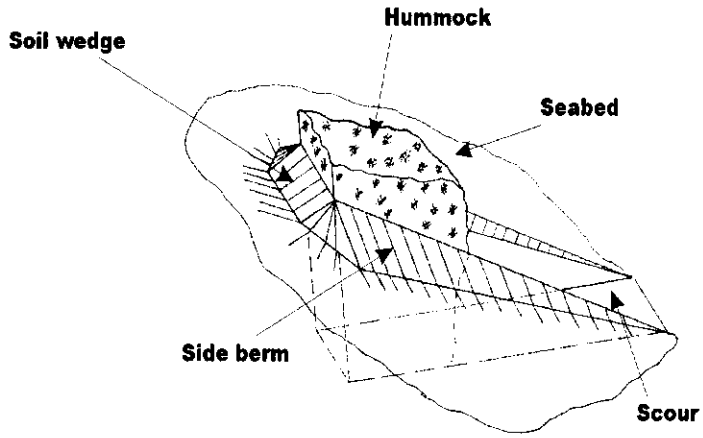

Figure A.1 Interaction of the model ice hummock with the seabed.

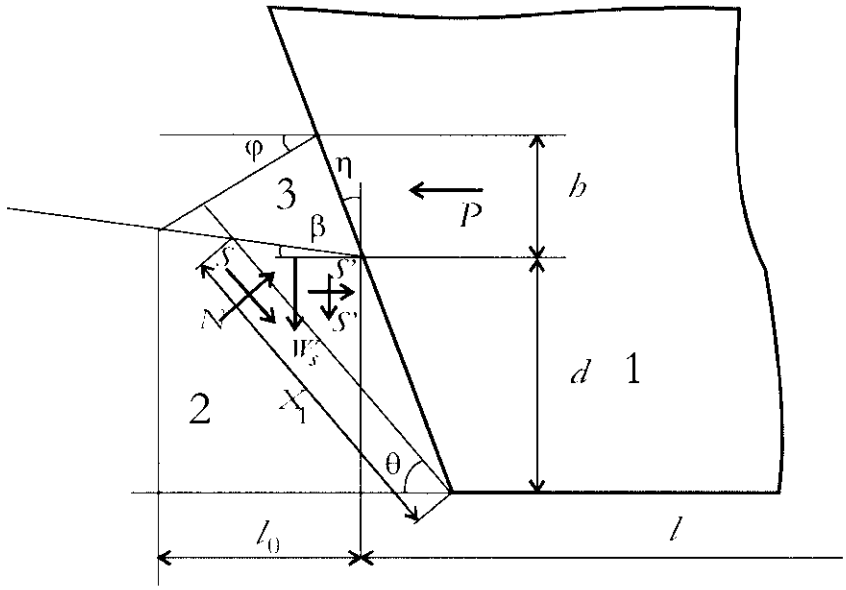

Where:

S,N = tangential and normal components of the force of interaction of the wedge with stationary soil

$\mathbf{W_s}$ = weight of the soil wedge

S' = friction on the sides of the wedge

1 = hummock

2 = seabed soil

3 = soil wedge

Figure A.2 Interaction of model ice hummock with the seabed.

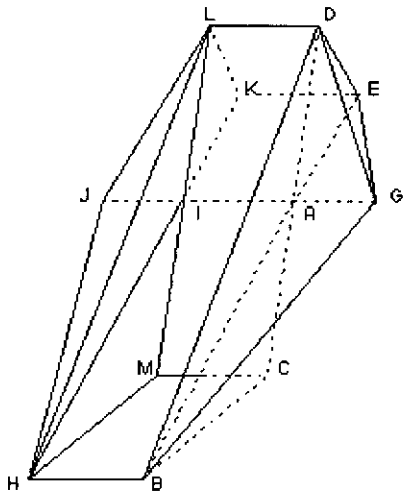

Figure A.3 The geometric representation of the form of the berms and furrow (furrow = HBCMIA, side berms = HIKLJ and BAEDG, front berm = IADLKE)

Appendix B

Subgouge Deformation Models

B.1 AARI Model

The mathematical formulation of the AARI model for the analysis of indirect interaction of a drift ice feature with a buried pipeline is based on a variant of the Winkler foundation model. Consider a buried pipeline subjected to vertical and horizontal loads as illustrated in Figure 1.3.2. The elastic semi-space is bounded by the xy-plane for $z > 0$. A beam of infinite length (L) parallel to the y-axis is situated within the semi-space at a depth (H) from the surface. Distributed loads (p_x, p_z) act on the surface (S) located in the xy-plane along the x-axis and z-axis, respectively.

Displacements of the semi-space point Q along the x-axis and z-axis can be defined as,

$$\begin{aligned} U_{x p_x}(Q) &= \int_S K_o^{xx}(Q,Q')\, p_x(Q')\, dQ' \\ U_{x p_z}(Q) &= \int_S K_o^{xz}(Q,Q')\, p_z(Q')\, dQ' \\ U_{z p_x}(Q) &= \int_S K_o^{zx}(Q,Q')\, p_x(Q')\, dQ' \\ U_{z p_z}(Q) &= \int_S K_o^{zz}(Q,Q')\, p_z(Q')\, dQ' \end{aligned} \qquad \text{(B.1)}$$

where $U_{i p_j}(Q)$ is the displacement of the semi-space point (Q) along the i-axis due to the distributed load (p_j) acting on the surface (S) along the j-axis, and $K_o^{ij}(Q,Q')$ is the displacement of the semi-space point (Q) along the i-axis due to a unit force acting at point (Q') along the j-axis.

The interaction forces per unit pipeline length, acting between the beam and semi-space, along the x-axis and z-axis can be defined as (q_x, q_z), respectively. Similarly, the displacements of point (Q) due to these forces applied to the semi-space along the beam axis can be expressed as,

$$
\begin{aligned}
U_{xq_x}(Q) &= \int_L K_o^{xx}(Q,Q')\,q_x(Q')\,dQ' \\
U_{xq_z}(Q) &= \int_L K_o^{xz}(Q,Q')\,q_z(Q')\,dQ' \\
U_{zq_x}(Q) &= \int_L K_o^{zx}(Q,Q')\,q_x(Q')\,dQ' \\
U_{zq_z}(Q) &= \int_L K_o^{zz}(Q,Q')\,q_z(Q')\,dQ'
\end{aligned}
\qquad \text{(B.2)}
$$

where $U_{iq_j}(Q)$ is the displacement of the semi-space point (Q) along the i-axis due to the interaction force (q_j) acting on the surface (S) along the j-axis, and $K_o^{ij}(Q,Q')$ is the displacement of the semi-space point (Q) along the i-axis due to the interaction force acting at point (Q') along the j-axis.

Beam axis displacement due to interaction forces (q_x, q_z) is defined by,

$$
\begin{aligned}
U_x(Q) &= \int_L K_{bx}(Q,Q')\,q_x(Q')\,dQ' \\
U_z(Q) &= \int_L K_{bz}(Q,Q')\,q_z(Q')\,dQ'
\end{aligned}
\qquad \text{(B.3)}
$$

where ($K_{bi}(Q,Q')$) represent a beam influence function defined to prevent rigid body displacement where the beam displacement at point (Q) along the i-axis due to the unit force acting at point (Q') along the i-axis.

To deduce equations defining interaction forces between the semi-space and the beam, set the beam displacements due to interaction forces equal to displacements of the semi-space along the line (L) due to external and interaction forces. The corresponding equations are expressed as,

$$
\begin{aligned}
U_x(Q_L) &= U_{xq_x}(Q_L)+U_{xp_x}(Q_L)+U_{xq_z}(Q_L)+U_{xp_z}(Q_L) \\
U_z(Q_L) &= U_{zq_x}(Q_L)+U_{zp_x}(Q_L)+U_{zq_z}(Q_L)+U_{zp_z}(Q_L)
\end{aligned}
\qquad \text{(B.4)}
$$

A system of two integral equations for two unknown interaction functions can be obtained through direct substitution of Equations (B.1), (B.2) and (B.3) into (B.4). Employing a system of linear algebraic equations, the solution can be calculated by numerical methods. The algorithm was based on the work of Mindlin (1953).

B.2 C-CORE Model

The soil deformation functions were derived from analysis of centrifuge modelling of ice gouge experiments conducted under PRISE. The basis has been presented by (CCORE, 1997) and Woodworth-Lynas et al. (1996). A three-dimensional spatial variation defined the subgouge deformation field (Figures 1.3.3 and 1.3.4). The coordinate system was comprised of two axes in the horizontal, *xy*-plane (Figure 1.3.4). The *y*-axis was collinear with the ice gouge centreline, in the direction of the gouge track, with the orthogonal *x*-axis at the ice keel base in contact with the seabed. The origin is located at the intersection of the *x*-axis and *y*-axis. This represents the maximum extent of Zone 1 (Figure 1.2.?), equal to the gouge depth (d) and demarcation for the subgouge deformation (Zone 2). The *z*-axis extends vertically from the origin with soil depth.

As illustrated in Figure 1.3.3, the maximum transverse horizontal displacement (u_o) for Zone 2 at the coordinate system origin [$(x,y,z) = (0,0,0)$] is,

$$u_o(0,0,0) = C_1\sqrt{wd} \tag{B.5}$$

where C_1 is a constant ($C_1 = 0.6$ for clay; $C_1 = 1.0$ for sand), w is the gouge width (m) and d is the gouge depth (m). The parameter (u_c) defines the vertical profile of horizontal soil displacement (Figure 1.3.3),

$$u_c(0,0,z) = u_o \exp\left[-\frac{2(z-d)}{3d}\right] \tag{B.6}$$

as a function of soil depth (z) and ice gouge depth (d). The longitudinal distribution of horizontal soil displacement (u_x), as shown in Figure 1.3.4, can be defined as a function of gouge width (w),

$$u_x(0,y,z) = \begin{cases} u_c & x \le \frac{w}{2} - \frac{w_l}{4} \\ \frac{u_c}{2}\left[1+\cos\left(\frac{4x-2w+w_l}{2w_l}\pi\right)\right] & \frac{w}{2} - \frac{w_l}{4} \le x \le \frac{w}{2} + \frac{w_l}{4} \\ 0 & x > \frac{w}{2} - \frac{w_l}{4} \end{cases} \quad \text{(B.7)}$$

where x is the perpendicular distance from the gouge centreline in the direction of gouge width (w) and w_l is the limited gouge width (m) expressed as the minimum of (w_l = *min[w, 20m]*). Equations (B.5), (B.6) and (B.7) completely define the three-dimensional subgouge displacement field.

Appendix C

Buried Pipeline Response Models

C.1 ASCE Model

ASCE (1984) present guidelines for modelling differential ground movement effects on buried pipelines. Soil load-deformation relationships for cohesive and granular soil are proposed. A summary of the formulations is presented. Specific details on the analytical and experimental basis applied to define the soil response functions are discussed in ASCE (1984).

Granular Soil

The yield axial (t), horizontal (p) and vertical downward (q) soil reaction loads per metre length (kN/m) for drained granular soil conditions are

$$\begin{aligned} t_u &= \frac{\pi D_o}{2} \gamma' H_s (1 + K_o) \tan\delta \\ p_u &= \gamma' H_s N_{qh} D_o \\ q_u &= \gamma' H_s N_q D_o + \frac{1}{2} \gamma D_o^2 N_\gamma \end{aligned} \qquad \text{(C.1)}$$

where D_o is the outside pipe diameter (m), γ' is the effective unit weight of soil (kN/m^3), H_s is the pipeline burial depth from the seabed surface to the pipeline neutral axis or springline (m), K_o is the coefficient of earth pressure at rest (Jaky, 1944) as,

$$K_o = 1 - \sin\phi \qquad \text{(C.2)}$$

where ϕ is the internal friction angle (degrees), δ is the interface friction angle (degrees) defined in the range $0.5\phi \le \delta \le 1.0\phi$ and N is the bearing interaction factor. For dense to loose sands, the yield axial (x), horizontal (y) and vertical downward (z) soil displacements are defined as,

$$\begin{array}{rcccl} 2.5mm & \leq & x_u & \leq & 5.0mm \\ 0.02(H_s + D_o) & \leq & y_u & \leq & 0.10(H_s + D_o) \\ 0.010\,D_o & \leq & z_u & \leq & 0.015\,D_o \end{array} \qquad \text{(C.3)}$$

Cohesive Soil

The yield axial (t), horizontal (p) and vertical downward (q) soil reaction loads per metre length (kN/m) for undrained cohesive soil conditions are

$$\begin{aligned} t_u &= \pi \mu D_o C_u \\ p_u &= N_{ch} D_o C_u \\ q_u &= N_c D_o C_u \end{aligned} \qquad \text{(C.4)}$$

where μ is the cohesion reduction factor.

For stiff to soft sands, the yield axial (x), horizontal (y) and vertical downward (z) soil displacements are defined as,

$$\begin{array}{rcccl} 5.0mm & \leq & x_u & \leq & 10.0mm \\ 0.03(H_s + D_o) & \leq & y_u & \leq & 0.05(H_s + D_o) \\ 0.010\,D_o & \leq & z_u & \leq & 0.015\,D_o \end{array} \qquad \text{(C.5)}$$

C.2 C-CORE Model

The response of a buried arctic marine pipeline subject to an ice gouge event is analysed by the finite element method. The procedure can be adapted for any soil/pipeline interaction problem with arbitrary deformations. Three coupled components define the numerical model, namely; ice

gouge/soil relationships, soil/pipeline interaction and finite element formulation. These issues are addressed in Section 1.

The finite element analyses were conducted using ABAQUS/Standard version 5.7. The soil/pipeline interaction model (Figure 1.4.1b) was discretised by two-dimensional beam elements (PIPE22) and one-dimensional spring elements (SPRINGA). The finite element model accounted for longitudinal symmetry and the geometric boundary conditions are illustrated in Figure C-1.

The beam element is based on Timoshenko beam theory assuming linear elastic, transverse shear behaviour. Three degrees of freedom per node are active and the behaviour is defined by quadratic shape functions. Two additional variables related to hoop strain account for internal pressurization. For a one-dimensional model, the constitutive relationship is defined by the Ramberg-Osgood formulation,

$$\varepsilon = \frac{\sigma}{E}\left[1+\alpha\left(\frac{\sigma}{\sigma_y}\right)^{n-1}\right] \tag{C.1}$$

where ε is the strain, σ is the applied stress, E is the elastic modulus, α is the plastic yield offset, σ_y is the yield stress and n is the hardening exponent. The default Simpson's rule (5-point) integration scheme is adopted. A von Mises yield criterion, with isotropic strain hardening, was employed and is shown in Figure C-2. For the analysis conducted in the present study, the hardening exponent (n) was adopted from INTEC (1998) and the plastic yield offset was calculated ($\alpha = 0.005\, E/\sigma_y - 1$). The defined pipeline response was slightly stiffer than the constitutive relationships presented by Walker and Williams (1995), as shown in Figure C-3.

The soil response is defined by nonlinear spring elements for the axial and horizontal soil deformation. An idealised bilinear, elastic, perfectly plastic load-deformation relationship is

considered. For a given pipeline burial depth, the subgouge deformation was determined for a particular gouge geometry and soil profile at the neutral axis (i.e. springline) of the buried pipeline. The resultant displacement field would be imposed on the horizontal spring elements as an initial displacement boundary condition. Thus, the relative soil displacement, due to the ice gouge event, would be coupled in the finite element model.

The finite element solution accounted for fully nonlinear behaviour (i.e. geometric and material) with large displacement and strain capabilities. The time step was subdivided into 50 increments with Newton's method employed for equilibrium iterations. In order to obtain a convergent solution, the longitudinal axis of the spring elements remained orthogonal to the reference datum (Figure C-1). This is due to the zero transverse stiffness of the element (SPRING A). The post-processing included beam element stress-strain data (output at the integration points), bending moments (averaged at the nodes) and nodal displacements. The data output for the spring elements included centroidal force and displacement.

The rationale for numerical modelling the coupled ice gouge/soil/pipeline interaction is illustrated in Figure C-3. Direct inputs for the finite element model are physical characteristics of the pipeline, the load-displacement relationship for the soil reaction springs and the imposed displacement field due to the scour event. Indirect parameters are pipeline burial depth, physical features of the scour event and geotechnical properties. Output from the finite element model includes the imposed displacement field, pipeline stress-strain response, soil reaction loads, soil deformation and stress history.

The finite element model has some inherent assumptions and limitations, such as the soil spring approximation of continuum behaviour. Furthermore, issues concerning buckling, ovalisation, and variation of soil displacement with soil strength are not addressed. In addition, the decoupling of the ice/soil and soil/pipe interactions may not be appropriate in some situations. These issues directly impact pipeline burial depth optimisation strategies

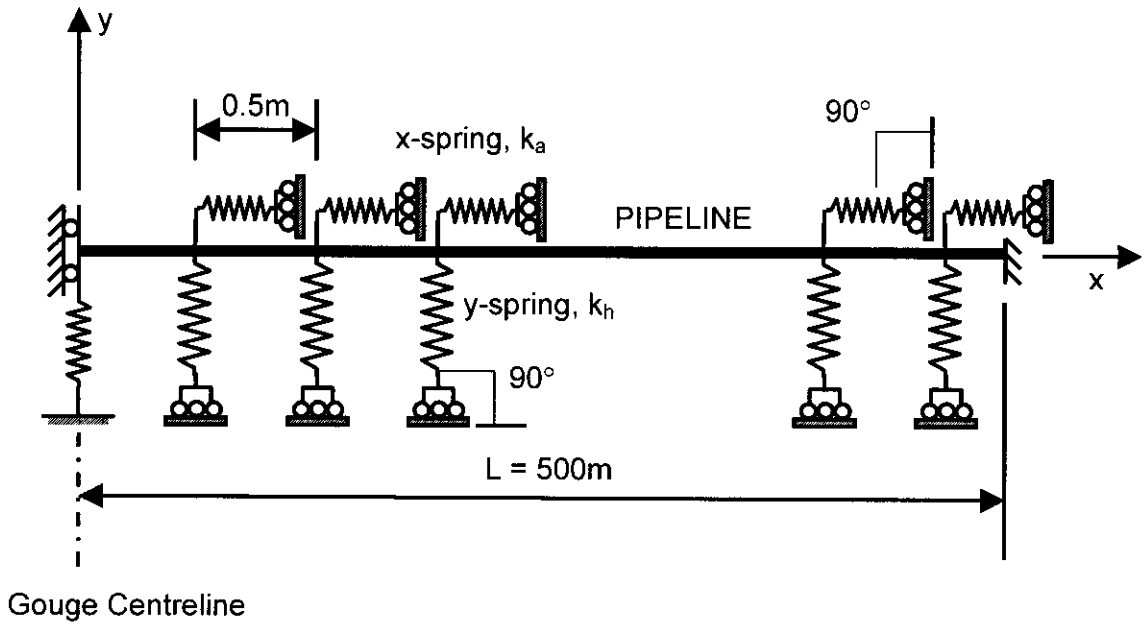

Figure C-1. Schematic illustration of finite element model and geometric boundary conditions.

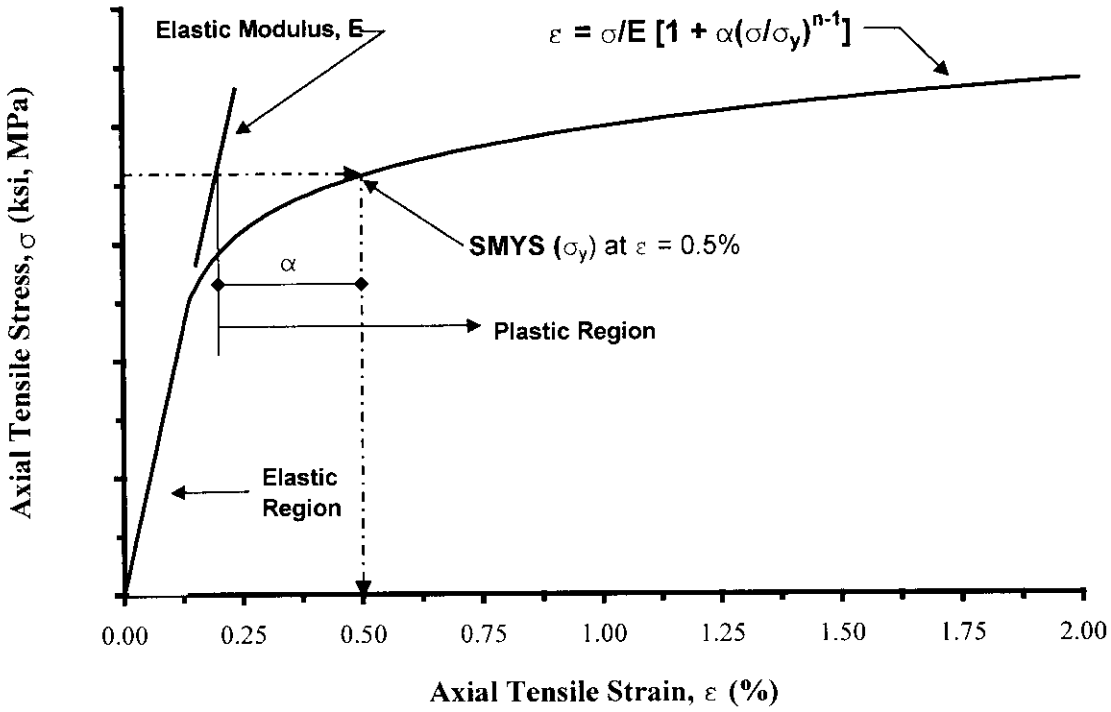

(a)

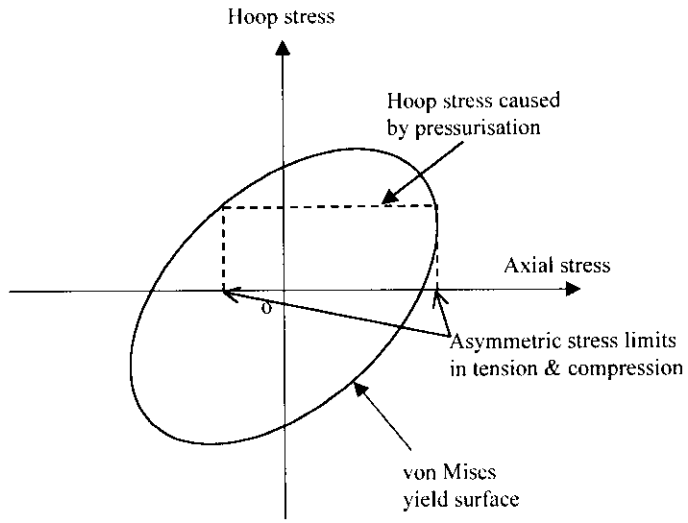

(b)

Figure C-2. Material Characterisation for the Pipeline Elements (a) Ramberg-Osgood Stress-Strain Response and (b) von Mises Yield Surface.

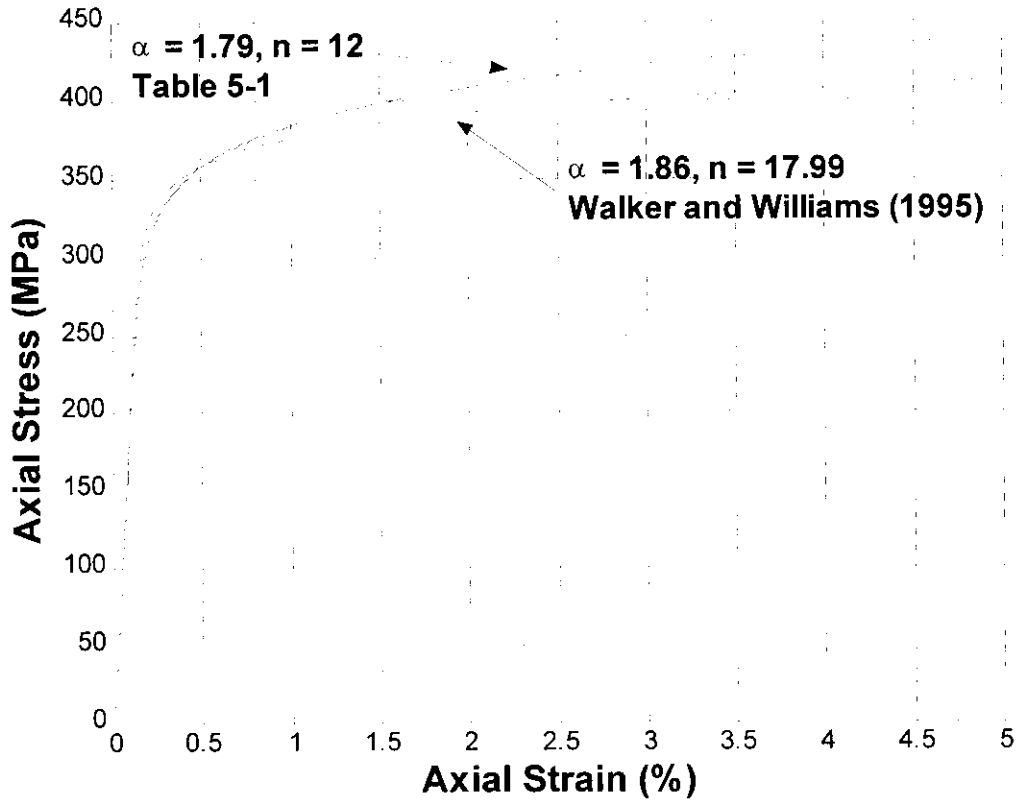

Figure C-3. Pipeline stress-strain characteristics defined by the Ramberg-Osgood formulation.

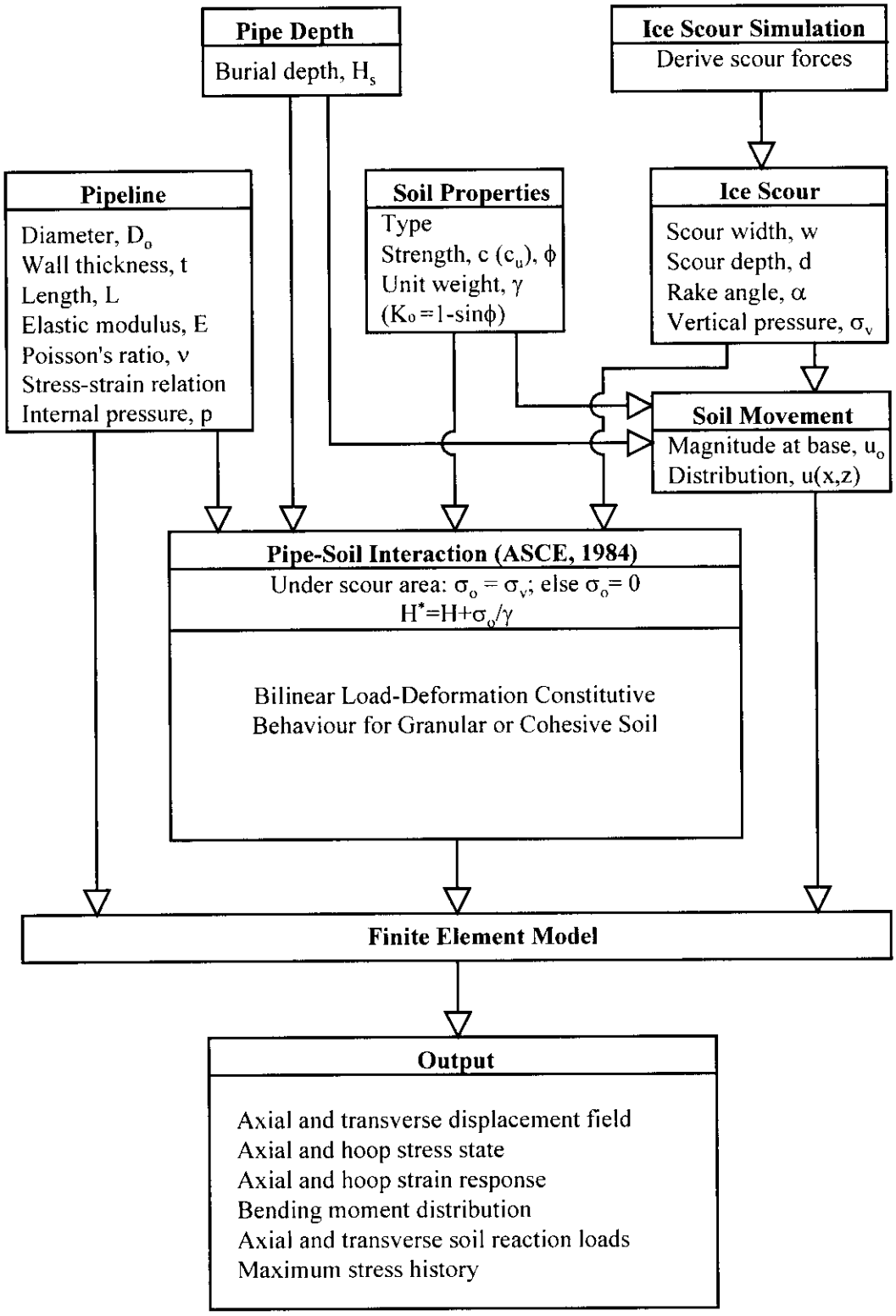

Figure C-4. Rationale for numerical modelling of ice gouge/soil/pipeline interaction.

Appendix D

Scour Forces and Subscour Deformations - Experimental Observations

Pressure Ridge Ice Scour Experiment, (C-CORE 1995, 1997a)

Subscour deformations:

Scour depths considered in the experimental program: for clay D=0.8 - 1.5 m and for sand D=0.2 - 2.2 m.

Horizontal subscour deformation:

For clay:

- Effect of scour depth: A definite pattern of subscour centreline horizontal displacement is apparent with a horizontal deformation of about 2.5D under scour, diminishing to 0 at a depth of about 4D.
- Effect of scour width: No significant effect of keel width has been observed.

For sand:

- Effect of strength: The effect of relative density is apparent in tests. Although the extent of subscour deformation is about the same for the dense and loose sands, the magnitude of horizontal deformation is greater for dense sand[1].

For both sand and clay: The effect of changes in attack angle of the keel on the horizontal centreline subscour deformation could not be determined.

Vertical subscour deformation:

For clay:

- Effect of scour depth: Vertical deformations are felt down to about seven scour depths below the keel.

For both sand and clay soils, no effect of scour width and keel angle on vertical subscour deformation could be determined.

[1] This is contrary to the results of previous small scale 1g tests (Poorooshasb et al. 1989), in that the magnitude of horizontal displacements in dense sand was greater near the surface but quickly decreased to zero with depth.

Scour forces:

Horizontal scour forces:

For clay:

- Effect of scour depth: Horizontal forces increase linearly with scour depth. For example:

  F_h=10.1 MN/m for scour depth D=0.8 m

  F_h=18 MN/m for scour depth D=1.49 m

  for the same clay material.
- Effect of attack angle: With increase of attack angle horizontal scouring force decrease.
- Effect of strength: As expected the horizontal scour force is greater as the strength of the seabed increases.

For Sand:

- Effect of scour depth: Horizontal forces increase with scour depth. For example:

  F_h=19.4 MN for scour depth 1.18 m

  F_h=40.2 MN for scour depth 2.14 m

  for the same sand material.
- Effect of attack angle: Steeper the attack angle smaller the scouring force.
- Effect of strength: Unexpectedly, the relative density of the sandy seabed did not significantly influence the horizontal scour force for the tests reported in this study.

Vertical to horizontal forces ratio:

For clay:

$F_v=\zeta.F_h$; ζ=1.03–2.67 with mean value of 1.91

For sand:

$F_v=\zeta.F_h$; ζ=0.85–1.04 with mean value of 0.99

Experimental Work by Lach (1996)

Centrifuge tests were performed at 100g using a soft clay (Speswhite Kaoline clay) to simulate the seabed.

Subscour deformation:

Range of scour depths analysed: D=0.4 - 2.2 m.

Horizontal subscour deformation:

- The magnitude of horizontal displacement at 0.1 m below the scour base ranged from 0.5 to 3.4m, with an average displacement of 1.6 m for all tests.
- The extent of the region of large displacement (i.e. larger than 0.2m) ranged from 1.4 to 3.1 m below the scour base, with an average depth of 2.5 m, corresponding to a normalised value of 2.5 scour depths.

Vertical subscour deformation:

- The magnitude of vertical displacement at the scour base ranged from 0.1 to 0.9 m, with an average displacement of 0.6 m for all tests.
- The extent of the region of large displacement ranged from 0.0 to 6.2 m below the scour base, with an average depth of 2.3 m, corresponding to a normalised value of 2.3 scour depths.

Scour forces:

Vertical to horizontal forces ratio ($Fv=\zeta.Fh$): ζ=1.9–3.9 with mean value of 3.0

Results of Field Observations (subscour deformations)

1. For clay soils of former glacial Lake Agassiz, Woodworth-Lynas and Guigne (1990), described scour marks 50-65m wide, 2-2.5m deep and 0.5-8.5km long. In the soils beneath one scour mark they documented normal faults with dip-slip displacements of at least 3.5m. The faults propagated to depths beyond 5.5m below the deepest part of scour mark. (Woodworth-Lynas 1992, Golder Assoc. 1990).

2. Woodworth-Lynas et. al. developed studies of a deep scour mark in layered granular and (Woodworth-Lynas 1998). The scour mark is steep sided, U-shaped, 10-m wide and 4 m deep with asymmetric berms of excavated diamict material. Scour-induced deformation has caused downward displacement of the lower diamict sequence boundary into underlying deltaic sands. Downward displacement has affected at least the top 2m of underlying sand, and sub-scour deformation can be traced to at least 4.5m below the deepest part of the scour mark.
3. More field observation results are documented by (Woodworth-Lynas 1998 and (Woodworth-Lynas et al. 1998).

Experimental 1g Work Documented by Golder Associates Ltd. (1990).

Golder indentor tests:

Subscour deformations:

- For clay: In cohesive soils, the rupture surface trajectory will generally be near horizontal and therefore subscour disturbance will be minimal.
- For sand: Effect of scour depth: The depth of subscour disturbance increases as the density of the sand subjected to scour decrease. Subscour disturbance would be relatively small for dense sands, which exhibit strain softening behaviour.

Remark: Inertial effects and pore pressure generation in sands due to rapid scouring are potentially important factors, based on a limited number of observations in this project. Conventional drained, static analysis may not be adequate.

Small scale ice scour modelling by C-CORE

For clay:

- Effect of scour depth: Stress changes may be expected at depths greater than 7 times the scour depth.

For sand:

- Effect of keel angle: An increase in rake angle from 15 to 30 degrees reduces the amount of deformation, which appears below the scouring iceberg. Also it changes the angle of the forces which react upon the advancing berg indicating a change in the orientation of a failure wedges in front of iceberg.
- Effect of strength: The denser the sand the less extensive subsurface deformations.

Appendix E

Pipeline Strain Response Analysis

Appendix A5

Pipeline Response Model

A deterministic, parametric analysis to investigate the response of a buried marine pipeline to ice gouge events was conducted. The issues addressed include internal pipeline material grade, pipeline diameter (D_o), gouge width (w), gouge depth (d), ice feature overburden stress (σ_v), subgouge displacement field, soil type (C_u,ϕ) and soil response functions (t_u–x_u, p_u–y_u). Pipeline trench depth was indirectly incorporated through the cover depth (H_c) parameter, which was held at a constant depth of 0.5m below the modelled gouge depth (i.e. $H_c = 0.5m + d$). The complex, nonlinear ice gouge/soil/pipeline interaction was analysed using the finite element method. The model is schematically illustrated in Figure A6-1. A detailed discussion on characteristics of the finite element model has been presented in Sections ??? and Appendices ???. The influence of the variant parameters on the baseline cases (Table 6-1) in terms of the longitudinal distribution of pipeline axial strain is presented.

A5.1 Longitudinal Pipeline Strain Response

A5.1.1 Pipeline Displacement Response

The imposed subgouge soil displacement and pipeline response profiles, for the baseline cases with granular and cohesive soil (Table 6-1), are illustrated in Figure A6-2. The pipeline response (solid, blue line) does not exhibit the steeper, "step-wise" gradient of the soil displacement field (dashed, red line). The moderated pipeline behaviour is due to the greater stiffness and the coupled axial/flexural response. Although the imposed gouge displacements for the granular soil was 1.5 times the cohesive soil peak displacement, similar pipeline displacement and curvature response was demonstrated. For strain based mechanisms such as ice gouging, the soil response functions, within the gouge footprint (dash-dot, black line), are characterised by yield behaviour due to the large magnitude, relative soil displacement field.

A5.1.2 Pipeline Geometry and Mechanical Properties

For the baseline cases of Table 6-1, the computed pipeline axial strains (ε_{11}) as a function of pipeline diameter and material grade are illustrated in Figure A6-3. In reference to Figure A6-1, the solid (blue) line represents integration point 1 ($\varepsilon_{11(1)}$ for pipe coordinate y–$D_o/2$) and the dashed (red) line represents integration point 5 ($\varepsilon_{11(5)}$ for pipe coordinate y+$D_o/2$). The strain profiles represent the longitudinal distribution of pipeline axial strain for the extreme fibers, where the sign convention is compression (-) and tension (+). The vertical dash-dot (black) line represents the extent of the ice gouge width (w).

Increasing the pipeline diameter or provides a more rigid system where the flexural stiffness (EI) is proportional to $EI \propto D_o^3 t$. The penalty for larger diameter pipelines is a reduction in the allowable curvature response with respect to specified strain limits in accordance with design codes or recommended practice. Furthermore, larger diameter pipelines attract a greater load due to the increased projected area, which is incorporated through the soil/pipeline models proposed by ASCE (1984) for example. Selecting higher strength grade material influences the stress–strain characteristics with an increased yield stress and higher flow stress levels.

A5.1.3 Gouge Geometry

Ice gouge geometry (e.g. width, depth) is a significant parameter that defines the subgouge displacement field magnitude and is proportional to $\sqrt{wd}$. The developed pipeline curvature was also influenced by the gouge width (w) through the stepwise change of the relative soil deformation as shown in Figure A6-2.

For the baseline cases of Table 6-1, the computed pipeline axial strains (ε_{11}) as a function of gouge width are illustrated in Figure A6-2. The pipeline response can be generally characterised

by an asymmetric response, which is related to the development of flexural (i.e. compressive and tensile bending deformation) and axial tensile (i.e. stretching) strains due to the large magnitude of the imposed relative soil deformation field. The attenuated strain response demonstrates that end effects arising from the geometric, pipeline boundary conditions are not present, where the modelled pipeline length was 1000m (3281ft).

The coupled interaction between gouge width (w) and pipeline curvature (i.e. strain response) is evident. The gouge width defines the magnitude ($u \propto \sqrt{wd}$) and profile, through the "step change" in soil displacements about the gouge width boundary (e.g. Figure 6-3), of the imposed relative soil deformation field. In combination, these factors influence the developed pipeline curvature and peak strain levels.

The pipeline strain response for granular soil (Figure A6-4) exhibited a similar dependence on gouge width (w) but with lower strain magnitudes in comparison with the medium stiff clay model (Figure A6-3). This was attributed to the more compliant material behaviour of the granular soil as shown in Table 6-1, which is related to the characteristic soil response functions (t_u–x_u, p_u–y_u). Although the imposed gouge displacement ($u_{max} = 2.343m$) was significantly greater than the cohesive soil load case ($u_{max} = 1.406m$) as shown in Figure 6-1, the pipeline was subjected to lower soil yield load and hence developed lower strain levels. The computed axial strain values are within recognized limits, such as those adopted for the proposed Northstar pipeline (Braden et al., 1998; INTEC, 1998).

The major influence of gouge depth (d) on the computed pipeline axial strain response, for both cohesive (Figure A6-5) and granular (Figure A6-6) soil load cases, was to increase the strain magnitudes.

A5.1.4 Gouge Bearing Stress

Local overburden stress arises due to the dynamic environmental driving forces acting on and the static mass of the ice feature penetrating the seabed. Consideration of the bearing stress in the soil/pipeline interaction model defines an effective burial depth (H^*) for the pipeline within the gouge footprint. The effective burial depth is calculated as

$$H^* = H_s + \frac{\sigma_v}{\gamma'} \quad \text{(A5.1)}$$

where γ' is the effective unit weight of soil (kN/m^3). For the current assessment study, overburden stresses (σ_v = 0kPa, 50kPa and 100kPa) were considered. In addition, the overburden pressure influences the bearing interaction factors (N) and the load-displacement response for granular soil, since these parameters are a function of the springline burial depth (H_s).

For the baseline parameters investigated with the cohesive soil load-deformation relationships, based on the ASCE (1984) guidelines, the influence of gouge bearing stress on pipeline response was insignificant. This is shown in Figure A6-7, which illustrates the longitudinal distribution of axial strain for the variation of ice feature overburden stress on the baseline parameters for the cohesive soil load case. Although defined as a function of burial depth, the horizontal (p_u–y_u) soil stiffness formulation for cohesive soils, as proposed by ASCE (1984), decreases with increasing burial depth. This is illustrated in Figure A6-8 where the normalised stiffness (K_N) is presented as a function of burial depth. The response is contrary to experimental observations of Paulin et al. (1995). For the finite element analysis conducted during the current study, a constant stiffness was adopted, for the p_u–y_u response of cohesive soil, when overburden stress was considered. The t_u–x_u curve for cohesive soil is not a function of burial depth. This area requires further consideration and investigations.

The soil response functions (t_u–x_u, p_u–y_u) for granular soil exhibit increasing stiffness proportional with burial depth. The pipeline axial strain magnitudes, for granular soil, exhibited

a significant dependence on increasing bearing stress, as illustrated in Figure A6-9. The enhanced overburden stress and pipeline strain response has been confirmed experimentally at C-CORE but the results are proprietary.

A5.1.5 Subgouge Displacement Field

A5.1.6 Soil Strength

The dominant influence of soil strength properties, for both cohesive (C_u) and granular (ϕ) soils, was to increase the axial strain magnitudes, through generalized stiffening of the mechanical response characteristics for the soil. This is illustrated in Figure A6-10 for cohesive soil and Figure A6-11 for granular soil. The pipeline strain behaviour was coupled to soil strength parameters through the load–displacement response functions (t_u–x_u, p_u–y_u) for the discretised "spring foundation stiffness". Increased soil strength is synonymous with higher soil yield loads levels and thus imposed pipeline forces and strain magnitudes. The longitudinal strain distribution was also a function of the combined relationship between gouge width (w), soil strength parameters (C_u, ϕ) and soil response functions (t_u–x_u, p_u–y_u).

A5.2 Peak Tensile Strain Response

A5.2.1 Pipeline Geometry and Mechanical Properties

A5.2.2 Gouge Geometry

A5.2.3 Gouge Bearing Stress

A5.2.4 Subgouge Displacement Field

A5.2.5 Soil Strength

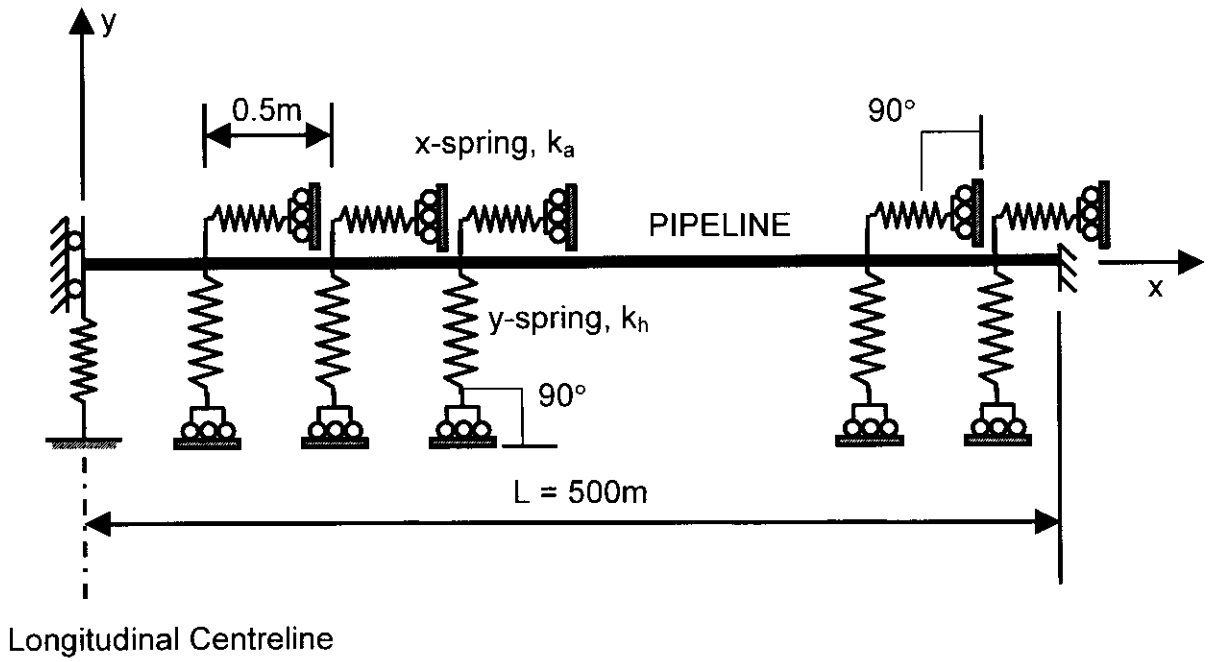

Figure A5-1. Schematic Illustration of the Finite Element Model for Soil/Pipeline Interaction Analysis and Geometric Boundary Conditions.

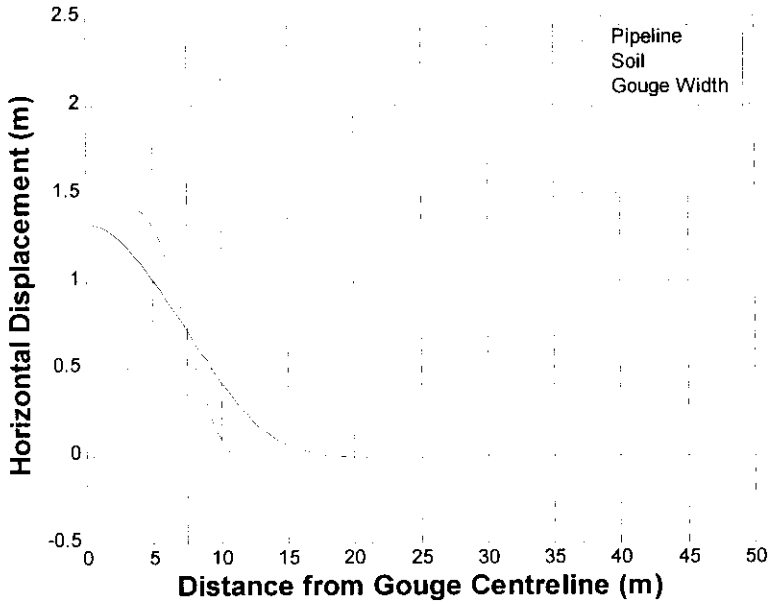

(a)

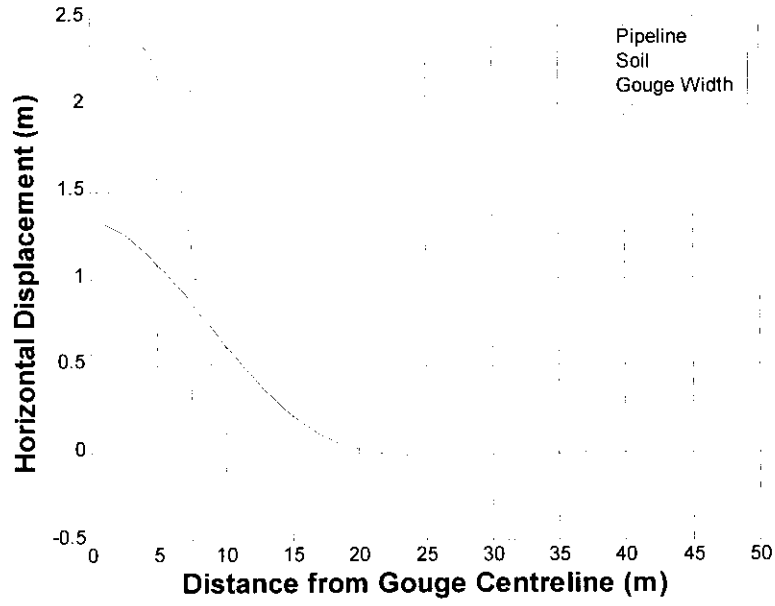

(b)

Figure A5-2. Displaced pipeline and soil profiles for the baseline cases of Table 5-1 with (a) cohesive soil ($C_u = 50kPa$) and (b) granular soil ($\phi = 35°$).

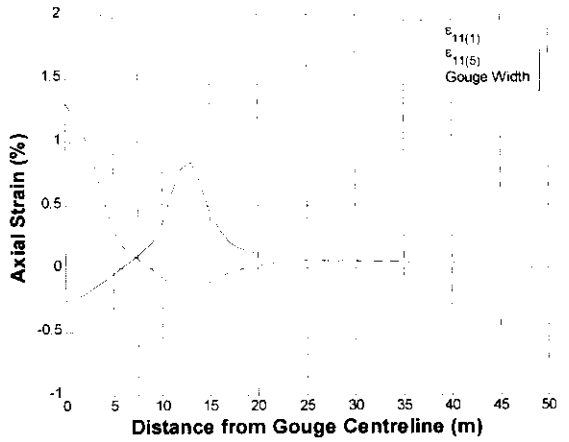

(a)

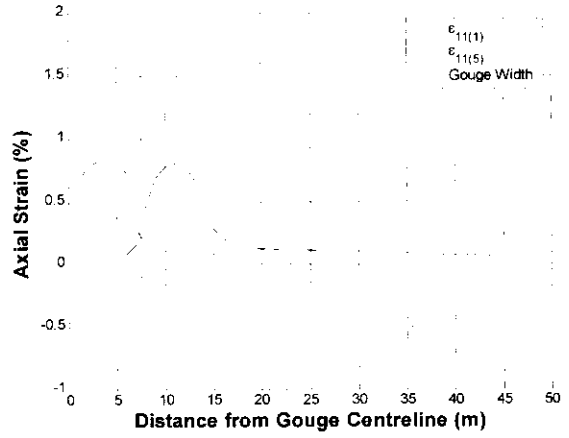

(b)

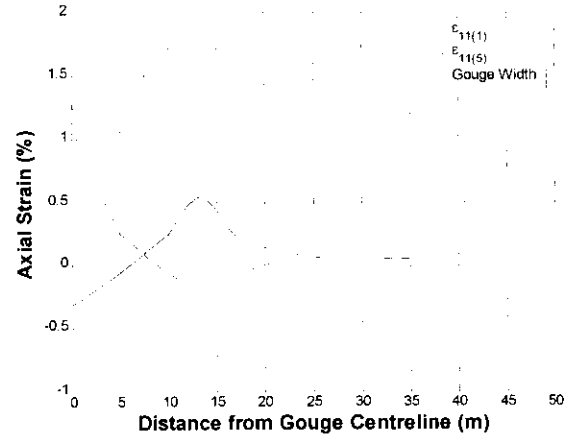

(c)

Figure A5-3. Pipeline axial strain response (ε_{11}) for pipeline diameter (D_o) and material grade variation on baseline case (Table 5-1) for cohesive soil with (a) API 5L X52, $D_o = 0.508m$, (b) API 5L X52, $D_o = 0.273m$ and (c) API 5L X65, $D_o = 0.508m$.

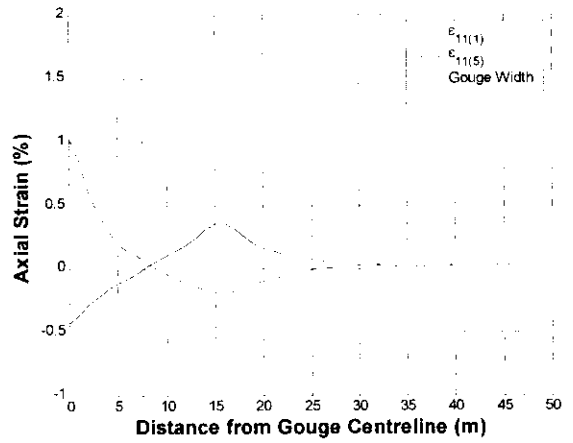

(a)

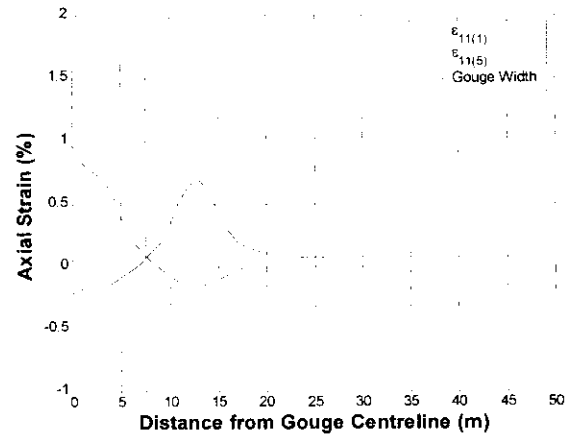

(b)

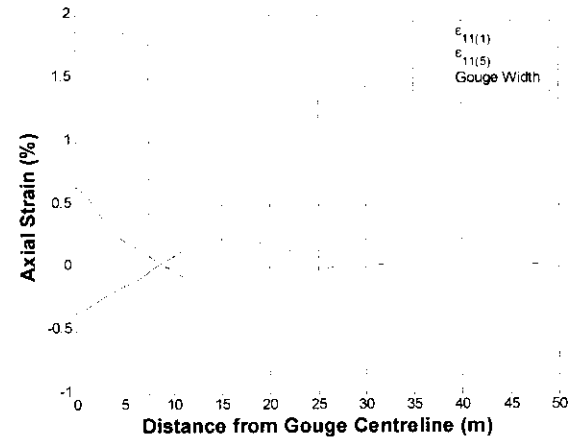

(c)

Figure A5-4. Pipeline axial strain response (ε_{11}) for pipeline diameter (D_o) and material grade variation on baseline case (Table 5-1) for granular soil with (a) API 5L X52, $D_o = 0.508m$, (b) API 5L X52, $D_o = 0.273m$ and (c) API 5L X65, $D_o = 0.508m$.

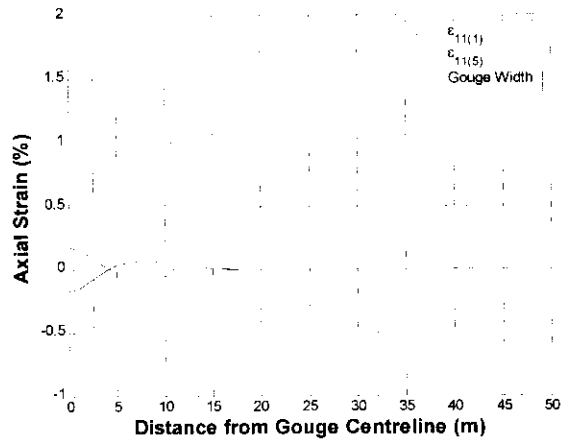

(a)

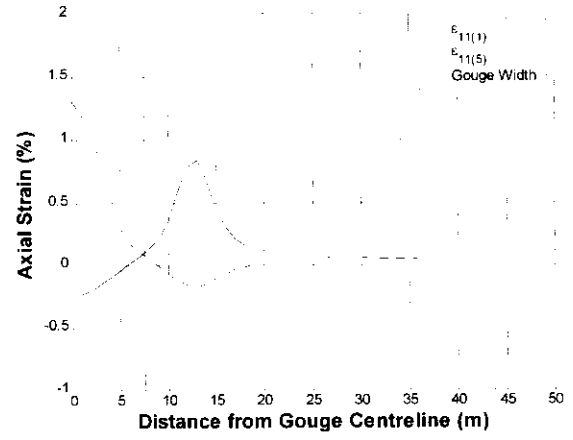

(b)

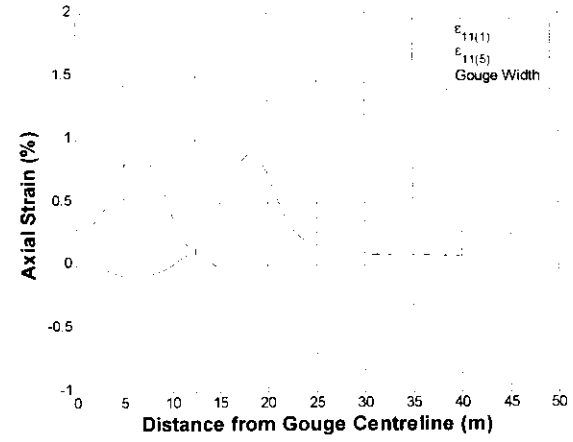

(c)

Figure A5-5. Pipeline axial strain response (ε_{11}) for gouge width (w) variation on baseline case (Table 5-1) for cohesive soil with (a) $w = 5m$, (b) $w = 15m$ and (c) $w = 25m$.

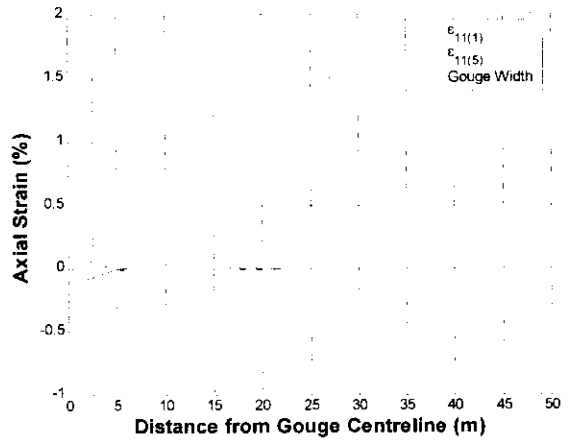

(a)

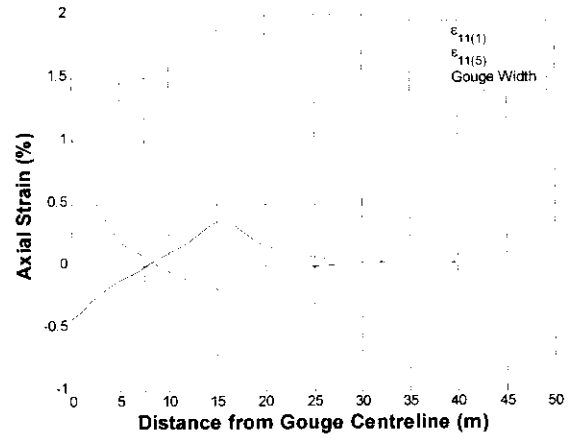

(b)

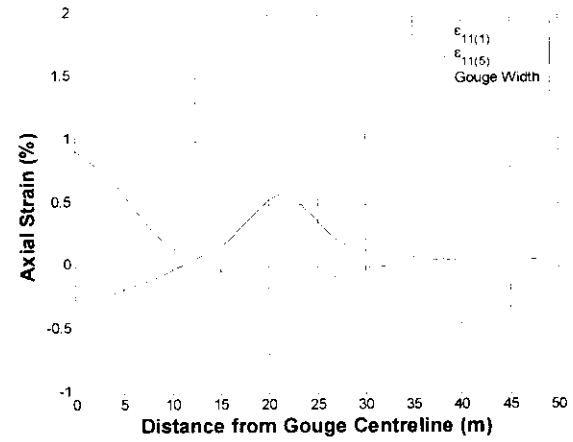

(c)

Figure A5-6. Pipeline axial strain response (ε_{11}) for gouge width (w) variation on baseline case (Table 5-1) for granular soil with (a) $w = 5m$, (b) $w = 15m$ and (c) $w = 25m$.

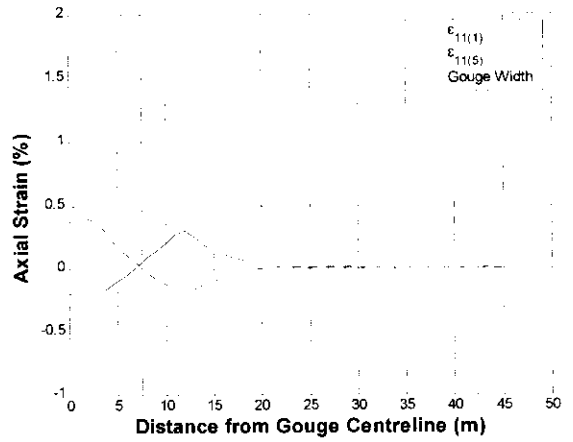

(a)

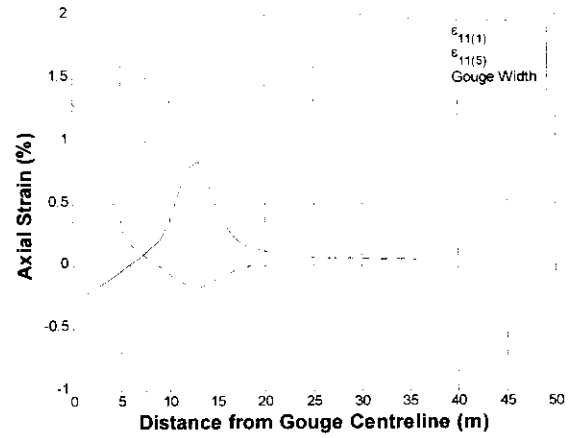

(b)

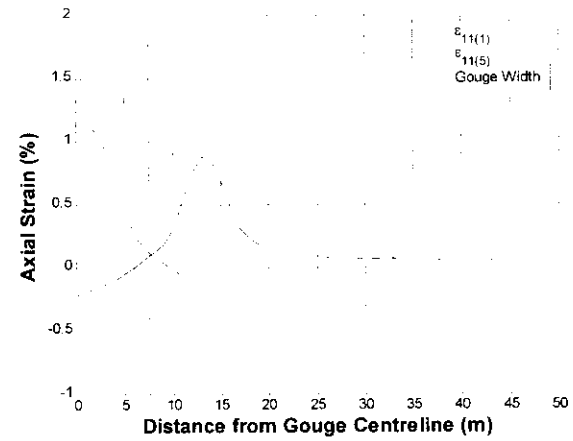

(c)

Figure A5-7. Pipeline axial strain response (ε_{11}) for gouge depth (d) variation on baseline case (Table 5-1) for cohesive soil with (a) $d = 0.5m$, (b) $d = 1.0m$ and (c) $d = 1.5m$.

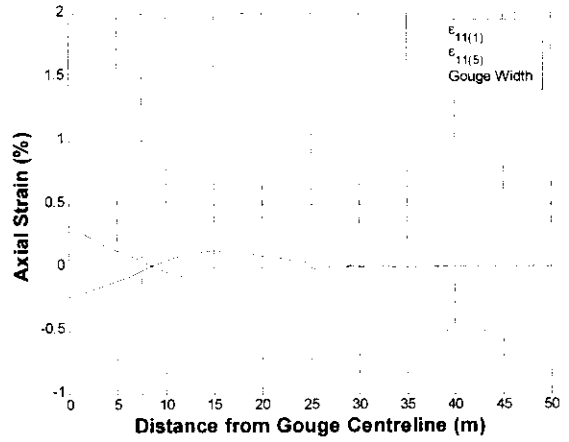

(a)

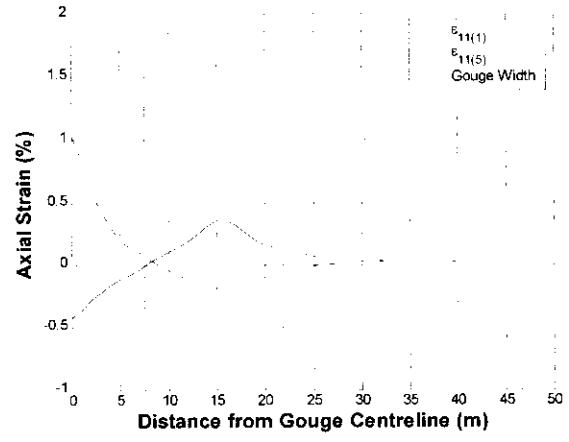

(b)

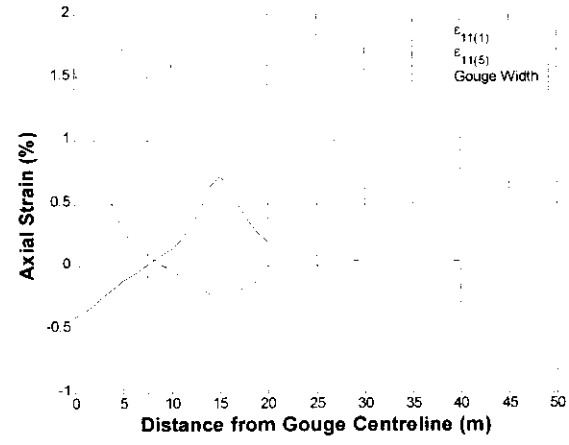

(c)

Figure A5-8. Pipeline axial strain response (ε_{11}) for gouge depth (d) variation on baseline case (Table 5-1) for granular soil with (a) $d = 0.5m$, (b) $d = 1.0$ and (c) $d = 1.5m$.

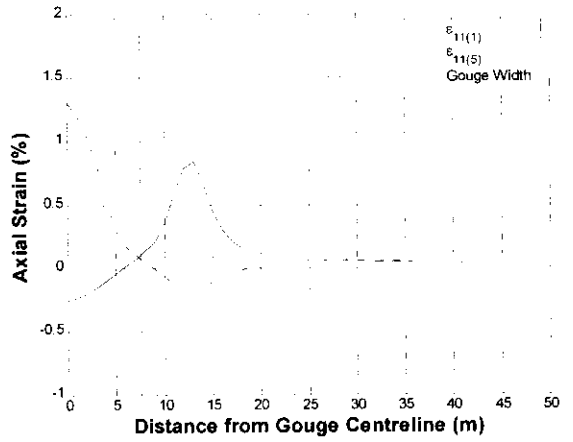

(a)

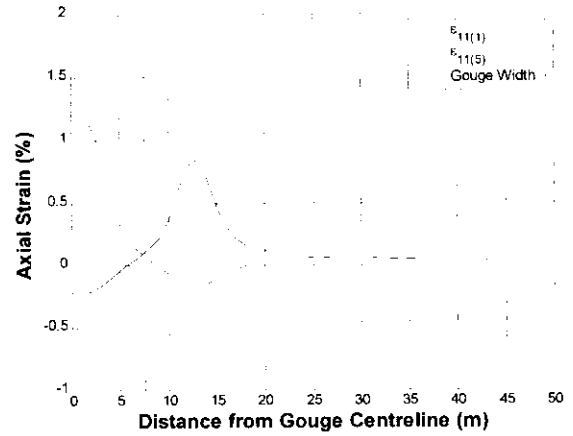

(b)

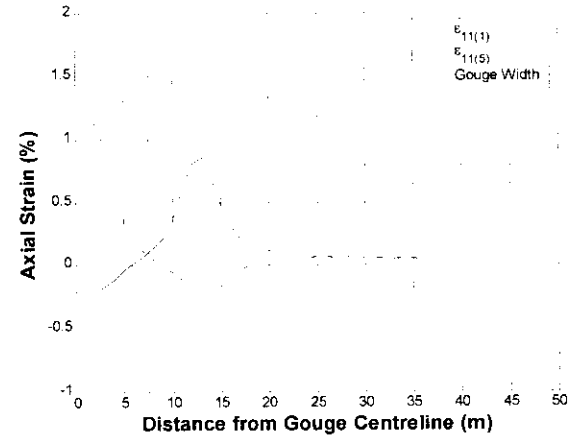

(c)

Figure A5-9. Pipeline axial strain response (ε_{11}) for overburden stress (σ_v) variation on baseline case (Table 5-1) for cohesive soil with (a) $\sigma_v = 0kPa$, (b) $\sigma_v = 50kPa$ and (c) $\sigma_v = 100kPa$.

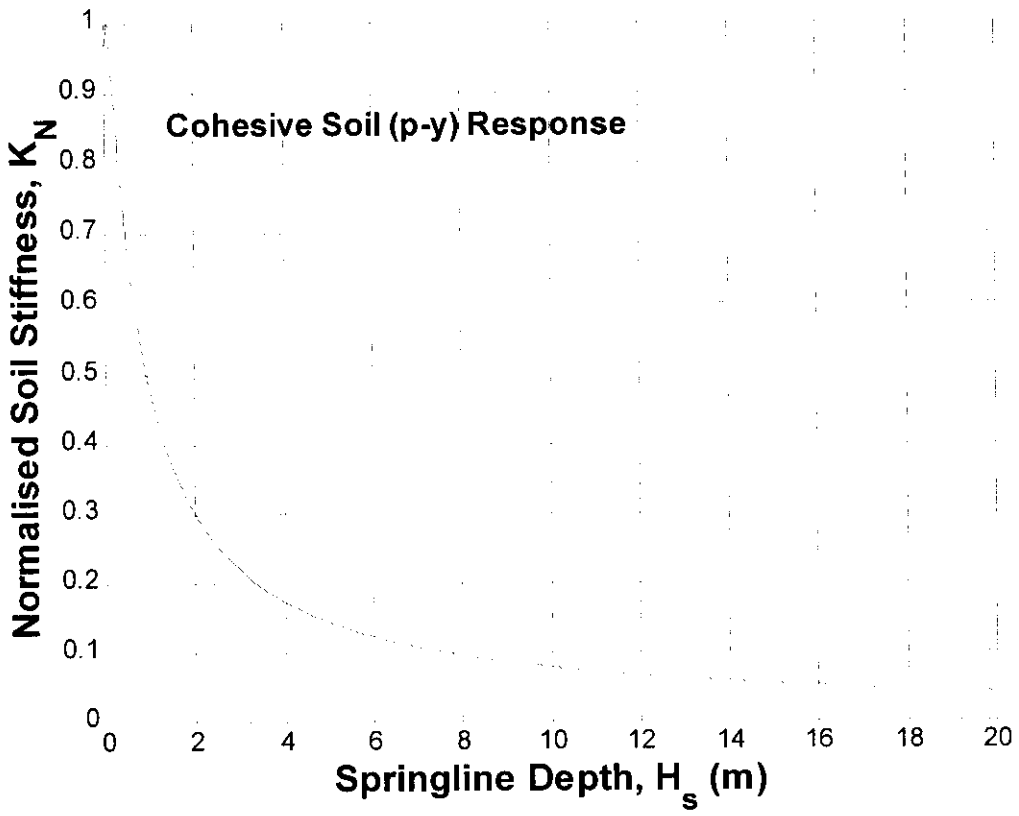

Figure A5-10. Normalised horizontal (p_u–y_u) soil stiffness for cohesive soil defined by ASCE (1984) guidelines.

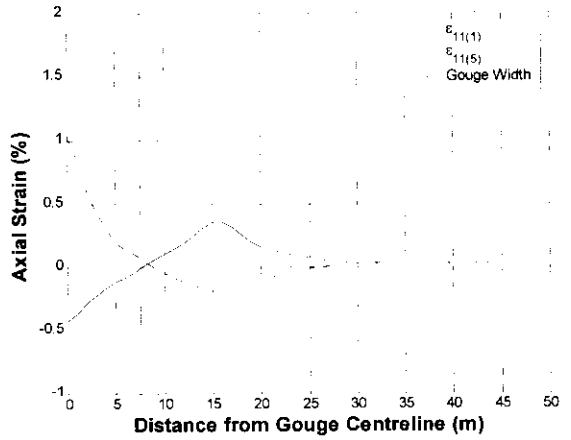

(a)

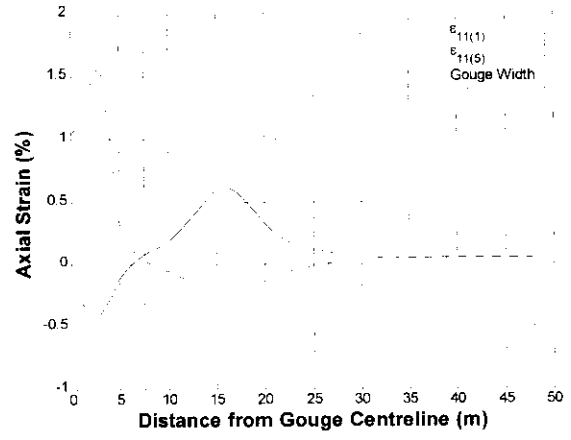

(b)

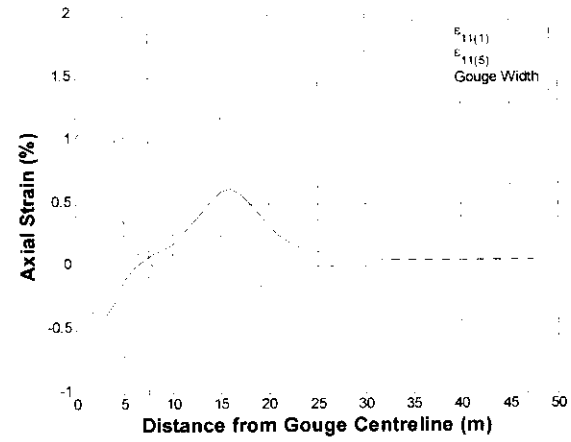

(c)

Figure A5-11. Pipeline axial strain response (ε_{11}) for overburden stress variation on baseline case (Table 5-1) for granular soil ($\phi = 35°$) with (a) σ_v=*0kPa*, (b) σ_v=*50kPa* and (c) σ_v=*100kPa*.

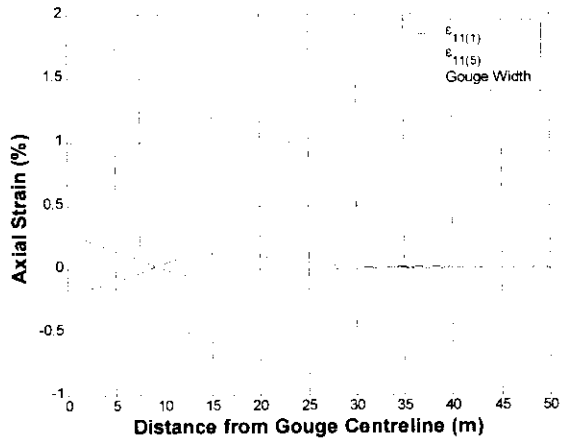

(a)

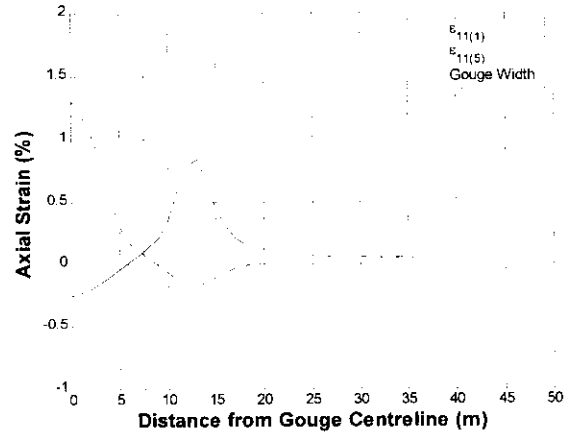

(b)

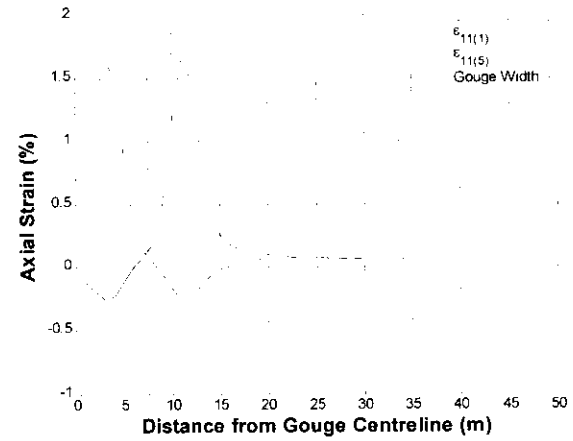

(c)

Figure A5-12. Pipeline axial strain response (ε_{11}) for soil strength (C_u) variation on baseline case (Table 5-1) for cohesive soil with (a) $C_u = 12.5kPa$, (b) $C_u = 50kPa$ and (c) $C_u = 100kPa$.

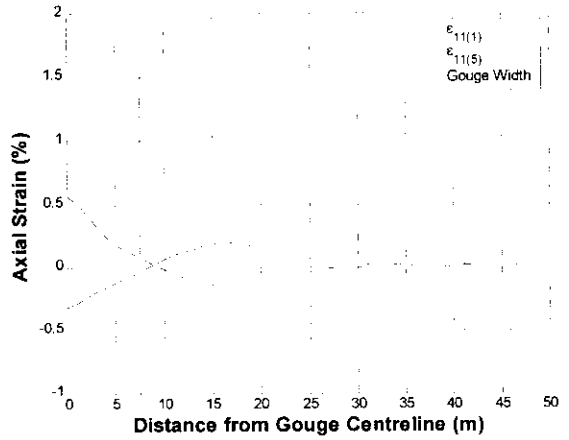

(a)

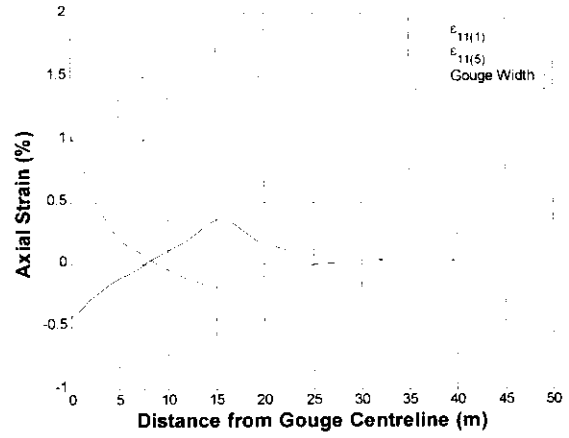

(b)

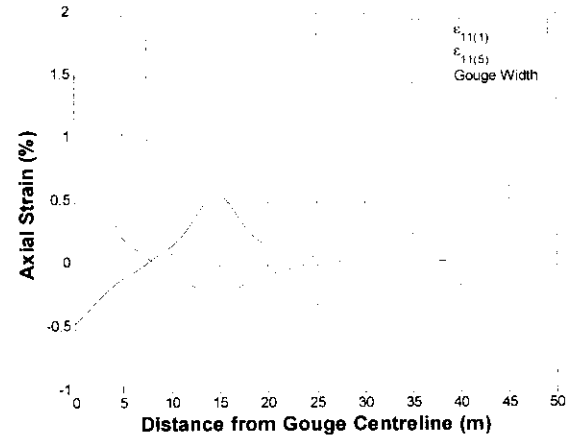

(c)

Figure A5-13. Pipeline axial strain response (ε_{11}) for soil strength (ϕ) variation on baseline case (Table 5-1) for granular soil with (a) $\phi = 30°$, (b) $\phi = 35°$ and (c) $\phi = 40°$.

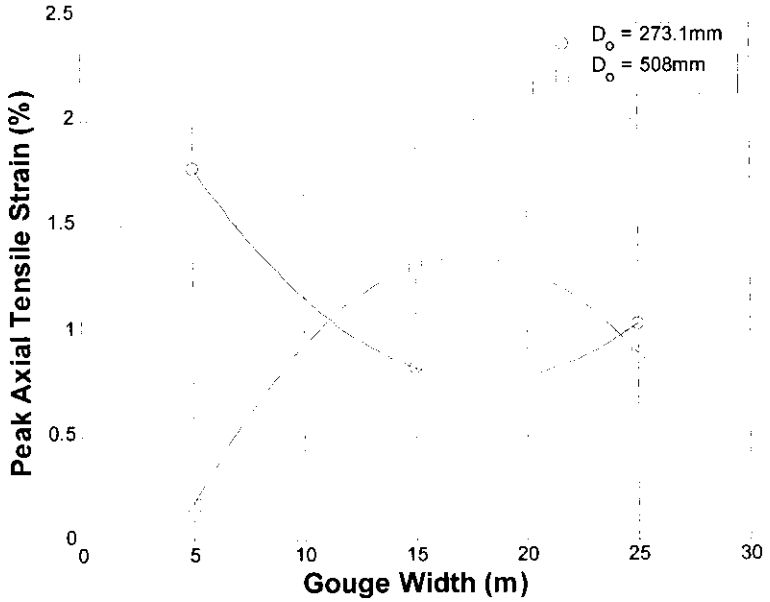

(a)

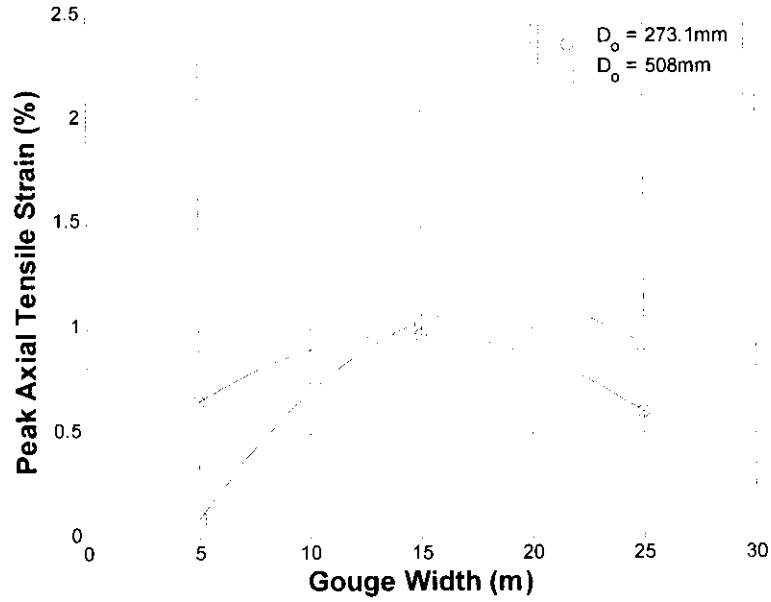

(b)

Figure A5-14. Peak axial tensile strain response (ε_{11}) as a function of gouge width (w) and pipeline diameter (D_o) for (a) cohesive soil and (b) granular soil. The gouge depth ($d = 1.0m$), soil strength ($C_u = 50kPa$, $\phi = 35°$) and overburden stress ($\sigma_v = 0kPa$) were held constant.

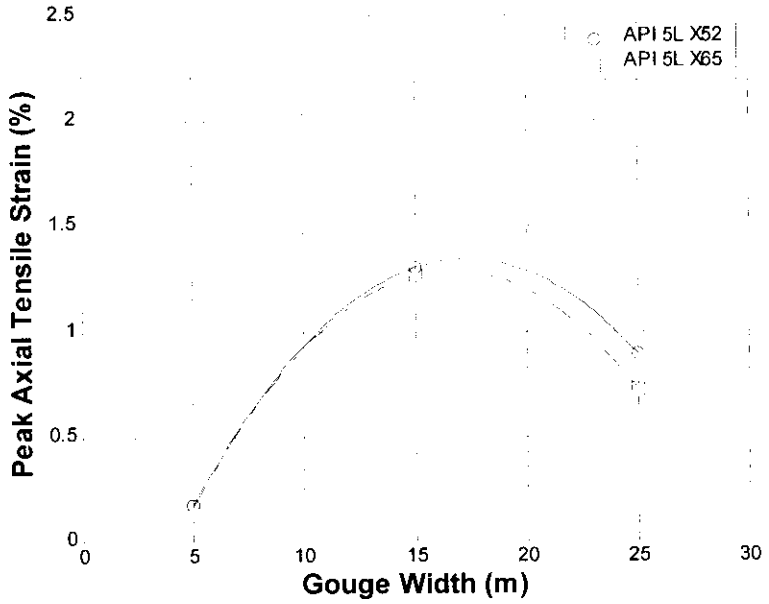

(a)

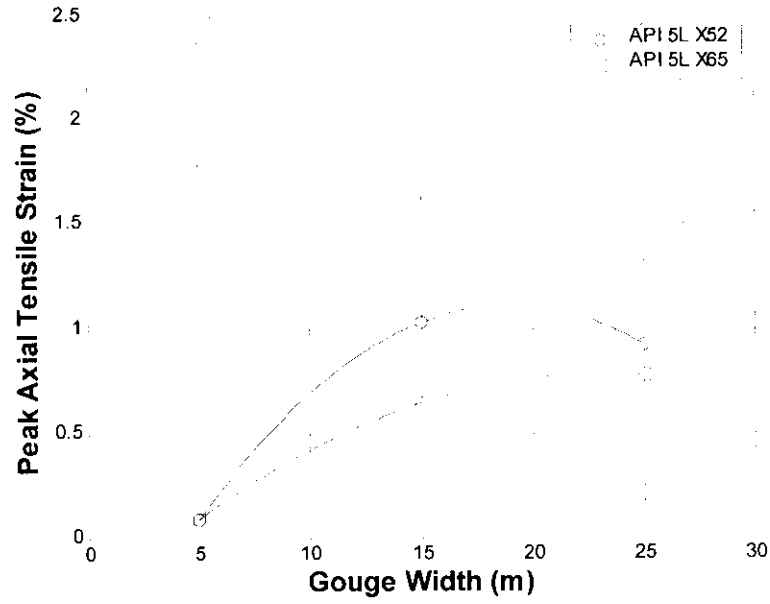

(b)

Figure A5-15. Peak axial tensile strain response (ε_{11}) as a function of gouge width (w) and pipeline grade for (a) cohesive soil and (b) granular soil. The gouge depth ($d = 1.0m$), soil strength ($C_u = 50kPa$, $\phi = 35°$) and overburden stress ($\sigma_v = 0kPa$) were held constant.

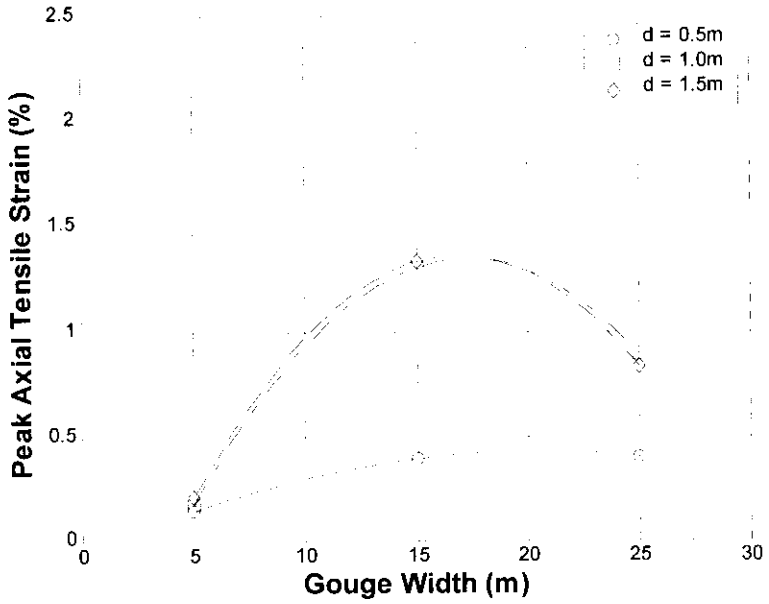

(a)

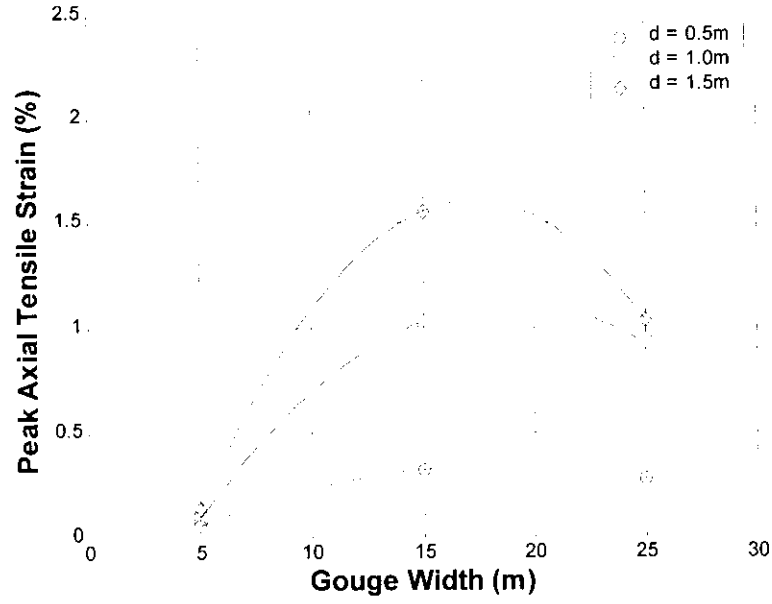

(b)

Figure A5-16. Peak axial tensile strain response (ε_{11}) as a function of gouge width (w) and gouge depth (d) for (a) cohesive soil ($C_u = 50kPa$) and (b) granular soil ($\phi = 35°$). The bearing stress ($\sigma_v = 0kPa$) was held constant.

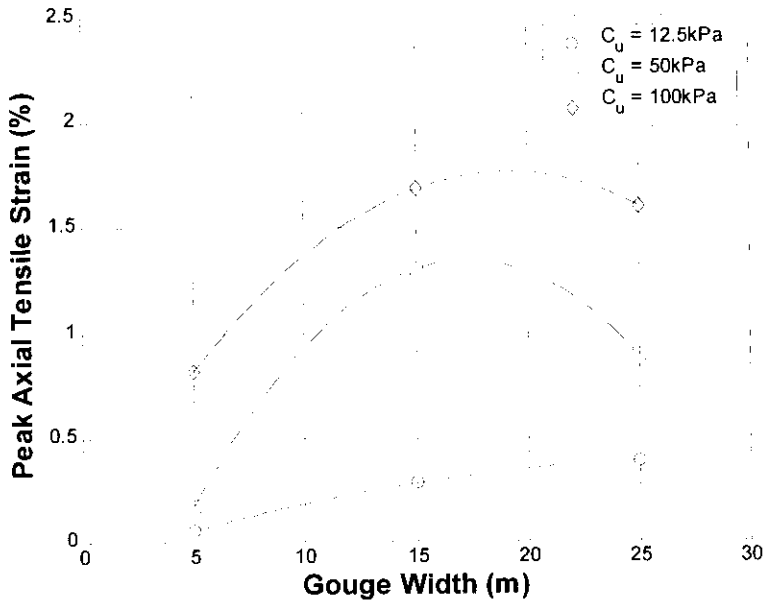

(a)

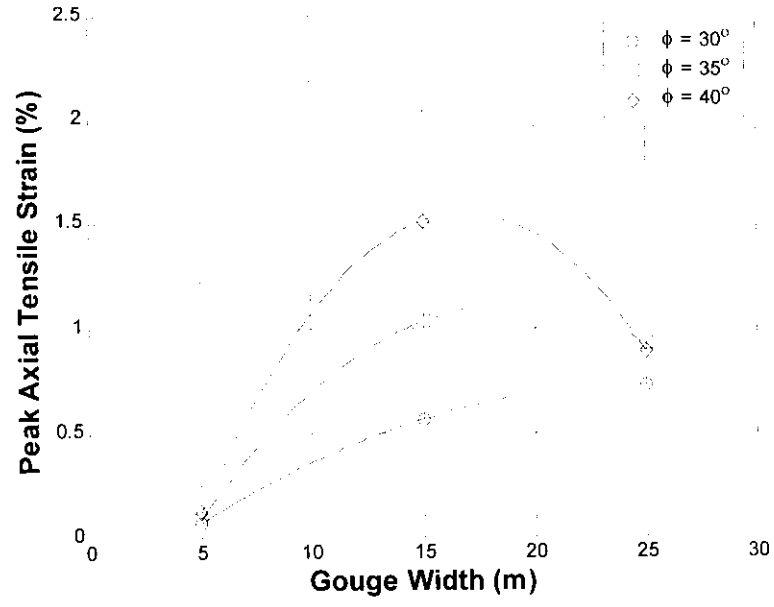

(b)

Figure A5-17. Peak axial tensile strain response (ε_{11}) as a function of gouge width (w) and soil strength (C_u, ϕ) for (a) cohesive soil and (b) granular soil. The gouge depth ($d = 1.0m$) and bearing stress ($\sigma_v = 0kPa$) were held constant.

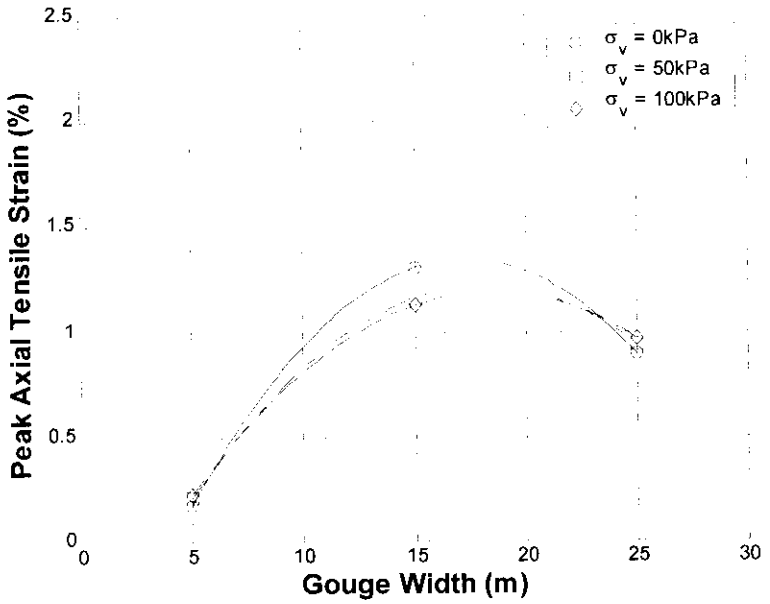

(a)

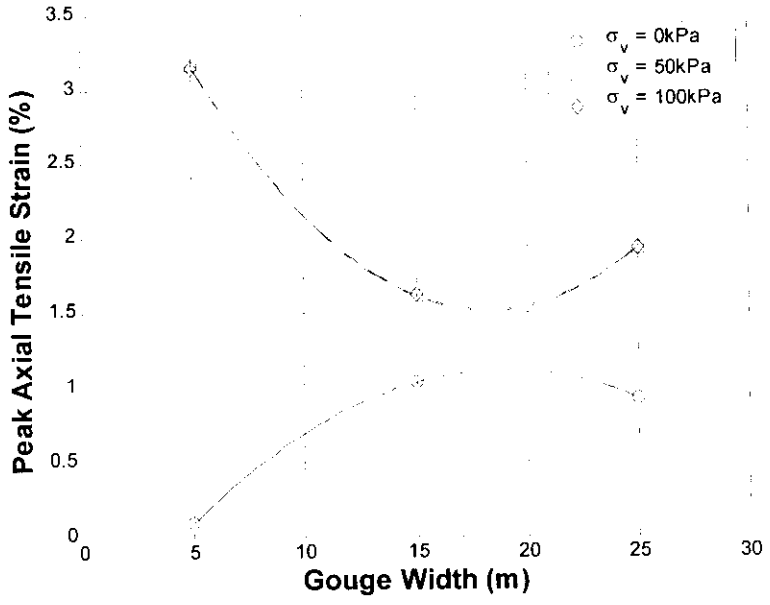

(b)

Figure A5-18. Peak axial tensile strain response (ε_{11}) as a function of gouge width (w) and overburden stress (σ_v) for (a) cohesive soil and (b) granular soil. The gouge depth ($d = 1.0m$) and soil strength ($C_u = 50kPa$, $\phi = 35°$) were held constant.

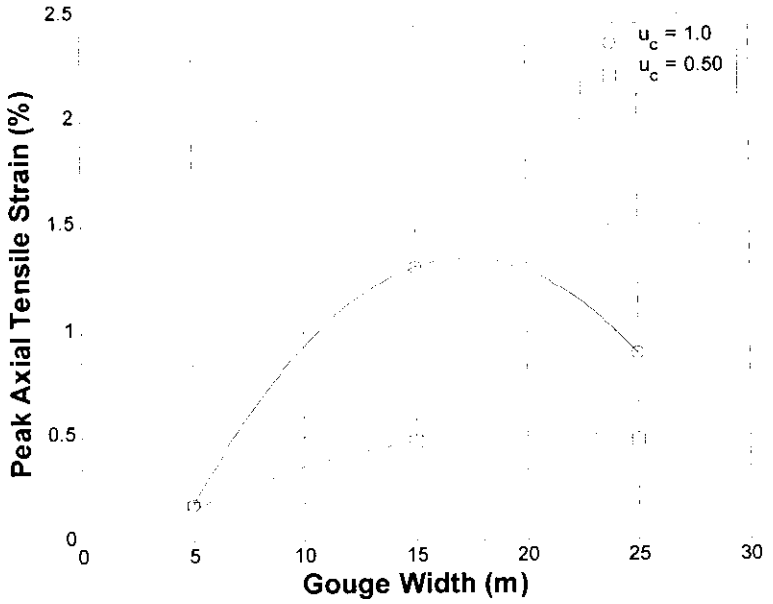

(a)

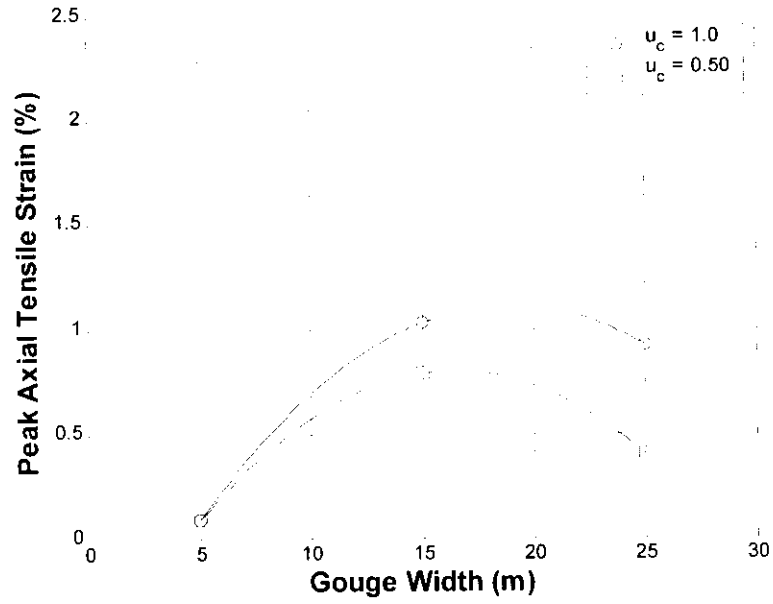

(b)

Figure A5-19. Peak axial tensile strain response (ε_{11}) as a function of gouge width (w) and subgouge displacement (u_c) for (a) cohesive soil and (b) granular soil. The gouge depth (d = *1.0m*), soil strength (C_u = *50kPa*, ϕ = *35°*) and overburden stress (σ_v = *0kPa*) were held constant.